PhD-FSTC-2016-18
The Faculty of Sciences, Technology and Communication

KTH, School of Electrical Engineering,
Signal Processing Laboratory

DISSERTATION

Defense held on 13/05/2016 in Luxembourg

to obtain the degree of

DOCTEUR DE L'UNIVERSITÉ DU LUXEMBOURG

EN INFORMATIQUE

AND

Doctor of Philosophy/Teknologie doktorsexamen

IN ELECTRICAL ENGINEERING

by

Ahmad GHARANJIK
Born on 21 March 1983 in Agh Ghala (Iran)

TRANSMISSION OPTIMIZATION FOR HIGH THROUGHPUT SATELLITE SYSTEMS

Dissertation defense committee

Dr Björn Ottersten, dissertation supervisor
Professor, Université du Luxembourg

Dr Mats Bengtssson, dissertation supervisor
Professor, KTH Royal Institute of Technology

Dr Joel Grotz, Chairman
SES S.A

Dr Wing-Kin Ma, Vice Chairman
Professor, The Chinese University of Hong Kong

Dr Mathini Sellathurai, Member
Professor, Heriot-Watt University

Dedicated to:
My loving wife Solmaz and my baby girl Sarina.

Abstract

Demands on broadband data service are increasing dramatically each year. Following terrestrial trends, satellite communication systems have moved from the traditional TV broadcasting to provide interactive broadband services even to urban users. While cellular and land-line networks are mainly designed to deliver broadband services to metropolitan and large urban centers, satellite based solutions have the advantage of covering these demands over a wide geography including rural and remote users. However, to stay competitive with economical terrestrial solutions, it is necessary to reduce the cost per transmitted bit by increasing the capacity of the satellite systems.

The objective of this thesis is to design and develop techniques capable of enhancing the capacity of next generation high throughput satellite systems. Specifically, the thesis focuses on three main topics: 1) Q/V band feeder link design, 2) robust precoding design for multibeam satellite systems, and 3) developing techniques for tackling related optimization problems.

Design of high bandwidth and reliable feeder links is central towards provisioning new services on the user link of a multibeam SatCom system. Towards this, utilization of the Q/V band and an exploitation of multiple gateway as a transmit diversity measure for overcoming severe propagation effects are being considered. In this context, the thesis deals with the design of a feeder link comprising $N + P$ gateways (N active and P redundant gateways). Towards satisfying the desired availability, a novel switching scheme is analyzed and practical aspects such as prediction based switching and switching rate are discussed. Building on this result, an analysis for the $N + P$ scenario leading to a quantification of the end-to-end performance is provided.

On the other hand, frequency reuse in multibeam satellite systems along with precoding techniques can increase the capacity at the user link. Similar to terrestrial communication channels, satellite based communication channels are time-varying and for typical precoding applications, the transmitter needs to know the channel state information (CSI) of the downlink channel. Due to fluctuations of the phase components, the channel is time-varying resulting in outdated CSI at the transmitter because of the long round trip delay. This thesis studies a robust precoder design framework considering requirements on availability and average signal to interference and noise ratio (SINR). Probabilistic and expectation based approaches are used to formulate the design criteria which are solved using convex optimization tools. The performance of the resulting precoder is evaluated through extensive simulations. Although a satellite channel is considered, the presented analysis is valid for any vector channel with phase uncertainty.

In general, the precoder design problem can be cast as power minimization problem or max-min fairness problem depending on the objectives and requirements of design. The power minimization problem can typically be formulated as a non-convex quadratically constrained quadratic programming (QCQP) problem and the max-min fairness problem as a fractional quadratic program. These problems are known to be NP-hard in general. In this thesis, the original design problem is transformed to an unconstrained optimization

problem using the specialized penalty terms. The efficient iterative optimization frameworks are proposed based on a separate optimization of the penalized objective function over its partition of variables at each iteration. Various aspects of the proposed approach including performance of the algorithm and its implementation complexity are studied.

This thesis is made under joint supervision agreement between KTH Royal Institute of Technology, School of Electrical Engineering, Stockholm, Sweden and University of Luxembourg, Luxembourg.

Acknowledgments

Firstly, I would like to thank my PhD supervisor Professor Björn Ottersten for his continuous support and encouragement throughout my PhD studies which was vital in making this thesis a reality. He would always take time out of his busy schedule to give good advice and guidance. I admire his respect, encouragement and positive attitude towards his team. I am grateful to him for providing me with the opportunity to pursue my PhD at both University of Luxembourg and KTH. I feel honored to have had a chance to work with him and learn from him.

I would also like to thank my co-supervisor at University of Luxembourg, Dr. Bhavani Shankar. He was actively involved in my research work while allowing me the space and freedom I needed to work. Throughout my PhD, I had numerous meeting with Dr. Shankar discussing various issues ranging from my research to daily issues. I am grateful for his friendly personality, I do not remember him getting impatient or angry even for once. Dr. Shankar was not only my supervisor, but also, sometimes acted as a big brother or a friend under different circumstances.

I am grateful to my supervisor at KTH, Professor Mats Bengtsson. Completing my PhD study at KTH would have been difficult without the support and help provided by Dr. Bengtsson. He was always ready to help and advise me on research problems or other administrative issues at KTH. I would like to thank my PhD committee member, Dr. Pantelis-Daniel Arapoglou. He has always had excellent answers to my questions related to Satellite Communication. His extensive knowledge and experience in the area of Satellite Communication helped me to be on right track with my research. I would also like to thank Dr. Mojtaba Soltanalian for introducing me to signal design and optimization area. Results of our fruitful scientific collaboration are presented in Chapter 6 and Chapter 7 of this thesis.

I wish to thank Professor Wing-Kin Ma for taking time to serve as opponent for this thesis and traveling from very far to attend the thesis defense. I also wish to thank the examination committee, Dr. Mathini Sellathurai, Dr. Joel Grotz and Dr. Mehrdad Sabetzadeh. Special thanks are dedicated to the friends and colleagues member of SigCom group in SnT for creating supportive and friendly environment.

Most importantly, I must express my gratitude to my family. My parents, brothers and sisters have always supported my studies. I would like to thank my wife Solmaz for her encouragement, love and patience that made this dissertation possible.

Ahmad Gharanjik
Luxembourg, April, 2016

Contents

Nomenclature

Mathematical Notation

Bold lowercase letters are used to denote the vectors and bold uppercase letters for matrices. The following mathematical notations are used throughout this thesis:

$\mathbf{x}(k)$	the k^{th} entry of the vector $\mathbf{x}$
$\|\mathbf{x}\|_n$	the ℓ_n-norm of $\mathbf{x}$, defined as $(\sum_k \|\mathbf{x}(k)\|^n)^{\frac{1}{n}}$
$\|\mathbf{x}\|$	ℓ_2-norm of $\mathbf{x}$
$\mathbf{X}^H$	the complex conjugate of a matrix $\mathbf{X}$
$\|x\|$	absolute value of a scalar x
$\mathbf{X}^T$	the transpose of a matrix $\mathbf{X}$
$\text{Tr}(\mathbf{X})$	the trace of a matrix $\mathbf{X}$
$\|\mathbf{X}\|_F$	the Frobenius norm of a matrix $\mathbf{X}$
$\mathbf{X} \otimes \mathbf{Y}$	the Kronecker product of two matrices $\mathbf{A}$ and $\mathbf{B}$
$\mathbf{X} \odot \mathbf{Y}$	the Hadamard element-wise product of two matrices
$\text{vec}(\mathbf{X})$	the vector obtained by column-wise stacking of $\mathbf{X}$
$\arg(\mathbf{X})$	the phase angle (in radians) of $\mathbf{X}$
$\Re\{\mathbf{X}\}$	the real part of $\mathbf{X}$
$\mathbf{X} \succ \mathbf{Y}$	$\mathbf{X} - \mathbf{Y}$ is positive definite
$\mathbf{X} \succeq \mathbf{Y}$	$\mathbf{X} - \mathbf{Y}$ is positive semidefinite
$\mathbf{I}_n$	the identity matrix of dimension n
$\mathbf{e}_n$	the n^{th} column of an identity matrix.
$\mathbb{C}$	the set of complex numbers
$\mathbb{R}$	the set of real numbers
$\mathbb{Z}$	the set of integer numbers
$[K]$	the set $\{1, 2, \ldots, K\}$
$\sigma_n(\mathbf{X})$	n^{th} maximal eigenvalue of $\mathbf{X}$
$[\mathbf{X}]_{ij}$	the $(i,j)^{\text{th}}$ element of a matrix $\mathbf{X}$
$\mathbf{E}\{\cdot\}$	the mathematical expectation of a random variable
$\text{diag}(\mathbf{X})$	denotes a vector formed by diagonal entries of the matrix $\mathbf{X}$
$\text{diag}(\mathbf{x})$	denotes a diagonal matrix formed by the entries of the vector $\mathbf{x}$
$\Pr\{\cdot\}$	denotes the probability of a random event

Chapter 1

Introduction

The thesis deals with some emerging challenges of the satellite communications (SatCom). Building on the literature, interactions with various stake holders, research topics of interest are identified. This chapter provides sufficient background to understand the problems considered in the latter chapters. Among them, we focus on broadband and multibeam satellite systems, interference cancellation, precoding design and Q/V band (50/60 GHz) feeder link. Further, the chapter also highlights the contribution of the thesis to the aforementioned areas. The mathematical system model, and detailed problem formulations are given in Chapter 2.

1.1 Broadband Satellite Systems

The main goal of the *broadband satellite systems* is to provide most of the services that are offered by terrestrial networks in a very large coverage area, particularly in the area wherein it is uneconomic for terrestrial solutions to be present. Among those services, fast Internet access and multimedia services are the main basis for development of broadband satellite systems [1,2]. Figure 1.1 shows the architecture of a traditional broadband satellite system. In the following, more details about each component of the system are provided.

- **Gateway**: Gateway (GW), also referred as *ground station*, is responsible for transmitting and receiving data, control and management of traffic to/from the user terminals (UT) via the satellite. Multiple gateways might be employed in the network if diversity is needed.
- **Satellite**: In the current work, we focus on satellites in the geostationary orbit (GEO) though other constellations exist. The relative stationarity of the satellite and the earth and high orbital distance allows for wider coverage area per satellite and avoids tracking on earth. The GEO satellite connects the gateway to the User Terminals (UTs), thanks to a set of feeder and user

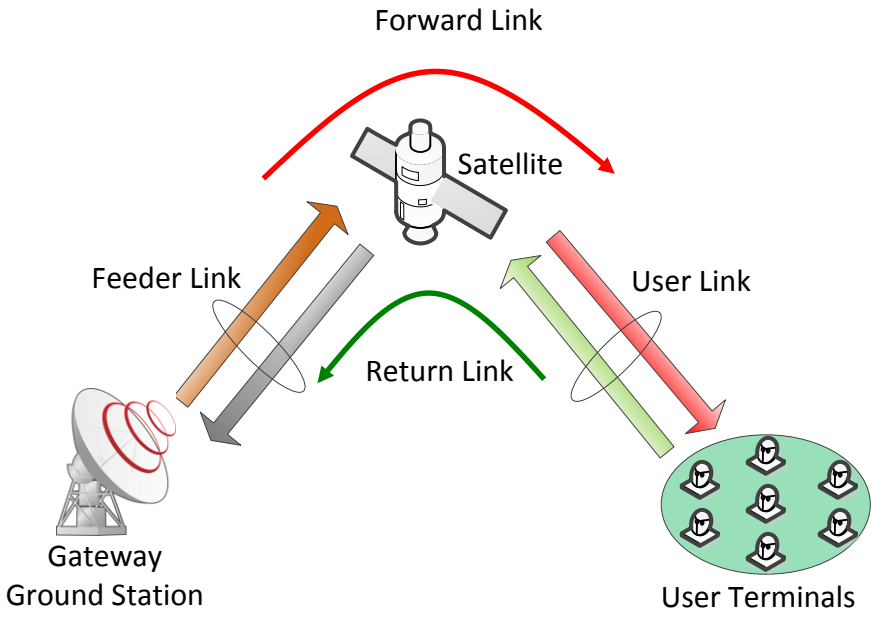

Figure 1.1. Architecture of a traditional broadband satellite system

links. Throughout the thesis, a bent-pipe satellite is considered where only amplification and frequency translations are performed on-board

- **User Terminal**: It is a device operating in a radio frequency (RF) band (e.g. Ku-band, Ka-band, etc). For broadband services it is a two-way terminal, that can both receive and transmit data from/to the satellite as an example very small aperture terminals (VSAT). User terminals usually are equipped with single antenna.
- **Feeder Link**: It is a radio link between the gateway and satellite at a given location to a space segment. It comprises both uplink and downlink. For current broadband satellite services, feeder links operate in Ka-band (20/30 GHz).
- **User Link**: The radio link between the satellite and UTs which comprise both uplink and downlink is called user link. This link operates in Ka-band as well. In order to allow several UTs to access the satellite and vise versa, multiple access techniques such as time division multiple access (TDMA) are deployed in this link [3].

- **Forward Link**: The end-to-end link from GW towards UTs is called forward link which includes uplink of the feeder link, satellite and downlink of user link. GW can transmit data to the UTs via the forward link. In this link, communication from GW to UT is based on satellite versions of DVB (DVB-S and DVB-S2) standards [4].
- **Return Link**: Unlike the forward link, the return link is the radio link from UT towards the GW and includes uplink of the user link, satellite and downlink of the feeder link. Through this link, the UT can transmit data to the GW. The DVB-Return Channel Satellite (DVB-RCS) standard provides the specification for the return traffic flows from UT to GW [5].

1.2 Multibeam Satellite Systems

Demands on broadband data service are increasing dramatically each year. Following terrestrial trends, satellite communication systems have moved from the traditional TV broadcasting to provide interactive broadband services even to urban users. While cellular and land-line networks are mainly designed to deliver broadband services to metropolitan and large urban centers, satellite based solutions have the advantage of covering these demands over a wide geography including rural and remote users.

However, to stay competitive with economical terrestrial solutions, it is necessary to reduce the cost per transmitted bit by increasing the capacity of the satellite systems [6, 7]. In legacy SatCom systems, a satellite provides coverage to a large area using a single beam which limits the capacity and efficiency of the system. Inspired by terrestrial cellular networks, modern SatCom systems deploy multiple, hundreds, beams. Using a multibeam architecture allows to reuse the frequency among the beams, resulting in capacity expansion of the system. Concurrently, the inter-beam interference is maintained within the acceptable limits to achieve a high spectral efficiency.

In general, modern satellites have multiple antennas in order to generate multiple spot beams. Various techniques can be used to create spot beams. The most straightforward technique is to use a *reflector* and *feed* (single beam per feed) architecture, where a dedicated feed chain (RF path) illuminates to the reflector so that the radiated radio waves from the reflector aperture generate the desired beam pattern. This solution usually offers high radiation efficiency and good isolation properties between the different beams [8]. In the receiving antennas, feeds are responsible for collecting the incoming radio waves from reflectors and transferring them to the subsequent elements of the RF chain. Figure 1.2 shows the schematic of satellite antennas that generate multiple spot beams. It can be seen that each beam is generated by a dedicated antenna feed and beams with same color are radiated from the same reflector.

Fig. 1.3 depicts the architecture of a modern SatCom system with 4-color reuse scheme where each color represents a frequency/polarization segment. In more

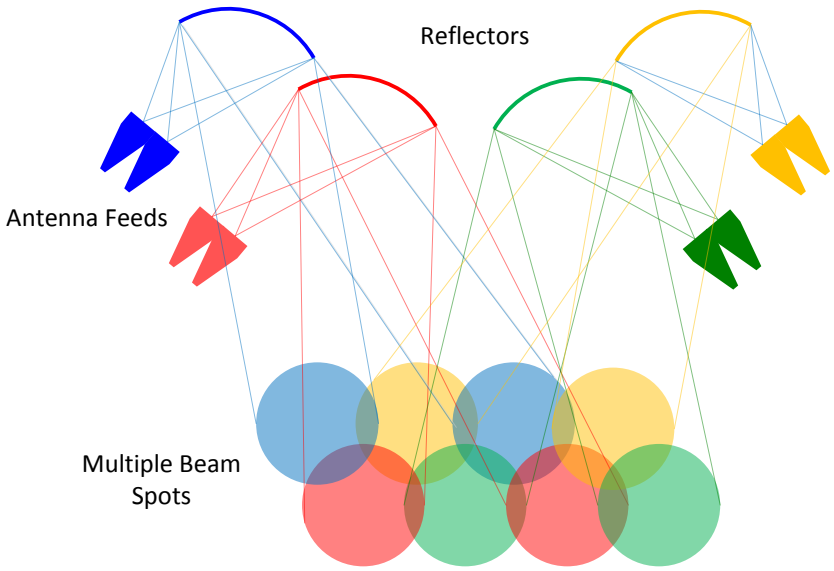

Figure 1.2. The schematic of the multibeam satellite antennas that generate multiple spot beams. It can be seen that each beam is generated by a dedicated antenna feed and beams with same color are radiated from the same reflector. Each color represents a frequency/polarization segment.

detail, a four color frequency reuse scheme can be achieved by partitioning the available frequency/polarization resources into four colors (segments), that each color defines half the available bandwidth and one polarization (right hand circular polarization- RHCP or left hand circular polarization- LHCP). In conventional multibeam systems, to reduce the inter-beam interference adjacent beams are allocated a different color.

Capacity of the current multibeam satellite systems is in the order of 100 Gbps, for example ViaSat-1 with 72 beams has capacity of 140 Gbps. To reduce the cost per transmitted bit, it is estimated that next generation satellites will require capacity of one Terabit/s (1000 Gbps) by 2020 [7]. The key challenge to achieve a Terabit/s broadband SatCom system is the limited available spectrum in the currently used Ka-band. At the user link, the capacity can be expanded by using multibeam structure and aggressively reusing the frequency resources. At feeder

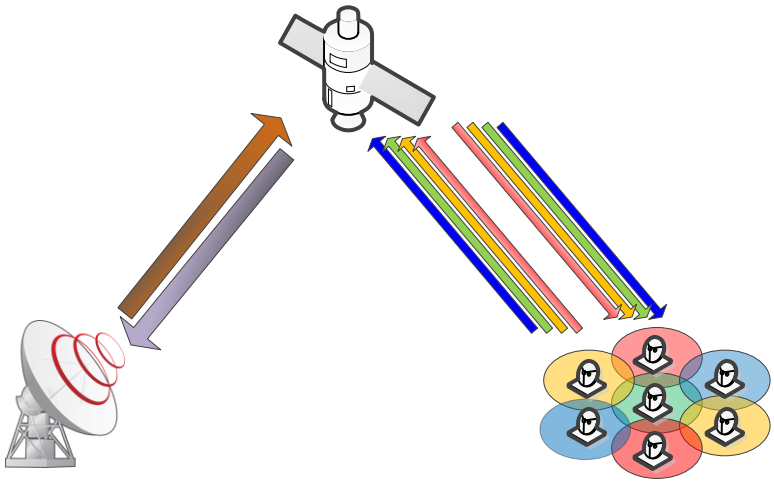

Figure 1.3. Architecture of a multibeam satellite system with a 4-color reuse scheme. A four color frequency reuse scheme can be achieved by partitioning the available frequency/polarization resources into four colors (segments), that each color defines half the available bandwidth and one polarization(RHCP or LHCP).

link, moving it from Ka-band to the Q/V-band (40/50 GHz)[1] is an attractive solution. In the following section, more details about these solutions are provided.

1.3 Solutions for High Throughput SatCom

1.3.1 Aggressive Frequency Reuse and Precoding Design

As discussed in the previous section, current multibeam SatCom systems use 4 color beam structure in order to increase the capacity while avoiding the inter-beam interference to a great extent. However, it has been known that this is greatly suboptimal from an information-theoretic point of view, since each beam can utilize only 1/4 of the total available physical resources, i.e. frequency band and polarization.

In recent years, a lot of research were carried out to improve upon conventional 4 color frequency reuse and consider advanced systems achieving full frequency reuse

[1] Q/V bands span 35-75 GHz but main frequency allocations for SatCom are the FSS bands, 37.5-42.5 GHz and 47.5-51.4 GHz.

where each beam can fully utilize the whole available resources. This, of course, comes at the cost of tremendous inter beam interference among the adjacent beams.

However, interference problem can be handled by employing advanced precoding techniques at GW. The precoding techniques require channel state information (CSI) which is a challenging task in SatCom channel due to long round trip delay (RTD). To allow the use of precoding in next generation satellite systems, it is essential to investigate the effect of imperfections induced by the RTD. Pursuing this goal, one may recognize that long RTD and time-varying phase components lead to outdated CSI at transmitter (CSIT), or more specifically an outdated estimate of the channel phase. Therefore, the performance of the system becomes unpredictable when the GW uses outdated CSIT due to phase uncertainty.

In the existence of uncertainty in CSI, robust precoding design paradigms can be considered in order to mitigate sensitivity of the precoding techniques to inaccurate CSIT. Developing a precoding framework that is robust to phase uncertainty is one of the main topics of this thesis. In general, design of the precoder can be cast as an optimization problem. Such problems are usually challenging to solve. The contributions of this thesis include modeling the phase uncertainty and developing new optimization techniques which can be employed for precoding design.

1.3.2 Moving Feeder Link to Q/V Band

In current Ka-band, a limited spectrum of about 2 GHz is available. Following the traditional trend, one solution for capacity expansion can be gradually shifting to a higher frequency band whenever the relevant technology is mature enough.

Therefore, an attractive solution is moving the feeder link from the Ka-band to the Q/V band where larger bandwidths, up to 5 GHz, are available [7,9,10]. Further, this move can free up the whole Ka-band spectrum for the user link. This is a very interesting solution for satellite operators since the feeder link requires almost the same spectrum as the user link but it does not provide any direct revenue. By moving the feeder link to the unused spectrum, satellite operators can use the freed bandwidth for commercial purposes. Moreover, it allows locating the gateways within the service area minimizing the interference between the feeder link and user link [10]. However, moving the feeder link to Q/V band imposes considerable strain on the link-budget, which is of the order of $15-20$ dB or more predominantly due to heavy rain attenuation [9]. The typical Fade Mitigation Technique (FMT) is the uplink power control. However, it can compensate only a few dBs and handle fades of short duration. These motivate the use of multiple GWs for transmit diversity to achieve the required availability in excess of 99.9% on the feeder link. Note that, it is preferable to first use FMTs then GW diversity techniques. Typically, FMTs include a fade prediction block and can handle short and small fades. If these techniques can counter the fade while providing the required performance, GW diversity techniques will not be triggered.

The traditional diversity scheme, where one GW is supported by another redundant GW, can be an acceptable solution for low/ medium throughput systems. On

the other hand, for high capacity satellite systems where tens of GWs are required, it is not efficient to use the traditional approach. This warrants an investigation into design of advanced diversity techniques. Another main topic of the thesis is to design of a Q/V band feeder link comprising multiple gateways.

1.4 Objectives and Outline of the Thesis

The objectives of this thesis are to design and develop techniques which are required for next generation high throughput satellite systems. More specifically, Q/V band feeder link design, robust precoding design and developing techniques for solving underlying optimization problems are main focus of the thesis. More details on contributions are given in Chapter 2, however a brief description of the contributions are as follows:

- **Q/V band feeder link design:** Design of high bandwidth and reliable feeder links is central towards provisioning new services on the user link of a multibeam SatCom system. Towards this, utilization of the Q/V band and an exploitation of multiple GW as a transmit diversity measure for overcoming severe propagation effects are being considered. In this context, the thesis deals with the design of a feeder link comprising $N + P$ GWs (N active and P redundant GWs). Towards satisfying the desired availability, a novel switching scheme is analyzed and practical aspects such as prediction based switching and switching rate are discussed. Unlike most relevant works, a dynamic rain attenuation model is used to derive analytically average outage probability in the fundamental $1+1$ gateway case. Building on this result, an analysis for the $N + P$ scenario leading to a quantification of the end-to-end performance is provided.

- **Robust precoding design framework:** While multibeam satellite systems with full frequency reuse provide an ideal application for introducing and exploiting precoding techniques, the precoding design must take practical limitations into account. We study robust precoding design on the user downlink channel of a multibeam satellite system. Due to fluctuations of the phase components, the channel is time-varying resulting in outdated channel state information at the transmitter because of the long round trip delay. Herein, we propose a model for the phase uncertainty and study a robust precoder design framework considering requirements on availability and average signal to interference and noise ratio (SINR). Probabilistic and expectation based approaches are used to formulate the design criteria which are solved using convex optimization tools. The performance of the resulting precoder is evaluated through extensive simulations. Although we considered a satellite channel, the presented analysis is valid for any vector channel with phase uncertainty.

- **Optimization techniques with application to precoding design:** In general, the precoding design is an optimization problem which can be cast as power minimization problem or max-min fairness problem depending on the objectives and requirements of design. The power minimization problem can typically be formulated as a non-convex quadratically constrained quadratic programming (QCQP) problem and max-min fairness problem as a fractional quadratic program. These problems are known to be NP-hard in general. In this thesis, using a penalized version of the original design problem, we derive a simplified reformulation of the problem in terms of the signal (to be designed). We propose an efficient iterative optimization framework based on a separate optimization of the penalized objective function over its partition of variables at each iteration. Various aspects of the proposed approach including performance of the algorithm and implementation complexity were studied.

Chapter 2

Background and Contributions

In this chapter, we introduce the system models presented in Chapter 1 in more mathematical details, and provide extensive background to the different topics of the thesis. We highlight the contributions of the thesis on each of the topic and introduce corresponding research articles.

The main system models and assumptions are presented in Section 2.1. The impacting impairments in the feeder link and user link are discussed in detail and system parameters including link budgets are provided. The feeder link design problem for Q/V band is discussed in Section 2.2 where the state of the art approaches along with our proposed method are presented. The robust precoding design under phase uncertainty is discussed in Section 2.3 and a review of robust precoding approaches is provided. New optimization techniques for solving signal design problems are introduced in Section 2.4. Finally, contributions which have not been included in the thesis are listed in Section 2.6

2.1 System Model

2.1.1 Satellite Feeder Link: Channel Model

Radio-wave propagation on the feeder links at Q/V band − and in general in millimeter wave frequencies − is impaired by different tropospheric effects [11, 12]:

- **Gaseous absorption due to oxygen and water vapor:** This effect is almost constant over time and its statistics can be calculated with the help of the model in ITU-R Recommendation P.676 [13].
- **Cloud attenuation:** This effect is very slowly varying over time (in minutes or hours) and its statistics can be calculated with the help of the model in ITU-R Recommendation P.840 [14].
- **Rain attenuation:** It varies slowly over time (order of minutes or few seconds) and its statistics can be calculated with the help of the relevant model

in ITU-R Recommendation P.618 [15].

- **Scintillations:** These are very fast variations (order of milliseconds) and their statistics can be calculated with the help of the relevant model in ITU-R Recommendation P.618.

Of the four effects above, the one driving the dynamics of the gateway diversity on the feeder link is rain attenuation, as gases and clouds are too slow and scintillations are too fast to track. Hence, we focus on rain attenuation as the main impairment throughout the thesis. Note that in typical Ka-band applications, feeder link is considered to be ideal since the impairments can be moderate by typical fade mitigation techniques (FMT) such as power control. But the case is not so when we go high on frequency band such as Q/V where rain attenuation can impair up to 20 dB.

The rain attenuation in dB has been traditionally modeled using a log-normal distribution and the same has been validated by many experimental results [16]. In fact, we can verify the log-normal model for rain attenuation as follows. Assume that $V_r(t)$ is time varying amplitude of the received signal voltage normalized to its non-faded level; i.e. $0 \leq V_r(t) \leq 1$ and $A(t)$ is time varying rain power attenuation in dB which defined as,

$$A(t) = \log_{10} \frac{1}{V_r^2(t)} = -20 \log_{10} V_r(t). \tag{2.1}$$

It can be assumed that rain attenuation is result of a sequence of many, say n_r, small attenuations $\{A_i(t)\}_1^{n_r}$ which are independent and identically distributed (i.i.d) random variables. So, we can write the total rain power attenuation as

$$A(t) = A_1(t)A_2(t) \cdots A_{n_r}(t). \tag{2.2}$$

Taking natural logarithm of $A(t)$, we have

$$\ln A(t) = \ln A_1(t) + \ln A_2(t) + \cdots + \ln A_{n_r}(t) = \sum_{i=1}^{n_r} \ln A_i(t). \tag{2.3}$$

Note that $\{\ln A_i(t)\}$ are i.i.d random variables. From central limit theorem, it is known that sum of many i.i.d random variables has a normal distribution. Therefore, $\ln A(t)$ has normal (Probability Density Function) PDF or equivalently $A(t)$ has log-normal PDF. Based on these results, the PDF of the rain attenuation, $A(t)$ (in dB), is modeled as a log-normal variable,

$$p_A(A) = \frac{1}{\sqrt{2\pi}\sigma_L A(t)} \exp\left(-\frac{(\ln A(t) - m_L)^2}{2\sigma_L^2}\right), \tag{2.4}$$

where m_L and σ_L are the long term mean and standard deviation of $\ln A(t)$, respectively. These quantities can be calculated by fitting a log-normal distribution

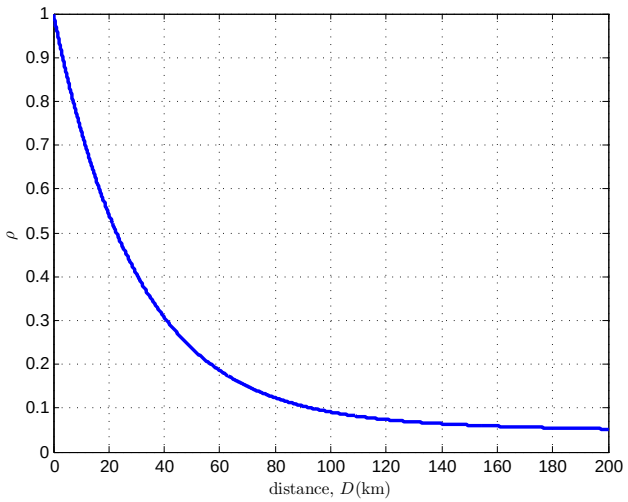

Figure 2.1. correlation between two diversity sites

to the empirical distribution included in ITU-R Recommendation P.618. Note that rain attenuation and channel gain is related as $A(t) = -10 \log_{10} |h(t)|^2$ where $h(t)$ is the channel gain between a gateway and satellite.

Since rain attenuation is a time varying process, in order to design a communication system robust to rain attenuation, it is necessary to model the dynamic behavior of rain. Several time series models to synthesize rain attenuation samples with temporal properties have been proposed [17]. The stochastic model of Maseng−Bakken [18], which was adopted as a new recommendation by the Study Group 3 of the ITU-R in 2009 (ITU-R P.1853) [19], has been the most popular one. This model is based on the fact that the rain attenuation in dB can be modeled as a first order Gauss Markov process of the Ornestein-Uhlenbeck type described by the following stochastic differential equation (SDE) [18], [20],

$$\frac{d\,x(t)}{dt} = -\beta x(t) + \sqrt{2\beta}\, w(t). \tag{2.5}$$

Here, $x(t) = (\ln A(t) - m_L)/\sigma_L$ and β is the parameter that describes the time dependency of the model. The PDF of the process that satisfies (2.5) is called transitional PDF and the process satisfying (2.5) can be described with a transitional PDF [18] having the form,

$$p_A\left(A(n)|A(n-1)\right) = \frac{1}{\sqrt{2\pi}\sigma_{\Delta t} A(n)} \exp\left(-\frac{(\ln A(n) - m_{\Delta t})^2}{2\sigma_{\Delta t}^2}\right), \tag{2.6}$$

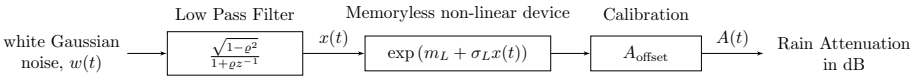

Figure 2.2. Block diagram of the rain attenuation time series synthesizer

where,

$$\sigma_{\Delta t} = \sigma_L \sqrt{1-\varrho^2}, \tag{2.7}$$

$$m_{\Delta t} = m_L\,(1-\varrho) + \varrho \ln A(n-1), \tag{2.8}$$

$$\beta = 2 \times 10^{-4}\,\text{sec}^{-1}, \tag{2.9}$$

$$\varrho = \exp(-\beta \Delta t), \tag{2.10}$$

and Δt is the sampling interval of the rain attenuation time series. Equation (2.6) models the PDF of rain attenuation $A(n)$ at instance $t = n\Delta t$ conditioned on the observation at the previous sampling instance, i.e. $A(n-1)$ at $t_0 = (n-1)\Delta t$.

While the above discussion can model a single GW to satellite link, for multiple gateway scenarios a model for multiple links is required. Towards this, a n-dimensional generalization was recently proposed in [21] to generate the space-time correlated rain attenuation time series of n links. However, inclusion of spatial correlation makes the analysis intractable and hence we assume spatially independent and identically distributed (i.i.d) links. Further the independence assumption is not unrealistic in the context of a multiple gateway diversity configuration. Typically, if a few tens of gateways are dispersed over Europe, the rain attenuation at their sites tends to be uncorrelated as it takes only few tens of kilometers to achieve decorrelation of rain attenuation. This becomes apparent from applying the correlation coefficient proposed by ITU-R Recommendation P.1815 [22] where the correlation drops to 0.1 at a distance of 90 km as given by

$$\rho = 0.94\,\exp(-D/30) + 0.06\,\exp[-(D/500)^2], \tag{2.11}$$

and can be seen in Figure 2.1.

Consider two GWs, $GW1$ and $GW2$, which are separated by a distance of D km. The joint PDF of the correlated rain attenuations on the corresponding two feeder links, takes the form given as,

$$p_{A_1,A_2}(A_1,A_2) = \frac{1}{2\pi A_1 A_2 \sigma_1 \sigma_2 \sqrt{1-\rho^2}} \exp\Big(-\frac{1}{1-\rho^2}\Big[u_1^2 - 2\rho u_1 u_2 + u_2^2\Big]\Big), \tag{2.12}$$

$$u_i = \frac{\ln A_{L_i} - m_{L_i}}{\sigma_{L_i}},\ i = 1,2.$$

Here, m_{L_i} and σ_{L_i} are the mean and standard deviation of $\ln A_i$ respectively.

Tables 2.1 details the propagation parameters for typical Central-European climate that were used for simulation purposes. These parameters are input to the

Table 2.1. propagation parameters

Q/V band Feeder Up-Link	Value
Orbit	GEO, $d_0 = 35786$ (km)
Carrier frequency	50 GHz
Elevation angle	32°
Polarization	Circular

empirical rain attenuation prediction model included in ITU-R Recommendation P.618. The output is long-term rain attenuation statistics, m_L and σ_L. Wherever Δt is used, it means that we consider a dynamic rain attenuation model which is based on ITU-R P.1853 [19]. Figure 2.2 depicts the block diagram of the rain attenuation synthesizer proposed in ITU-R P.1853 [19]. In this method, rain attenuation samples are synthesized from a discrete white Gaussian noise process. In the first step, the white Gaussian noise is low-pass filtered and then transformed from a normal distribution to a log-normal distribution. Finally, it is calibrated to match the specific probability of rain.

Note that when analyzing the end to end performance of the gateway diversity schemes in Chapter 3 and Chapter 4, similar channel model is used for the user link but with different link budget which will be described wherever needed.

2.1.2 Satellite User Link: Multibeam Channel

For the precoding design problems, a typical Ka-band multibeam satellite system with K beams is considered where a full frequency reuse is employed, that is all the beams operate at the same frequency [23]. A single feed per beam scenario is assumed where K antenna feeds at the satellite are used to form the K fixed beams. Further, the i^{th} feed has a constraint on the maximum power. Towards focusing on the precoding design, a single GW is assumed to manage K adjacent beams and that the feeder-link is considered ideal; such assumptions are commonplace in the related literature [23, 24] where appropriate fade mitigation techniques (GW switching, power control,...) are assumed to be employed. Time division multiple access (TDMA) is utilized on the user downlink (link between satellite and user) wherein a single user is served in a beam for every time slot. Further, we assume that users are equipped with single antenna.

Since the beams are not perfectly isolated, each user receives transmissions from all the K feeds [23]. This combined with the use of TDMA results in a user being interfered by $K-1$ co-channel users. Such a system then resembles the traditional multiuser multi-input single-output (MISO) downlink, thereby facilitating further analysis. So, in this scenario it can be assumed that all K feeds are used to transmit to all K users.

In the considered Ka-band scenarios with fixed users, the downlink propagation

Table 2.2. Link Budget and System Parameters

Parameter	Value
Downlink Band	Ka-Band, $f = 20$ (GHz)
Number of beams	$K = 7$
Beam radius	250 (km)
Boltzmann's constant	$\kappa = 1.38 \times 10^{-23}$ (J/m)
Noise bandwidth	$B = 50$ (MHz)
Satellite antennae gain	$G_{s,k} = 38$ (dBi)
Receiver gain to noise temperature	$G_{r,i}/T = 15$ (dB/K)
3dB Angle	$\theta_{3\text{dB}} = 0.4^\circ$
TWTA RF Power @ Saturation	$P_i = 200$ (W)

channel is typically line of sight (LOS) with minimal scattering. The predominant quantities defining such a frequency flat channel are:

- beam gains,
- time varying rain attenuation,
- frequency dependent path loss.

Therefore, the time varying equivalent channel vector between the K satellite transmit antennas and i^{th} user, which includes the satellite processing and propagation effects, can be expressed as,

$$\mathbf{h}_i(t) = \sqrt{r_i(t)\, C_i}\; \mathbf{b}_i^{\frac{1}{2}} \odot e^{\mathrm{j}\boldsymbol{\theta}_i(t)} \tag{2.13}$$

where $r_i(t)$ represents the time varying rain attenuation between the satellite antennas and the i^{th} user. It can be assumed that all sub-channels, channels between each antenna and each user experience identical rain attenuation. As discussed in previous section, the rain attenuation in dB, $10\log_{10}(r_i(t))$, has a log-normal distribution. $\boldsymbol{\theta}_i(t)$ is a vector that represents the phase components of the channel including the phase noise introduced by the local oscillator (LO). We let $\boldsymbol{\theta}_i(t) \triangleq [\theta_{i1}(t), \theta_{i2}(t), \ldots, \theta_{iK}(t)]^T$ where $\theta_{ik}(t)$ denotes the channel phase between i^{th} user and k^{th} satellite antenna. C_i and $\mathbf{b}_i$, respectively represent a constant factor collecting deterministic link budget parameters and the satellite antenna gain for beam i.

As shown in Fig. 2.3, the first tier of 7 beams is considered for performance evaluation in this thesis. The reason for considering 7 beams is that the majority of interference arises from adjacent beams. Also, this number of beams is typically handled by a single GW in practical systems. We can find the corresponding channel vector for each user based on the model described above and the link budget and system parameters given in Table 2.2.

Given the i^{th} user's location within a beam, we define the angle subtended by the chord between i^{th} user and the k^{th} beam center at the satellite as $\varphi_{k,i}$. The

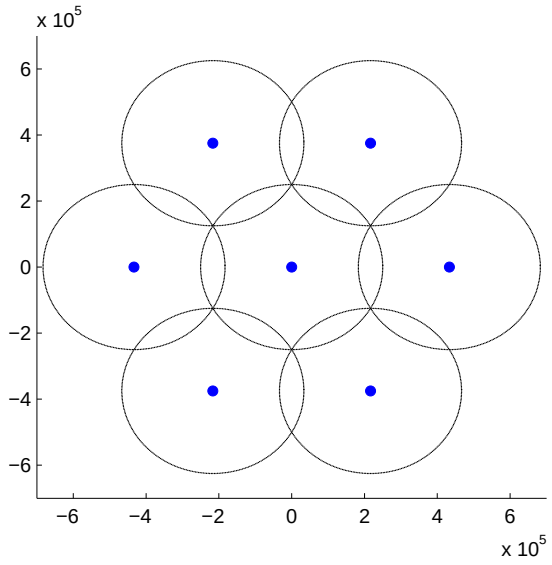

Figure 2.3. Locations of 7 beams(radius is 250km)

3 dB angle for the k^{th} beam is denoted by $\varphi_{k3\text{dB}}$, which is a constant. The beam gain from the k^{th} antenna to i^{th} user in (2.13) is then approximated by [25],

$$\mathbf{b}_i(k) = G_{s,k}\left(\frac{J_1(u_k)}{2u_k} + \frac{36J_3(u_k)}{u_k^3}\right)^2, \tag{2.14}$$

where $G_{s,k}$ is the satellite transmit antenna gain for the k^{th} beam and

$$u_k = 2.07123\left(\frac{\sin(\varphi_{k,i})}{\sin(\varphi_{k3\text{dB}})}\right). \tag{2.15}$$

Here, J_1 and J_3, respectively, are the first and third order Bessel functions of first kind. In (2.13), the coefficient C_i is defined as,

$$C_i = \left(\frac{\nu}{4\pi f d_0}\right)^2 \frac{G_{r,i}}{\kappa BT}, \tag{2.16}$$

to include effects of the free space loss, $(\nu/(4\pi f d_0))^2$, i^{th} UT receive antenna gain, $G_{r,i}$, and noise power at the receiver, κBT. We normalized the noise power by κBT, so it becomes equal to one. In (2.16), ν is the speed of light, f is the operating frequency of the downlink, κ is the Boltzmann's constant, B is the noise bandwidth and T is the receiver noise temperature.

Note that, the amplitude of the channel is also affected by cloud attenuation and the gaseous absorption. The magnitude of these components are negligible compared to rain attenuation in the Ka-band. Further, variations in these components are slower than the rain attenuation. For these reasons, we focus only on rain attenuation on the user link.

2.2 Research Direction: Feeder Link Design

2.2.1 Background

In Chapter 1, it was briefly discussed that to increase the capacity of SatCom systems, one solution is to move the feeder link from the Ka-band to the Q/V band. This move can free up the whole Ka-band spectrum for the user link. However, rain attenuation at Q/V band feeder link imposes considerable strain on the link-budget, which is of the order of $15-20$ dB or more predominantly due to severe rain attenuation [9]. The typical Fade Mitigation Technique (FMT) can not compensate more than a few dBs, thereby motivating the use of multiple GWs for transmit diversity to achieve the required availability in excess of 99.9% on the feeder link.

The traditional $1+1$ diversity scheme [26], where one GW is supported by another redundant GW, can be an acceptable solution for low/ medium throughput systems. On the other hand, for high capacity satellite systems where tens of GWs are required, it is not efficient to use the traditional approach. This warrants an investigation into design of advanced GW diversity techniques.

An interesting GW transmit diversity technique is the $N+P$ diversity scheme, which was studied in [6, 7, 27–29]. In this scheme, there are N active GWs and P redundant or idle GWs. When one of the active GWs is in outage, switching occurs and traffic of the active GW is rerouted to one of the idle GWs. Smart GW diversity is another technique which was firstly presented in [30] for Ka-band, and has been studied and developed for Q/V band in [28] and [6]. The benefit of this scheme is that all N GWs are active and there is no need for redundant GWs but its disadvantage is that the throughput of users served by GWs sharing the traffic from their affected counterpart will be reduced or each GW should have some spare capacity available in order to support other GWs in case of outage; hence GWs need to be over dimensioned in capacity. Also, some level of intelligence is required in the user terminals. In this thesis, we will focus on the $N+P$ scheme and present our contributions for this scenario.

Most of the works that studied $N+P$ scheme take a high-level approach for the system design without a rigorous mathematical analysis. To the best of our knowledge, the only work that has analyzed GW diversity mathematically is [7] where authors derive the availability in a $N+P$ scenario. However, the authors in [7] do not describe if and how such an availability could be achieved. Further, the switching rate, which is an important system parameter, has not been studied in [7]. A high switching rate can lead to severe overheads and instability thereby warranting its further analysis. In [6], the authors used a simple probabilistic

model to study the availability improvement induced by $N + P$ scheme. They assumed the link to be either fully available or unavailable. The absence of a rigorous analysis taking into account the dynamic rain attenuation characteristics and practical requirements on switching motivate a further study of the multiple GW paradigm for Q/V band applications.

2.2.2 Contribution of the Research

The contributions of this thesis in the feeder link design domain are:

- The $1+1$ diversity scheme is studied as a building block of $N+P$ scheme. A correlated rain fading channel is considered and impact of distance between two GWs is investigated and performance of this scheme is evaluated. Apart from the theoretical analysis of the outage performance, practical issues such as end-to-end (transparent) link performance, the effect of erroneous threshold selection are also addressed.

- The thesis undertakes outage analysis incorporating a dynamic model for the rain attenuation samples. For this model, we analytically derive the average outage probability expression for $N+P$ scenario. The analysis highlights the interplay of switching interval and time correlation as well as the impact of these parameters on performance. Effect of other parameters related to the dynamic modeling (like sampling interval) are studied through simulations.

- Towards accommodating for the latencies incurred during the switching process, we resort to the prediction of Signal-to-Noise-Ratio (SNR). In particular, we find the Minimum Mean Square Error (MMSE) predictor of SNR exploiting the dynamic rain fading model and employ the predicted value for switching. The system performance based on the use of predicted values is further studied. The results can also be seen as providing insight into the sensitivity of the switching mechanism to errors in channel estimation.

- An efficient switching scheme suited for the $N + P$ gateway scenario is presented. Building on the results from $1 + 1$, a closed form expressions for the average outage performance and switching probability on the feeder link are derived. These expressions provide critical insights into system sizing. The average outage probability study is also extended to the end-to-end system which can be further used in system performance evaluations.

The corresponding results are presented in Chapter 3 and Chapter 4. The $1+1$ diversity scheme considering temporally independent but spatially correlated rain attenuation samples is the subject of Chapter 3. The general $N+P$ diversity scheme with spatially independent but temporally correlated rain attenuation samples is discussed in Chapter 4.

2.3 Research Direction: Robust Precoding Design

2.3.1 Background

Downlink precoding techniques have been widely studied in the context of multiuser terrestrial communication systems because of their potential to enhance communication efficiency [31]. A key objective of such techniques is to optimize the system utility while meeting certain Quality of Service (QoS) considerations as well as a variety of system constraints [32]. Following terrestrial trends, satellite communications have moved from the traditional TV broadcasting to provide interactive broadband services even to urban customers (see ViaSat's Exede service in the US) [33]. Such a development is triggered by the emergence of multiple spot beam satellites where the frequency reuse provides a trade-off between available bandwidth and co-channel interference (CCI).

While precoding techniques have been studied in terrestrial systems to mitigate CCI, of late, they have also attracted significant research interest among academia and industry for application in multibeam satellite systems with high frequency reuse factors [23, 24, 34]. Furthermore, precoding is now supported in terms of framing and signaling in the latest extension of the DVB-S2 (digital video broadcasting over satellite 2) standard; see in particular [35, Annex E].

We note that the usual requirement to ensure effective precoding is the availability of accurate CSIT [36]. This has been assumed to be the case in [23,24]. Unlike the terrestrial counterparts, GEO satellite communication systems work with long RTD between the gateway and user terminals. In particular, the two-hop propagation delay in the GEO orbit is about 250 milliseconds (ms) [34] compared to the few milliseconds in cellular systems.

To allow the use of precoding in next generation satellite systems, it is essential to investigate the effect of imperfections induced by the RTD. Pursuing this goal, one may recognize that the main time-varying component affecting the *channel amplitude* is the rain attenuation whose variations are typically slow [37,38]. Hence, it can be assumed that the channel amplitude is fixed during the feedback interval. On the other hand, there is a significant variation in the *channel phase* arising from the different time-varying phase components [39] with phase noise of the onboard local oscillator being the dominant one. Thus, the time-varying nature of the channel and a high RTD lead to outdated CSIT, or more specifically an outdated estimate of the channel phase. Therefore, the performance of the system becomes unpredictable when the GW uses outdated CSIT due to phase uncertainty.

Robust precoding design paradigms have been considered in the literature in order to mitigate the sensitivity of the precoding techniques to inaccurate CSIT [40–44]. The literature focuses on the general additive uncertainty model where it is assumed that actual CSIT, $\mathbf{h}$, can be modeled as,

$$\mathbf{h} = \widehat{\mathbf{h}} + \mathbf{e}, \tag{2.17}$$

here, $\widehat{\mathbf{h}}$ is the estimate of CSI and $\mathbf{e}$ represents the uncertainty in the CSI. In

general, there are several different strategies to obtain robustness against channel uncertainty [45]: (a) Probabilistic design using a stochastic uncertainty model and optimizing the performance at a certain outage level [41–44]. (b) Expectation-based design using a stochastic uncertainty model but optimizing the average performance [45]. (c) Worst-case design using a deterministic uncertainty model, where the true value is known to be within a certain interval, and optimizing the performance of the worst-case situation. This is sometimes called max-min robustness [40].

In multibeam broadband satellite systems, phase uncertainty impacts the channel estimation; this manifests itself as a multiplicative uncertainty as,

$$\mathbf{h}_i = \widehat{\mathbf{h}}_i \odot \mathbf{q}_i, \tag{2.18}$$

where $\widehat{\mathbf{h}}_i$ is a known channel vector for i^{th} user and $\mathbf{q}_i$ is a random vector arising out of the phase uncertainty.

The purpose of this investigation is twofold: first it models the phase uncertainty induced by the outdated feedback in a multibeam satellite system and then designs a precoder which is robust against the phase uncertainty.

Consider a multibeam satellite system with K feeds where each user receives transmissions from all K feeds. Let $s_i(t)$ denote the complex signal intended for user i with $\mathbf{E}\{|s_i(t)|^2\} = 1$. Prior to transmission, each $s_i(t), i \in [K]$ is weighted at the GW by the corresponding precoding vector $\mathbf{w}_i \in \mathbb{C}^K$, and the resulting transmitted signal from the GW is given by,

$$\mathbf{x}(t) = \sum_{i=1}^{K} \mathbf{w}_i s_i(t). \tag{2.19}$$

The assumptions on ideal feeder link and lossless processing on-board the satellite allows us to consider $\mathbf{x}(t)$ as the signal transmitted from the satellite. At time instance t_2, the signal $\mathbf{x}(t)$ is acted upon by the channel vectors $\{\mathbf{h}_i\}_i^K$ and the signal received by the i^{th} user is (time index is dropped for ease of comprehension),

$$r_i = \mathbf{h}_i^H \mathbf{w}_i s_i + \mathbf{h}_i^H \sum_{j \neq i} \mathbf{w}_j s_j + n_i, \tag{2.20}$$

where n_i is the circularly symmetric complex Gaussian noise with zero mean and variance N_0. This additive receiver noise is i.i.d. across the users. The received SINR at the i^{th} user then takes the form,

$$\text{SINR}_i = \frac{\text{Tr}(\mathbf{R}_i \mathbf{W}_i)}{\sum_{ji} \text{Tr}(\mathbf{R}_i \mathbf{W}_j) + N_0}, \tag{2.21}$$

where $\mathbf{W}_i \triangleq \mathbf{w}_i \mathbf{w}_i^H$ and,

$$\begin{aligned} \mathbf{R}_i \triangleq \mathbf{h}_i \mathbf{h}_i^H &= \text{diag}(\widehat{\mathbf{h}}_i)\, \mathbf{Q}_i\, \text{diag}(\widehat{\mathbf{h}}_i^H) \\ &= \widehat{\mathbf{h}}_i \widehat{\mathbf{h}}_i^H \odot \mathbf{Q}_i, \end{aligned} \tag{2.22}$$

and $\mathbf{R}_i \in \mathbb{C}^{K\times K}$ is the instantaneous channel correlation matrix. In (2.22), $\widehat{\mathbf{h}}_i$ is the known (estimated) channel vector and $\mathbf{Q}_i = \mathbf{q}_i\mathbf{q}_i^H$ is a random matrix which conveys the phase uncertainty and makes the SINR random. If the perfect CSI (zero phase uncertainty) is assumed in the system, $\mathbf{q}_i$ will become the all one vector, viz. $\mathbf{1}^T$.

Considering different robust approaches and objectives, four different problem formulations are considered:

- **Probabilistic Approach - Power Minimization:** The objective of this formulation is to minimize the total transmit power while enforcing the constraints on the availability for each user considering the per-antenna power constraints.

$$\begin{aligned}\mathcal{B}_1 : \underset{\mathbf{W}}{\text{minimize}} \quad & \sum_{i=1}^{K} \text{Tr}\left(\mathbf{W}_i\right) \\ \underset{\forall i\in[K]}{\text{subject to}} \quad & \Pr\Big\{ \text{SINR}_i \geq \gamma_{\text{th}} \Big\} \geq \alpha_i, \\ & \Big[\sum_{j=1}^{K} \mathbf{W}_j\Big]_{i,i} \leq P_i, \\ & \mathbf{W}_i \succcurlyeq 0,\ \text{rank}(\mathbf{W}_i) = 1,\end{aligned}$$

  where α_i is the required availability for i^{th} user and γ_{th} is a SINR threshold. P_i denotes the per antenna power limit.

- **Probabilistic Approach - Max-Min Fairness:** Let us define availability of each user by $f_i(\mathbf{W}) = \Pr\Big\{ \text{SINR}_i \geq \gamma_{\text{th}} \Big\}$. The objective of this formulation is to maximize the minimum of availability of users. The optimization problem can be written as,

$$\begin{aligned}\mathcal{B}_2 : \underset{\mathbf{W}}{\text{maximize}} \quad & \min\{f_1(\mathbf{W}), \ldots, f_K(\mathbf{W})\} \\ \underset{\forall i\in[K]}{\text{subject to}} \quad & \Big[\sum_{j=1}^{K} \mathbf{W}_j\Big]_{i,i} \leq P_i, \\ & \mathbf{W}_i \succcurlyeq 0,\ \text{rank}(\mathbf{W}_i) = 1.\end{aligned}$$

- **Expectation Based Approach - Power Minimization:** In this formulation, expectation based approach is used which minimizes the total transmit

power subject to satisfying the required average SINR for each user.

$$\begin{aligned} \mathcal{B}_3: \ \underset{\mathbf{W}}{\text{minimize}} \quad & \sum_{i=1}^{K} \text{Tr}(\mathbf{W}_i) \\ \underset{\forall i \in [K]}{\text{subject to}} \quad & \mathbf{E}\{\text{SINR}_i\} \geq \gamma_{\text{th}}, \\ & \left[\sum_{j=1}^{K} \mathbf{W}_j\right]_{i,i} \leq P_i, \\ & \mathbf{W}_i \succcurlyeq 0, \ \text{rank}(\mathbf{W}_i) = 1. \end{aligned}$$

Since evaluating exact value of $\mathbf{E}\{\text{SINR}_i\}$ is difficult, it is approximated by SINR'_i as,

$$\text{SINR}'_i \triangleq \frac{\mathbf{E}\left\{ \text{Tr}(\mathbf{R}_i \mathbf{W}_i)\right\}}{\mathbf{E}\left\{ \sum_{j \neq i} \text{Tr}(\mathbf{R}_i \mathbf{W}_j)\right\} + N_0}. \tag{2.23}$$

- **Expectation Based Approach - Max-Min Fairness:** This formulation intends to maximize the minimum of SINR'_i subject to per-antenna power constraints.

$$\begin{aligned} \mathcal{B}_4: \ \underset{\mathbf{W}}{\text{maximize}} \quad & \min\{\text{SINR}'_1, \ldots, \text{SINR}'_K\} \\ \underset{\forall i \in [K]}{\text{subject to}} \quad & \left[\sum_{j=1}^{K} \mathbf{W}_j\right]_{i,i} \leq P_i, \\ & \mathbf{W}_i \succcurlyeq 0, \ \text{rank}(\mathbf{W}_i) = 1. \end{aligned}$$

2.3.2 Contribution of the Investigation

The contributions of this investigation in robust precoding design area are:

- The thesis introduces and investigates different time-varying phase components which describe the satellite communication channel. It is argued that phase noise of the on-board LO has a predominant impact on these variations and we employ an appropriate model to study its impact. While the literature focuses on the additive uncertainty model for robust designs [32, 40–45], the current study employs a multiplicative model for the phase induced channel uncertainty. The use of such an uncertainty model, and the ensuing analysis are novel.

- A framework for robust precoding design is developed intended for stochastic phase uncertainty. The multiplicative nature of the phase uncertainty model

makes the robust design difficult. However, using some approximations, we transform the robust design problems to tractable optimization problems. These transformations and the subsequent analysis are novel and not straightforward.

- Depending on the required QoS goals, an appropriate design approach to guarantee the requirements is used. An important QoS measure is the user availability which is defined as (1− outage probability× 100%). Another important QoS measure is the average SINR. Therefore, we focus on these two measures in the robust design formulations. The robustness is imparted to the design by modeling the phase uncertainty as a random process and ensuring that the QoS measures are maintained at desired levels.

  Since a stochastic model is used to represent the phase uncertainty, the (a) probabilistic approach and (b) expectation-based approach are suitable for the robust precoding design.

Detailed results on robust precoding design are presented in Chapter 5.

2.4 Research Direction: Optimization Techniques

2.4.1 Background

Optimization techniques are the key tool for solving many signal processing problems including the precoder design problem. In this thesis, we are interested in two NP-hard optimization problems that have many applications in signal processing domain: Nonconvex quadratically constrained quadratic program (QCQP) and Max-Min fractional quadratic programming.

Nonconvex QCQP can be formulated as,

$$\boxed{\begin{aligned} \mathcal{P}_1 : \min_{\mathbf{w}} . \quad & \mathbf{w}^H \mathbf{A}_0 \mathbf{w} \\ \text{s. t.} \quad & \mathbf{w}^H \mathbf{A}_i \mathbf{w} \leq c_i, \quad \forall i \in [M], \end{aligned}} \tag{2.24}$$

where $\mathbf{A}_0$ and $\mathbf{A}_i$ are Hermitian matrices for all $i \in [M]$ and $\mathbf{w} \in \mathbb{C}^N$ and $c_i \in \mathbb{R}$. In this thesis, we are interested in *a subclass of nonconvex* QCQP problems with *convex* objective and *nonconvex* constraints, $\mathbf{A}_0$ is a positive definite (PD) matrix and $\mathbf{A}_i$ are Hermitian matrices with at least one negative eigenvalues [46]. This class of nonconvex QCQP problems captures many problems that are of interest to the signal processing and communications community such as beamforming design [47–49], radar optimal code design [50–53], multiple-input multiple-output (MIMO) and multiuser estimation and detection [54], as well as phase retrieval [55, 56]. The application is also extended to other domains such as portfolio risk management in financial engineering [57]. Nonconvex QCQP is known to be an NP-hard problem, i.e. at least as hard NP-complete problems which are particularly deemed by optimization community to be difficult [58].

Due to its wide area of application, the nonconvex QCQP problem has been studied extensively in the optimization and signal processing literature. The NP-hardness of the problem has motivated the search for various efficient approaches to solve $\mathcal{P}$ including those based on the *semidefinite relaxation* (SDR) [54, 59], the *reformulation linearization technique* (RLT) [60, 61], and the *successive convex approximation* (SCA) [62–64]. Recently a variant of SCA known as *feasible point pursuit-successive convex approximation (FPP-SCA)* has also been proposed in [65]. To the best of our knowledge, SDR is yet the most prominent and widely–used technique employed for tackling nonconvex QCQP.

Another NP-hard problem [48, 49] of interest is Max-Min fractional quadratic programming which can be written as following optimization problems,

$$\boxed{\begin{aligned} \mathcal{P}_2 : \max_{\mathbf{w}} . \quad & \min_{i\in[K]} \left\{ \frac{\mathbf{w}^H \mathbf{A}_i \mathbf{w}}{\mathbf{w}^H \mathbf{B}_i \mathbf{w}} \right\} \\ \text{s. t.} \quad & \mathbf{w} \in \Omega_1 \end{aligned}} \tag{2.25}$$

where $\mathbf{w} \in \mathbb{C}^N$, $\mathbf{A}_i \in \mathbb{C}^{N\times N}$ and $\mathbf{B}_i \in \mathbb{C}^{N\times N}$ are PSD matrices and Ω_1 is the feasible set of the problem which is determined by the constraint on the signal $\mathbf{w}$.

Problem $\mathcal{P}_2$ has been studied extensively in the literature, particularly when Ω denotes a total-power or per-antenna power constraint (see e.g., [48, 66–72] and the references therein). For precoder design application different approaches have been proposed to solve the design problem including those based on uplink-downlink duality [66], the Lagrangian duality [68] and quasi-convex formulations [72]. The semidefnite relaxation (SDR) is, however, the most prominent approach to the type of problems related to $\mathcal{P}_2$. Defining $\mathbf{W} = \mathbf{w}\mathbf{w}^H$ and $\mathbf{W} \in \Omega_2$, $\mathcal{P}_2$ can be equivalently reformulated as,

$$\begin{aligned} \mathcal{R}_1 : \max_{\mathbf{W}} . \quad & \min_{i\in[K]} \left\{ \frac{\mathrm{Tr}\left(\mathbf{A}_i \mathbf{W}\right)}{\mathrm{Tr}\left(\mathbf{B}_i \mathbf{W}\right)} \right\} \\ \text{s. t.} \quad & \mathbf{W} \in \Omega_2 \, , \mathbf{W} \succeq 0 \, , \mathrm{rank}(\mathbf{W}) = 1. \end{aligned} \tag{2.26}$$

Relaxing the rank-one constraint and noting that objective function is quasi-concave, we can write the corresponding feasibility problem as follows,

$$\begin{aligned} \mathcal{R}_2 : \text{find} \quad & \mathbf{W} \\ \text{s. t.} \quad & \frac{\mathrm{Tr}\left(\mathbf{A}_i \mathbf{W}\right)}{\mathrm{Tr}\left(\mathbf{B}_i \mathbf{W}\right)} \geq \upsilon \, , \qquad \forall i \in [K], \\ & \mathbf{W} \in \Omega_2 \, , \mathbf{W} \succeq 0 \, . \end{aligned} \tag{2.27}$$

An optimal value of υ can be found using bisection method. We stop the bisection iteration whenever increment in υ become bounded by 10^{-5}. Note that $\mathcal{R}_2$ along with bisection procedure is equivalent to $\mathcal{R}_1$. For any given υ, $\mathcal{R}_2$ is a convex optimization problem and can be solved using an standard solver such as CVX [73].

Let us denote the solution of $\mathcal{R}_2$ by $\mathbf{W}^\star$. Due to the rank relaxation in $\mathcal{R}_2$, $\mathbf{W}^\star$ will not, in general, be rank-one. In this case, the Gaussian randomization method [54, 74–76] can be used to extract the rank-one solutions. However, the SDR technique doesn't always result in rank-one solutions and is computationally costly method. In order to alleviate these issues, new optimization methods are investigated in this thesis.

2.4.2 Contributions of the Investigation

This thesis proposes novel optimization frameworks that can efficiently tackle $\mathcal{P}_1$ and $\mathcal{P}_2$. Using a penalized version of the original design problems, we derive a simplified reformulations of the problem in terms of the signal (to be designed). Each iteration of the proposed design frameworks consist of a combination of power method-like iterations (for problem $\mathcal{P}_1$ power method iterations) and some readily solvable subproblems. As a result, the proposed optimization framework enjoys a low computational cost. More details on the frameworks for $\mathcal{P}_1$ and $\mathcal{P}_2$ are provided in Chapters 6 and Chapter 7, respectively.

2.5 Publications

Most of the research results have already been published or have been submitted for publication as listed in the following. Unless otherwise stated, in all publications the main idea, the problem formulations, the analysis and the numerical evaluation are contributions of the author of this thesis.

2.5.1 Journals

- [37] Ahmad Gharanjik, Bhavani Shankar Mysore Rama Rao, Pantelis-Daniel. Arapoglou, and Björn Ottersten. Gateway switching in Q/V band satellite feeder links. *IEEE Communications Letters*, 17(7):1384–1387, 2013.

- [38] Ahmad Gharanjik, Bhavani Shankar Mysore Rama Rao, Pantelis-Daniel Arapoglou, and Björn. Ottersten. Multiple gateway transmit diversity in Q/V band feeder links. *IEEE Transactions on Communications*, 63(3):916–926, March 2015.

- [77] Ahmad Gharanjik, Bhavani Shankar Mysore Rama Rao, Pantelis-Daniel Arapoglou, Mats Bengtsson, and Björn Ottersten. Phase uncertainty in multi-beam satellite channels: Modeling and robust precoding design. *to be submitted to IEEE Transactions on Wireless Communications*, 2016.

- Ahmad Gharanjik, Bhavani Shankar Mysore Rama Rao, Mojtaba Soltanalian, and Björn Ottersten, An Iterative Approach to Nonconvex QCQP with Applications in Signal Processing, to be submitted to *IEEE Transaction on Signal Processing, 2016.*

- Mojtaba Soltanalian, Ahmad Gharanjik, Bhavani Shankar Mysore Rama Rao, and Björn Ottersten, Grab-n-Pull: A Max-Min Fractional Quadratic Programming Framework with Applications in Signal Processing, to be submitted to *IEEE Transaction on Signal Processing, 2016.*

  In this work and in the conference version of it (ICASSP 2016 paper), the author of this thesis initiated the research work and contributed to the problem formulation, the performance comparison with SDR technique, implementing the algorithm, and numerical evaluations.

2.5.2 Conferences

- [78] Ahmad Gharanjik, Bhavani Shankar Mysore Rama Rao, Pantelis-Daniel Arapoglou, and Björn Ottersten. Large scale transmit diversity in Q/V band feeder link with multiple gateways. In *2013 IEEE 24th International Symposium on Personal Indoor and Mobile Radio Communications (PIMRC)*, pages 766–770, September 2013.
- [79] Ahmad Gharanjik, Bhavani Shankar Mysore Rama Rao, Pantelis-Daniel Arapoglou, Mats Bengtsson, and Björn Ottersten. Robust precoding design for multibeam downlink satellite channel with phase uncertainty. In *IEEE International Conference on Acoustics, Speech and Signal Processing, ICASSP*, pages 3083–3087, April, 2015.
- [80] Ahmad Gharanjik, Bhavani Shankar Mysore Rama Rao, Pantelis-Daniel Arapoglou, Mats Bengtsson, and Björn Ottersten. Precoding design and user selection for multibeam satellite channels. In *IEEE International Workshop on Signal Processing Advances in Wireless Communications (SPAWC)*, pages 420–424, June, 2015.
- Ahmad Gharanjik, Bhavani Shankar Mysore Rama Rao, Mojtaba Soltanalian, and Björn Ottersten, An Iterative Approach to Nonconvex QCQP with Applications in Signal Processing, submitted to *IEEE SAM 2016.*
- [81] Mojtaba Soltanalian, Ahmad Gharanjik, Bhavani Shankar Mysore Rama Rao, and Björn Ottersten. Grab-n-Pull: An optimization framework for fairness-achieving networks. *accepted to IEEE International Conference on Acoustics, Speech and Signal Processing (ICASSP)*, 2016.

2.6 Contribution outside of the Thesis

Some of the results are not included to keep the coherency of the thesis :

- [82] Ahmad Gharanjik, Konstantinos Liolis, Bhavani Shankar, and Björn Ottersten. Spatial multiplexing in optical feeder links for high throughput satellites. In *Signal and Information Processing (GlobalSIP), 2014 IEEE Global Conference on*, pages 1112–1116. IEEE, 2014.

- Phase Retrieval via Upper-Bound Tightening: to be submitted to *IEEE Transaction on Signal Processing.*

Chapter 3

Gateway Switching in Q/V band Feeder Links (1 + 1)

3.1 Introduction

Moving feeder link to Q/V band provides for higher bandwidth that can accommodate a broadband SatCom system with a high number of beams (>200) and aggressive frequency reuse. Further, it can free-up the whole Ka-band spectrum for the user link. However, heavy fading caused by rain attenuation in Q/V band necessitates the use of gateway diversity techniques to ensure the required availability [9].

Although GW site diversity reception is a familiar and mature technique with rich literature [83], very little attention has been given in SatCom systems on realizing a transmit gateway diversity scheme in the forward link. Equal gain combining (EGC) and maximum ratio combining (MRC) have been studied in [9] towards achieving transmit diversity. However, these techniques require accurate channel phase information while both the GWs need to be active, which demands challenging synchronization processes. Switch and Stay Combining (SSC) and Selection Combining (SC) which do not require phase information and employ a single active transmitter at any instance have been proposed in terrestrial communications [84–86].

In this chapter, building on the SSC, we propose and analyze a novel diversity scheme for Q/V band feeder links suffering from correlated rain fading. This Modified SSC (MSSC) scheme exploits beacons for attenuation measurement and activates only one GW in a manner that lowers the GW switching rate without performance degradation. This makes it an ideal candidate for SatCom and avoids frequent GW switching that causes system overhead. Further, MSSC does not warrant any modification of the user terminal and naturally lends itself to the smart GW concepts that have been proposed recently for multi-GW configurations [7]. Apart from the feeder link, also the benefit of this diversity scheme over the end-

to-end (feeder and user) link is analyzed.

3.2 System Model

Two gateways, GW_1 and GW_2, separated on ground by a distance of D km communicate with a GEO satellite over a feeder link operating in the Q/V band with only one of them being active in each transmission time slot. Assume that the active GW transmits the signal $s(t)$ having an average power $E_1 = \mathbf{E}\{|s(t)|^2\}$. The decision on switching is taken at discrete time instants $t = nT$, where n is an integer and the T is the interval between switching instants. The channel between GW_i and the satellite at $t = nT$ is denoted by,

$$h_i[n] = |h_i[n]|e^{j\alpha_i}, \quad i = 1, 2, \tag{3.1}$$

where α_i is the phase component. The channel amplitude, $|h_i[n]|$, can be estimated using a beacon signal received from the satellite. The clear sky signal-to-noise ratio (SNR) for the feeder uplink is then defined as $\gamma_{CS_{UL}} = E_1/N_1$ where N_1 is the noise variance at the satellite front-end. The actual SNR for the link between GW_i and the satellite at $t = nT$ can be obtained by,

$$\gamma_{i,n} = \frac{E_1|h_i[n]|^2}{N_1} = |h_i[n]|^2\gamma_{CS_{UL}}, \quad i = 1, 2. \tag{3.2}$$

As discussed in Chapter 2, in the Q/V band the main impairment is the rain attenuation which is typically modeled by the lognormal distribution [15]. The other clear-sky effects are assumed to be compensated by a fixed fade margin or an uplink power control scheme. The rain attenuation and the channel gains are related as,

$$A_{i,n} = -10\log_{10}|h_i[n]|^2, \quad i = 1, 2. \tag{3.3}$$

The model for the rain attenuation is detailed in Chapter 2 and the joint PDF of the correlated rain attenuations on the two feeder links is given in (2.12).

According to the MSSC scheme, gateway switching from active GW_i to the alternative GW_j occurs if $\gamma_{i,n} < \theta$ and $\gamma_{j,n} > \theta, i \neq j$ where θ is the switching threshold. In contrast, conventional SSC results in switching when $\gamma_{i,n} < \theta$ regardless of $\gamma_{j,n}$, while in SC, switching always ensures that the active GW has the higher SNR (irrespective of its relation to θ). The proposed MSSC strategy can be implemented without any feedback, with each GW estimating its SNR by employing a beacon signal from the satellite (no phase information needed). In case of switching, the traffic is rerouted to the redundant GW via a terrestrial fiber interconnection.

Note that in this chapter we consider temporally independent and identically distributed rain attenuation samples, that is $A_{i,n}$ and $A_{i,n-1}$ are independent and identically distributed. This assumption results in a performance bound for the 1+1 diversity scheme. In Chapter 4, a dynamic model for rain attenuation samples will be considered and its impact on the performance will be highlighted.

3.3 Performance Analysis

3.3.1 Outage Analysis of the Feeder Link

We now study the outage performance of MSSC. Denoting the SNR of the active feeder link by γ_n, it follows that,

$$\gamma_n = \gamma_{1,n} \iff \begin{cases} \gamma_{n-1} = \gamma_{1,n-1}\ ,\ \gamma_{1,n} \geq \theta \\ \gamma_{n-1} = \gamma_{1,n-1}\ ,\ \gamma_{1,n} < \theta\ ,\ \gamma_{2,n} < \theta \\ \gamma_{n-1} = \gamma_{2,n-1}\ ,\ \gamma_{2,n} < \theta\ ,\ \gamma_{1,n} \geq \theta \end{cases} \tag{3.4}$$

for the MSSC. Further, $\gamma_n = \gamma_{2,n}$ can be obtained similarly. The cumulative distribution function (CDF) of γ_n follows as,

$$F_{\gamma_n}(u) = \Pr\{\gamma_n = \gamma_{1,n}, \gamma_{1,n} \leq u\} + \Pr\{\gamma_n = \gamma_{2,n}\,, \gamma_{2,n} \leq u\}. \tag{3.5}$$

Using (2) and the fact that $\gamma_{1,n}$ and $\gamma_{2,n}$ are identical, (3) can be further simplified by following an approach similar to Appendix of [87] as,

$$\begin{aligned} F_{\gamma_n}(u) \quad = \quad & \Pr\{\theta \leq \gamma_{1,n} \leq u\} + \Pr\{\theta \leq \gamma_{1,n} \leq u\,, \gamma_{2,n} \leq \theta\} \\ & + \Pr\{\gamma_{1,n} \leq \theta\ ,\ \gamma_{1,n} \leq u\ ,\ \gamma_{2,n} \leq \theta\}\ . \end{aligned} \tag{3.6}$$

A system outage occurs if $\gamma_n < \gamma_{th}$, where the outage threshold γ_{th} depends on the operational set-up. The outage probability, $P_{out}(\gamma_{th}) = F_{\gamma_n}(\gamma_{th})$, can be obtained from (3.6) as,

$$\begin{aligned} P_{out}(\gamma_{th}) \quad = \quad & \Pr\{\theta \leq \gamma_{1,n} \leq \gamma_{th}\} + \Pr\{\theta \leq \gamma_{1,n} \leq \gamma_{th}, \gamma_{2,n} \leq \theta\} \\ & + \Pr\{\gamma_{1,n} \leq \theta, \gamma_{1,n} \leq \gamma_{th}, \gamma_{2,n} \leq \theta\}\ . \end{aligned} \tag{3.7}$$

Setting a predetermined θ is an important system design issue and significantly affects P_{out} of the system. For a given γ_{th}, the optimal θ minimizing P_{out} is given by $\theta = \gamma_{th}$ [88, Ch.9.8.1]. In this case, (3.7) reduces to the outage of the SC scheme,

$$P_{out}(\gamma_{th}) = \Pr\{\gamma_{1,n} \leq \gamma_{th}\ ,\ \gamma_{2,n} \leq \gamma_{th}\}\ . \tag{3.8}$$

Using the expression of $\gamma_{i,n}$ from Section 3.2 and (3.8), we have,

$$\begin{aligned} P_{out}(\gamma_{th}) &= \Pr\{10^{-\frac{A_1}{10}}\gamma_{CS_{UL}} \leq \gamma_{th}\ ,\ 10^{-\frac{A_2}{10}}\gamma_{CS_{UL}} \leq \gamma_{th}\} \\ &= \Pr\{A_1 > \Gamma_{CS} - \Gamma_{th}\ ,\ A_2 > \Gamma_{CS} - \Gamma_{th}\}, \end{aligned} \tag{3.9}$$

where $\Gamma_{CS} = 10\log\gamma_{CS_{UL}}$ and $\Gamma_{th} = 10\log\gamma_{th}$. The expression for the outage probability can be derived simply as

$$P_{out}(\gamma_{th}) = \int_{\Gamma_{CS}-\Gamma_{th}}^{\infty}\int_{\Gamma_{CS}-\Gamma_{th}}^{\infty} p_{A_1,A_2}(A_1, A_2)\ dA_1 dA_2\,, \tag{3.10}$$

where $p_{A_1,A_2}(A_1, A_2)$ is defined in (2.12). Using [89, Eq. 233.1.8] and after some manipulation, P_{out} of the MSSC scheme in the feeder uplink can be obtained as,

$$P_{out}^{UL}(\gamma_{th}) = \frac{1}{2\sqrt{2\pi}} \int_{\beta_2}^{\infty} \left(\exp\left(-x^2/2\right) \operatorname{erfc}\left(\frac{\beta_1 - \rho x}{\sqrt{2\left(1-\rho^2\right)}} \right) \right) dx, \tag{3.11}$$

where

$$\beta_i = \frac{\ln\left(\Gamma_{CS} - \Gamma_{th}\right) - m_i}{\sigma_i},\ i = 1, 2. \tag{3.12}$$

Integral in (3.11) can be evaluated numerically.

3.3.2 End-to-End Outage Analysis

Vast majority of SatCom systems are transparent − the satellite repeater only down-converts the signal received on the feeder link and amplifies it before re-transmitting onto the user link. Given that the user link will operate in a band (like Ka) lower than the feeder link, it is interesting to investigate the improvement of the end-to-end link due to MSSC. Although a similar geometry has been modeled in terrestrial dual hop radio relay system [90], to the best of our knowledge this is first time the satellite link is analyzed for this diversity technique.

Towards this, the satellite repeater gain, denoted by G_s, ensures that the output power level is fixed to E_2. Therefore, the amplifying factor can be obtained by

$$G_s^2 = \frac{E_2}{|h[n]|^2 E_1 + N_1}, \tag{3.13}$$

where $h[n]$ is the corresponding channel of the active GW. The signal received by the user terminal from the satellite is

$$r'[n] = g[n] G_s \left(h[n]s[n] + n_1[n]\right) + n_2[n], \tag{3.14}$$

where $g[n]$ is the channel between the satellite and the user, while $n_2[n]$ is the receiver additive white Gaussian noise (AWGN) of variance N_2. The equivalent SNR at the receiver can be written as,

$$\gamma_{eq} = \frac{\gamma_g \gamma_h}{(\gamma_g + \gamma_h + 1)}\ , \tag{3.15}$$

where $\gamma_h = \gamma_n = E_1|h|^2/N_1$ and $\gamma_g = E_2|g|^2/N_2$ with the time index n dropped for simplicity. The clear sky SNR for downlink is defined as $\gamma_{CS_{DL}} = E_2/N_2$. Finally,

Table 3.1. Markov Chain Modeling

State	γ_n	γ_{n-1}	$\gamma_{1,n}$	$\gamma_{2,n}$	Description
1	$\gamma_{1,n}$	$\gamma_{1,n-1}$	$\geq \theta$	$\cdot$	GW_1 continues to be active
2	$\gamma_{1,n}$	$\gamma_{1,n-1}$	$< \theta$	$\leq \theta$	2 GWs in outage, no switching
3	$\gamma_{2,n}$	$\gamma_{1,n-1}$	$< \theta$	$> \theta$	GW_1 in outage, GW_2 better
4	$\gamma_{2,n}$	$\gamma_{2,n-1}$	$\cdot$	$\geq \theta$	GW_2 continues to be active
5	$\gamma_{2,n}$	$\gamma_{2,n-1}$	$\leq \theta$	$< \theta$	2 GWs in outage, no switching
6	$\gamma_{1,n}$	$\gamma_{2,n-1}$	$> \theta$	$< \theta$	GW_2 in outage, GW_1 better

the end-to-end outage probability, $P_{out}^{e2e}(\gamma_{th})$, can be calculated as

$$\begin{aligned} P_{out}^{e2e}(\gamma_{th}) &= \Pr\{\gamma_{eq} \leq \gamma_{th}\} = \int_0^{\infty} \Pr\left(\frac{\gamma_g \gamma_h}{\gamma_g + \gamma_h + 1} \leq \gamma_{th} | \gamma_g\right) f_{\gamma_g}(\gamma_g)\, d\gamma_g \\ &= \int_0^{\gamma_{th}} \Pr(\gamma_h > z|\gamma_g)\, f_{\gamma_g}(\gamma_g)\, d\gamma_g + \int_{\gamma_{th}}^{\infty} \Pr(\gamma_h \leq z|\gamma_g)\, f_{\gamma_g}(\gamma_g)\, d\gamma_g \\ &= P_{out}^{UL}(\gamma_{th}) + \int_{\gamma_{th}}^{\infty} P_{out}^{UL}(z) f_{\gamma_g}(\gamma_g) d\gamma_g > P_{out}^{DL}(1 - P_{out}^{UL}) + P_{out}^{UL} \end{aligned} \quad (3.16)$$

where

$$z = \frac{\gamma_{th}(\gamma_g + 1)}{\gamma_g - \gamma_{th}}, \quad (3.17)$$

$$P_{out}^{DL} = \Pr\{\gamma_g < \gamma_{th}\}, \quad (3.18)$$

and $f_{\gamma_g}(\gamma_g)$ is the PDF of the γ_g. This equation shows the impact of feeder link improvement on the overall performance of the system. It is worth mentioning that the lower bound (last inequality of (3.16)) is the outage performance when the satellite is operating in the regenerative mode.

3.3.3 Switching Rate

When a GW switching strategy is used in the transmission side, the switching rate becomes an important issue. Clearly, reduced switching rate for a given performance is desirable from a system implementation and operation view while a high switching rate can make the system unstable. Towards this, we analyze the switching rate of MSSC by employing a Markov chain model [84]. We define six states as in Table 3.1.

Clearly, whenever the active GW is in state 3 or 6, switching occurs. So, the probability of switching is given by $\pi_3 + \pi_6$ where π_i is the probability that GW is in state i. Based on the MSSC switching strategy, the transitional probability

matrix $\mathbf{P}$ of the Markov chain can be obtained as,

$$\mathbf{P} = \begin{bmatrix} 1-p & p_{12} & p-p_{12} & 0 & 0 & 0 \\ 1-p & p_{12} & p-p_{12} & 0 & 0 & 0 \\ 0 & 0 & 0 & 1-p & p_{12} & p-p_{12} \\ 0 & 0 & 0 & 1-p & p_{12} & p-p_{12} \\ 0 & 0 & 0 & 1-p & p_{12} & p-p_{12} \\ 1-p & p_{12} & p-p_{12} & 0 & 0 & 0 \end{bmatrix}. \tag{3.19}$$

Here,

$$p_{12} = \Pr\{\gamma_{1,n} \leq \theta, \gamma_{2,n} \leq \theta\}, \tag{3.20}$$

$$p = \Pr\{\gamma_{1,n} \leq \theta\} = \Pr\{\gamma_{2,n} \leq \theta\}. \tag{3.21}$$

By using the facts that $\overrightarrow{\pi} = \overrightarrow{\pi}\mathbf{P}$ and $\sum_{i=1}^{6} \pi_i = 1$, where $\overrightarrow{\pi} = [\pi_1, \pi_2, ..., \pi_6]$, the MSSC switching probability can be calculated as

$$P_{sw} = \pi_3 + \pi_6 = p - p_{12}. \tag{3.22}$$

Finally, the switching rate is calculated by $R_{sw} = (p - p_{12})/T$. The switching probability of the conventional SSC was obtained in [84] as $P_{sw} = p$ and for SC easily can be found as 0.5. In Section 3.3.1 and in [86], respectively, it was shown that by selection of a proper switching threshold, both, MSSC and SSC will have the same outage performance as SC. However, (3.22) shows that MSSC has the advantage of a lower switching rate compared to both SC and SSC.

3.4 Numerical Results and Discussion

Table 3.2 details the propagation parameters that were used as input to the empirical rain attenuation prediction model included in ITU-R Recommendation P.618 [15]. Table 3.3 presents the forward-link budget that has been used in the numerical results.

Figure 3.1 compares the analytically obtained outage performance of the proposed scheme with that of MRC [9] on the feeder uplink for GW separation of 20Km. Also, the Monte-Carlo simulation of the MSSC scheme is plotted to corroborate the analytical results. While these schemes have relatively similar outage performance, MRC is not a realistic option for realizing GW diversity since it assumes that two GWs transmit to the satellite in a synchronized fashion. However, MSSC is not beset with these issues.

Figure 3.2 illustrates the outage probability of the MSSC for different non-optimal values of the switching threshold (θ). It is clear that the system has the best performance when the switching threshold is set to the outage threshold ($\theta = \gamma_{th}$). It is also worth mentioning that, in the event of an erroneous threshold selection, over-estimation of θ yields better outage.

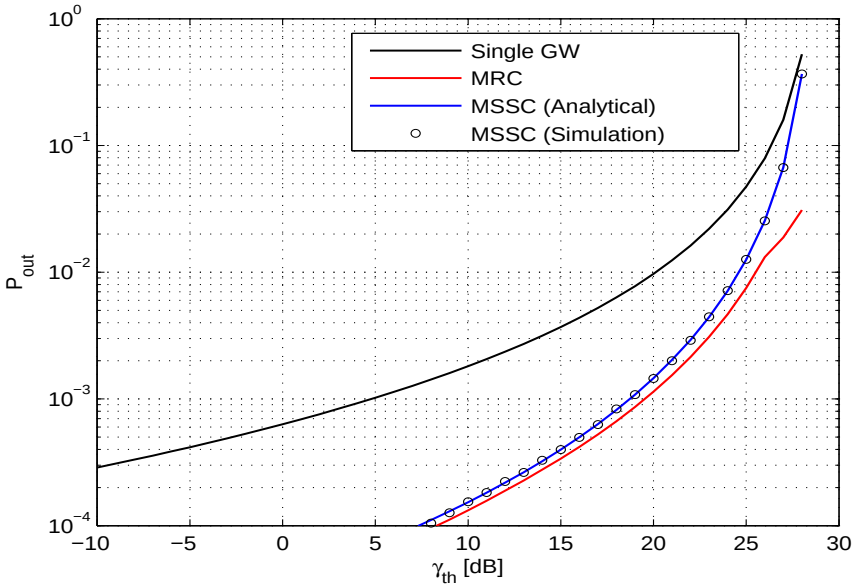

Figure 3.1. Outage of GW diversity strategies on the feeder uplink (D=20 Km)

Table 3.2. propagation assumptions

V Band Up-Link	**Value**
GWs Location	Luxembourg (49.36°N; 6.09°E)
Carrier frequency	50GHz
Elevation angle	32°
Polarization	Circular
Ka Band Down-Link	
Receiver Location	Amsterdam (52.3°N; 4.8°E)
Carrier frequency	20GHz
Elevation angle	35°
Polarization	Circular

Figure 3.3 shows the influence of spatial correlation on the feeder uplink performance. It can be inferred from the plots that for $D > 100$Km, the GWs can be assumed to be spatially uncorrelated.

Figure 3.4 plots the end to end outage performance of the system. For a typical

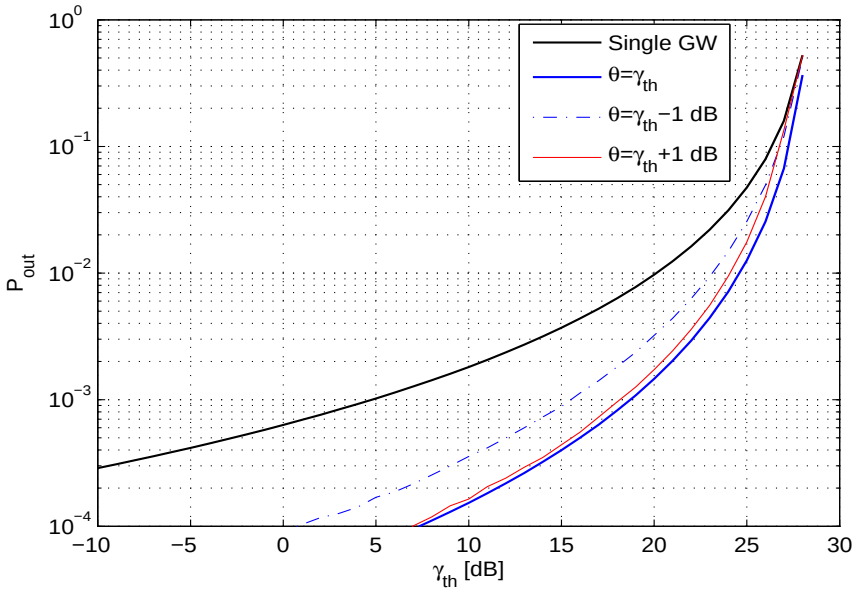

Figure 3.2. Outage results with non-optimal switching threshold θ (D=20 Km)

Table 3.3. Forward (up/down) link budget

Description	Value
EIRP_{GW} including back-off	76.5 dBW
UL free space loss	218.3 dB
$(\text{G/T})_{Sat}$	31.45 dB
$\gamma_{CS_{UL}}$	28.3 dB
EIRP_{sat} including back-off	72.5 dBW
DL free space loss	210.5 dB
$(\text{G/T})_{UT}$	20.3 dB
$\gamma_{CS_{DL}}$	21.3 dB

availability of 99.9% (outage 10^{-3}) diversity gains for MSSC is 7.8 dB and for MRC is about 9.3 dB compared to single GW when $D = 20$ Km. For $D = 100$ Km, these values increase to 9 dB and 10.7 dB respectively.

Figure 3.5 depicts the switching probability of the traditional SSC and the proposed MSSC. It can be seen that the switching probability of the GWs is slightly improved but at the expense of requiring both GW's SNR unlike the SSC which

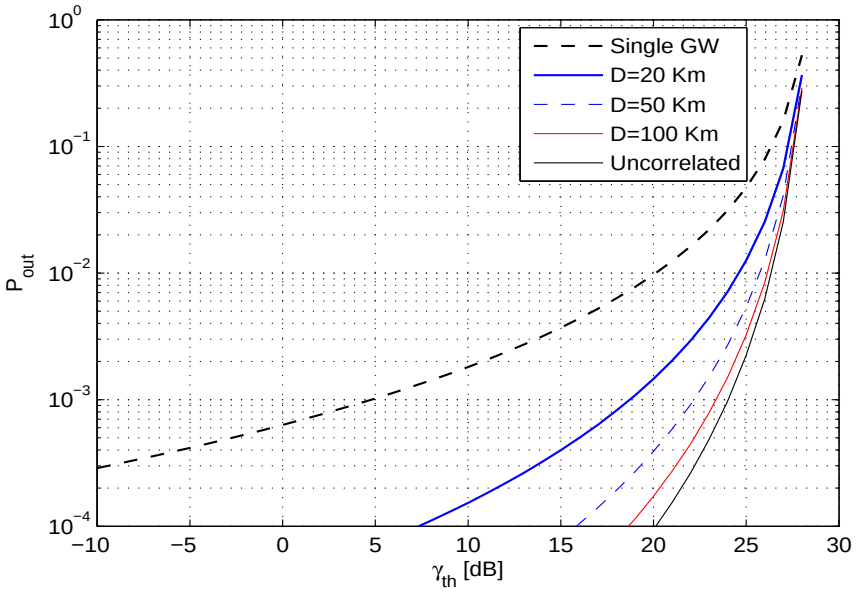

Figure 3.3. Influence of the spatial correlation on the outage performance

requires only SNR of the active GW. However, it is not the case for SatCom as the SNR can be easily obtained employing beacon signals.

3.5 Summary

In this chapter, a modified switch and stay scheme for Q/V band feeder link has been studied. Although being one of the few realistic GW diversity strategies − since it involves a single GW transmitting at each instant − it has not been hitherto studied for a correlated rain fading channel. Apart from the theoretical analysis of the outage performance, we also address practical issues such as performance of the end-to-end (transparent) link, the effect of erroneous threshold selection, as well as the switching rate between the GWs. Proposed scheme achieves performance comparable to the optimal one with a lower complexity.

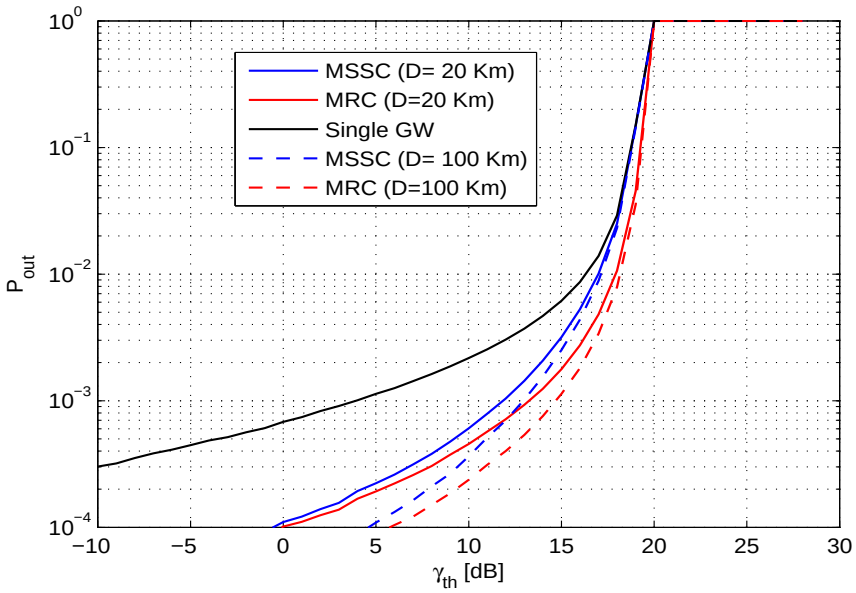

Figure 3.4. End-to-End outage performance of the satellite forward link

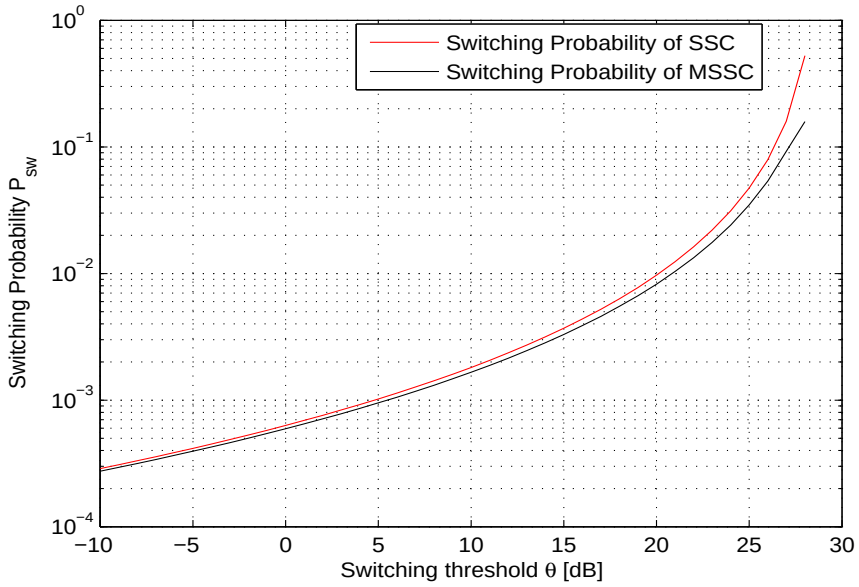

Figure 3.5. Switching Probability of different strategies (D=20 K)

Chapter 4

Multiple Gateway Diversity in Q/V Band ($N + P$)

4.1 Introduction

In this chapter, the $N + P$ GW diversity scheme is presented where there are N active GWs and P redundant GWs. N active GWs are used for multiplexing purpose and P redundant GWs are employed for diversity purpose. Unlike Chapter 3, the dynamic rain model is used for analysis of the GW diversity scheme. Considered dynamic rain model was described in Chapter 2.

The remainder of this chapter is organised as follows. Section 4.2 studies the switching strategy for the $1+1$ diversity scheme as the building block of the general $N+P$ scheme. The difference with respect to Chapter 3 is that here a dynamic rain model is considered that impacts the whole analysis. In Section 4.3, the proposed $N + P$ switching scheme is presented and its performance is evaluated analytically in terms of average outage probability and switching rate. Numerical results are presented in Section 4.4. Concluding remarks are provided in Section 4.5.

4.2 $1 + 1$ GW Configuration

4.2.1 Switching Strategy

The $1+1$ GW switching scheme is the building block of the general $N+P$ scheme. Hence we first analyze this scheme assuming a dynamic rain attenuation model. We consider a feeder link with an active GW, denoted as G, and an idle GW, denoted as $\bar{\mathsf{G}}$. We assume that they are located far away from each other so that they experience independent rain [37]. The GWs sample the beacon signal, assumed to be in the appropriate frequency, every Δt seconds. The channel between the gateways and the satellite at $t = n\Delta t$ is denoted by $h_{i,n} = |h_{i,n}|e^{j\alpha_{i,n}}$ where $\alpha_{i,n} \in (0, 2\pi]$ is

the uniformly distributed phase component[1] and $i \in \{1, 2\}$ ($i = 1$ for active GW and $i = 2$ for idle GW). The channel amplitudes, $|h_{i,n}|$, can be estimated at each GW using a beacon signal received from the satellite. In practice, the beacons measure the total atmospheric attenuation. However, since the gaseous and cloud components are assumed to vary slowly compared to the rain attenuation, their bearing on the decision to switch gateways can be accounted by using a fixed (statistical) margin.

It is a standard engineering task to derive the rain attenuation from the measured beacon value with some margin of error. This error margin will vary depending on the auxiliary equipment used on the gateway site. For example, if the gateway is equipped with a radiometer, cloud attenuation can be estimated with high accuracy and be removed from the total attenuation. Further, if the gateway is equipped with a rain gauge, it may improve the deduction of rain attenuation from total attenuation. For the gaseous contribution, a fixed value will be removed from the total attenuation.

Note that, the scintillations are too fast to track, so no attempt is made in the prediction of these fast variations. Thus by measuring the beacon, the decision to switch gateway stations is made in relative terms based on an initial calibration of the beacon signal at each gateway. This is common practice in all operational satellite systems. Motivated by this, we incorporate the simplifying assumption that $|h_{i,n}|$ denotes rain attenuation. As mentioned earlier, the variations in rain attenuation are slow; hence, it is possible to track them and estimate $|h_{i,n}|$ fairly accurately. Since the focus is on the feeder link, the GW exhibits a high clear-sky SNR due to large antenna/ high power amplifier. These arguments corroborate the assumption of an ideal estimation of the channel amplitude in the ensuing analysis. Therefore, the corresponding SNR for the active and idle GWs at $t = n\Delta t$ can be obtained as $\gamma_i(n) = |h_{i,n}|^2 \gamma_{CS}$ where γ_{CS} is the clear-sky SNR for the feeder uplink. Thus the measurements can be equivalently seen as providing SNR estimates. The rain attenuation and the channel gains are related as $A_i(n) = -20 \log_{10} |h_{i,n}|$.

In our work, the other clear-sky effects are assumed to be compensated by a fixed fade margin or an uplink power control scheme. For tractability of the analysis, we assume identical rain attenuation statistics among the different GWs. Under these assumptions, the corresponding rain attenuations $A_1(n)$ and $A_2(n)$ are i.i.d random variables.

We assume that the GWs are connected to a Network Control Centre (NCC) node which has access to the channel state information of the GWs so that it can estimate $\gamma_1(n)$ and $\gamma_2(n)$ every Δt seconds based on the beacon signal from the satellite. We use two realizations of the time series synthesizer (one per GW) using ITU-R P.1853 [19] summarized in the Section 2.1.1. Note that, these two series are spatially i.i.d but each exhibits a temporal autocorrelation based on the transitional PDF given in (2.6). After SNR estimation, the NCC investigates the necessity of

[1]The phase component is time varying and random due to the imperfections of on-ground and on-board Local Oscillators as well as due to the satellite movement within its station keeping box.

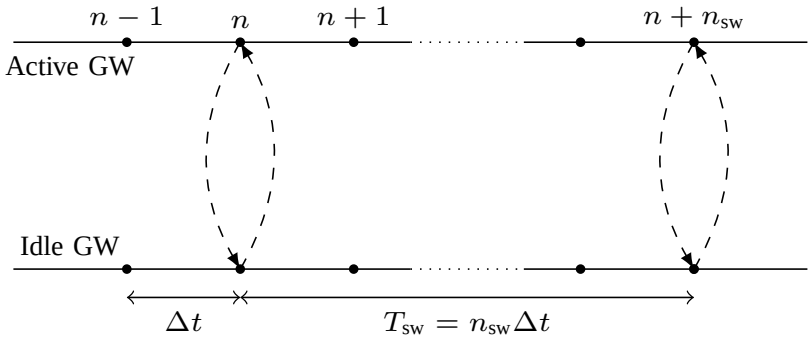

Figure 4.1. Switching intervals in 1 + 1 Configuration

switching at intervals of T_{sw} based on the obtained SNR measurements. For ease of implementation, we assume that $T_{\text{sw}} = n_{\text{sw}}\Delta t$, where n_{sw} is the number of beacon (SNR) samples that NCC uses to perform the GW switching. Figure 4.1 illustrates the switching and beacon sample intervals. In general, evaluating the outage performance of the system for the dynamic rain attenuation model is not mathematically tractable. Therefore we first analytically study the outage performance for the special case of $n_{\text{sw}} = 1$ or $T_{\text{sw}} = \Delta t$, and subsequently attempt the general case of $n_{\text{sw}} > 1$. A numerical evaluation illustrating the effect of setting different n_{sw} is presented in Section 4.4.

4.2.2 Average Outage Probability for 1 + 1 Scheme ($n_{\text{sw}} = 1$)

The objective of the study is to analyze the outage performance of the considered multiple GW scheme. The outage enumeration is related to the underlying switching scheme and in this work, we consider the MSSC (modified switch and stay combining) scheme proposed in [37]. According to this scheme, when $T_{\text{sw}} = \Delta t$, the NCC investigates the necessity of switching every Δt and undertakes switching only if SNR of the active GW is below the threshold (γ_{th}) and that the SNR of the idle GW is above the threshold. Denoting the index of the active GW at $t = n\Delta t$ as $\mathcal{A}_n$ and its SNR as $\gamma(n)$, the MSSC is described as,

$$\mathcal{A}_n = 1 \Longleftrightarrow \begin{cases} \mathcal{A}_{n-1} = 1, \gamma_1(n) \geq \gamma_{\text{th}} \\ \mathcal{A}_{n-1} = 1, \gamma_1(n) < \gamma_{\text{th}}, \gamma_2(n) < \gamma_{\text{th}} \\ \mathcal{A}_{n-1} = 2, \gamma_2(n) < \gamma_{\text{th}}, \gamma_1(n) \geq \gamma_{\text{th}} \end{cases} \tag{4.1}$$

Further, $\mathcal{A}_n = 2$ can be obtained similarly.

To exploit the temporal correlation, we exploit the fact that the NCC knows the attenuation from all the GWs at time instances $\{(n-k)\triangle t\}_{k\geq 1}$. Further, the NCC also knows the GW active at instances $\{(n-k)\triangle t\}_{k\geq 1}$. The instantaneous

outage probability at $t = n\Delta t$ exploiting time correlation then takes the generic form,

$$\Pr\left\{\gamma(n) \leq \gamma_{\text{th}} | \{\gamma_1(n-k), \gamma_2(n-k), \mathcal{A}_{n-k}\}_{k\geq 1}\right\}. \tag{4.2}$$

Using the fact that rain attenuation is a first-order Markov [18], the aforementioned expression reduces to

$$\Pr\left\{\gamma(n) \leq \gamma_{\text{th}} | \gamma_1(n-1), \gamma_2(n-1), \mathcal{A}_{n-1}\right\}. \tag{4.3}$$

Since $\gamma_k(n-1)$ are random variables, so is, $\Pr\{\gamma(n) \leq \gamma_{\text{th}} | \gamma_1(n-1), \gamma_2(n-1), \mathcal{A}_{n-1}\}$ and towards defining a statistical measure of outage at $t = n\Delta t$, we define,

$$P_n = \mathbf{E}\left\{\Pr\{\gamma(n) \leq \gamma_{\text{th}} | \gamma_1(n-1), \gamma_2(n-1), \mathcal{A}_{n-1}\}\right\}, \tag{4.4}$$

where $\mathbf{E}(\cdot)$ is the expectation operation over $\{\gamma_k(n-1)\}$ and $\mathcal{A}_{n-1}$. Note that, the PDF of $\gamma_k(n-1)$ (in dB) can be obtained from (2.4) and that we assume $\mathcal{A}_{n-1}$ takes values $\{1, 2\}$ equally likely. The last assumption follows from the identical distribution of the rain attenuation across the two GWs. While P_n is no longer a random variable, it is time varying. The time variations are further averaged to yield the *average outage probability* of $1+1$ scheme as,

$$\bar{P}_{1+1}(\gamma_{\text{th}}) = \frac{1}{N_r}\sum_{n=1}^{N_r} P_n \,. \tag{4.5}$$

where N_r is the number of samples in the time series.

The discussion so far has been agnostic to the switching strategy. We now incorporate the MSSC strategy for further simplification. Specializing to the case of $\mathcal{A}_{n-1} = 1$ and employing (4.1), we have,

$$\begin{aligned}&\Pr\{\gamma_n \leq \gamma_{\text{th}} | \gamma_1(n-1), \gamma_2(n-1), \mathcal{A}_{n-1} = 1\}\\ &= \Pr\{\gamma_1(n) \leq \gamma_{\text{th}},\ \gamma_2(n) \leq \gamma_{\text{th}} | \gamma_1(n-1), \gamma_2(n-1)\},\end{aligned} \tag{4.6}$$

wherein we exploit the first order Markov property of rain attenuation [18] and the fact that the first GW was active at the instance $n-1$. Using the spatial independence of the rain attenuations, (4.6) can be simplified as,

$$\begin{aligned}&\Pr\{\gamma_1(n) \leq \gamma_{\text{th}},\ \gamma_2(n) \leq \gamma_{\text{th}} | \gamma_1(n-1), \gamma_2(n-1)\}\\ &= \Pr\{\gamma_1(n) \leq \gamma_{\text{th}} | \gamma_1(n-1)\} \Pr\{\gamma_2(n) \leq \gamma_{\text{th}} | \gamma_2(n-1)\}.\end{aligned} \tag{4.7}$$

Using the relation between the rain attenuation and the SNR, we further simplify (4.7) as,

$$\begin{aligned}&\Pr\{\gamma_1(n) \leq \gamma_{\text{th}},\ \gamma_2(n) \leq \gamma_{\text{th}} | \gamma_1(n-1), \gamma_2(n-1)\}\\ &= \Pr\{A_1(n) > \alpha_{\text{th}} | A_1(n-1)\} \Pr\{A_2(n) > \alpha_{\text{th}} | A_2(n-1)\},\end{aligned} \tag{4.8}$$

where $\alpha_{\rm th} = 10\log(\gamma_{CS}/\gamma_{\rm th})$. Further, a similar result holds when $\mathcal{A}_{n-1} = 2$. Using the identical distribution of the $A_k(n), k = 1, 2$ and equally like occurrence of $\mathcal{A}_{n-1} = 1, 2$, it is shown in Appendix A, that

$$P_n = \frac{1}{4}\,\mathrm{erfc}\left(\frac{\ln\alpha_{\rm th} - m_L}{\sqrt{2}\sigma_L}\right)^2. \tag{4.9}$$

Using (4.9), the average outage probability can be finally written as

$$\bar{P}_{1+1}(\gamma_{\rm th}) = \frac{1}{4}\,\mathrm{erfc}\left(\frac{\ln\alpha_{\rm th} - m_L}{\sqrt{2}\sigma_L}\right)^2. \tag{4.10}$$

Remark 1. *Effect of Time Correlation: The average outage probability in* (4.10) *is independent of Δt. In fact, (4.10) can be easily deduced as the outage probability when considering time-independent rain attenuation samples [37]. One could argue that the use of the current SNR sample for switching invalidates the introduction of the time correlation. However, the outage probability expressions are derived for MSSC which implicitly exploits time correlation. This non-appearance of the time correlation is made possible because the outage threshold in* (4.8) *is independent of $A_k(n-1)$ unlike, for example, derivations involving the evaluation of Bit Error Rates for fading channels. However, it should be stressed that, unlike the temporally independent scenario,*

$$\bar{P}_{1+1}(\gamma_{th}) \neq \Pr\{\gamma(n) \leq \gamma_{th} | \gamma_1(n-1), \gamma_2(n-1), \mathcal{A}_{n-1}\} \tag{4.11}$$

when the dynamic model is exploited. The observation implies that the correlation between rain samples, as dictated by (2.6), can have favorable as well as adverse effects.

4.2.3 Average Outage Probability for $1 + 1$ Scheme ($n_{\rm sw} > 1$)

We now study the outage probability for the $1 + 1$ configuration when $n_{\rm sw} > 1$. This considers a switching interval, $T_{\rm sw}$, that includes $n_{\rm sw}$ SNR samples. In such a scenario, it is natural to include the number of outages in addition to their occurrence. Hence, we extend the definition of (4.4) to

$$P_k = \frac{1}{n_{\rm sw}}\Big(\mathbf{E}\{\Pr\{\gamma(k) < \gamma_{\rm th} | \{\gamma_m(k-1)\}_m, \mathcal{A}_{k-1}\}\} + \mathbf{E}\left\{n_{\rm out}(k)\right\}\Big) \tag{4.12}$$

where $n_{\rm out}(k)$ is the number of SNR samples (measured at the active GW) that are in outage during the interval $[k+1, k+n_{\rm sw}-1]$ and the expectation is over $\{\gamma_m(k-1)\}_m, \mathcal{A}_{k-1}$. While the first term provides the outage at the switching instance, $\mathbf{E}\left\{n_{\rm out}(k)\right\}$ results in the average number of outages in the remaining $n_{\rm sw} - 1$ samples. Thus the measure gives the notion of probability and reduces to (4.4) when $n_{\rm sw} = 1$.

Further, $\mathbf{E}\{n_{\text{out}}(k)\}$ can be expressed as,

$$\mathbf{E}\left\{n_{\text{out}}(k)\right\} = \sum_{l=1}^{n_{\text{sw}-1}} l\,\mathbf{E}\left\{\Pr\{n_{\text{out}}(k) = l\,|\gamma(k-1)\}\right\}. \tag{4.13}$$

Evaluation of each of the terms in (4.13) involves correlated rain samples, thereby making it involved if not untractable. In the following, we illustrate with an example that not all terms are independent of $\beta\Delta t$ as in the case of $n_{\text{sw}} = 1$.

Example: Consider $n_{\text{sw}} = 3$ and we consider $n_{\text{out}} = 2$. It can be shown that

$$\begin{aligned}&\mathbf{E}\left\{\Pr\{n_{\text{out}} = 2\,|\gamma_{k-1}\}\right\} \\ &= \int_0^{\gamma_{th}}\int_0^{\gamma_{th}} f\left(x, y; (m_L, \sigma_L^2), (m_L, \sigma_L^2), e^{-\beta\Delta t}\right)\, dx\, dy\end{aligned} \tag{4.14}$$

where $f\left(x, y; (m_L, \sigma_L^2), (m_L, \sigma_L^2), e^{-\beta\Delta t}\right)$ is the bi-variate log-normal distribution with the variables x, y having m_L as mean, σ_L as variance and $e^{-\beta\Delta t}$ as the correlation [91].

Remark 2. *A key observation is that P_k has components that are no longer independent of $\beta\Delta t$. While it is difficult to characterize their effect analytically, the effects of the dynamic model are further discussed in Section 4.4 where their effects are illustrated through numerical evaluations.*

While we have derived the expression for $n_{\text{sw}} = 2$, a similar exercise for $n_{\text{sw}} > 2$ becomes rather involved. However, we can find an approximate expression by assuming the SNR samples to be i.i.d spatially and temporally. In this case, it can be written as,

$$\sum_{i=0}^{n_{\text{sw}-1}} i\binom{n_{\text{sw}} - 1}{i} p^i (1-p)^{n_{\text{sw}}-1-i}, \tag{4.15}$$

where,

$$p = \Pr\{\gamma(k) < \gamma_{\text{th}}\} = \frac{1}{2}\,\text{erfc}\left(\frac{\ln\alpha_{\text{th}} - m_L}{\sqrt{2}\sigma_L}\right),\ \forall k,\ kn_{\text{sw}} + 1 \le j < (k+1)n_{\text{sw}} \tag{4.16}$$

wherein we exploit the identical distribution of attenuation samples for all GWs. The average outage probability, $\bar{P}_{1+1}$, can be approximated by,

$$\bar{P}_{1+1} \approx \frac{p^2 + (n_{\text{sw}} - 1)p}{n_{\text{sw}}}. \tag{4.17}$$

When $n_{\text{sw}} = 1$ (4.17) reduces to (4.10). Further, if $n_{\text{sw}} = 1$, average outage probability will be p^2 regardless of the correlation between the sample (as it was

shown for correlated samples in subsection 4.2.1) and it naturally means that we will get the best performance when switching is checked for every sample. If $n_{\text{sw}} \to \infty$, we will have $\bar{P}_{1+1} = p$. This means that if the time interval between switching instances is too long, the system will not benefit from the second GW since its performance is equal to the single GW system. Numerical simulations corroborating this observation is presented in Section 4.4.

4.2.4 Switching Based on SNR Prediction

In practice, the switching operation is not instantaneous and there is a latency between making the decision and executing it. This implies that actual switching is effected only at $t+t_d$ if the decision to switch is made at t. However, the value of the SNRs at the actual switching instance would be different from those resulting in the decision. One way to solve this problem is to predict the rain attenuation t_d seconds ahead, derive the corresponding SNR and make a decision based on these predicted values.

There are different methods for the fade predicting depending on the model assumed for the channel, see [92–94]. For the channel model assumed in this chapter, we can exploit (2.6) to derive the MMSE estimator which is used to estimate the $A(t + t_d)$ based on the observed $A(t)$. It is known that the MMSE estimator is the mean of the posterior PDF [95]. The posterior PDF of $A(t + t_d)$ given the observation $A(t)$ can be obtained by (2.6) and the MMSE estimate as follows,

$$\hat{A}(t + t_d) = \exp\left(m_{t_d} + \sigma_{t_d}^2/2\right), \tag{4.18}$$

where m_{t_d} and σ_{t_d} similar to (2.6) with Δt replaced by t_d. During the switching interval (time duration between making the decision and executing it) we assume that the active GW continues serving the users until switching is effected.

While the instantaneous estimation of the channel using beacon is assumed to be ideal, errors would be induced by the prediction. Use of predicted values can be seen as a representative case towards evaluating the performance of the system with decision errors and indicative of its sensitivity to imperfect channel information. Further the quality of the estimate is indicative of the correlation and hence switching based on prediction reflects the influence of time correlation as well. Clearly, increasing t_d reduces correlation and enhances prediction errors; Section 4.4 will discuss the effect of t_d on the performance of the system.

4.3 $N + P$ GW Configuration

In this section, we consider a generalized switching scheme with N active GWs and P idle GWs. Similar to the 1+1 analysis, we continue the use of the dynamic rain fading model for every link, while assuming the links themselves to be spatially i.i.d. The latter assumption, used for mathematical tractability, is motivated in Section 2 and implies that all GWs have the same rain attenuation statistics and

are independent. We have dropped n (time sample index) from the expressions for simplicity. Based on the MSSC strategy in Section 4.2.1, a switching scheme for $N+P$ scenario is presented first (see also [78]), followed by an analysis of the outage probability as well as switching rate.

4.3.1 $N+P$ GW Switching Strategy

Fig. 4.2 illustrates the switching strategy in detail and the different steps are explained in detail below.

- **Acquisition**: In the first step, NCC collects the SNR of all GWs, both active and idle.
- **Sorting**: After acquisition, the NCC sorts the active and idle GWs based on their SNR in *decreasing* order (this is same as sorting the GWs based on their rain attenuation in *increasing* order). The mth largest SNR amongst the active GWs and the corresponding GW index are denoted by μ_m and G_m, respectively. Similarly, for the idle GWs, the kth largest SNR and the corresponding GW index are depicted by $\bar{\mu}_k$ and $\bar{\mathsf{G}}_k$, respectively. Therefore, we can write $\mu_1 \geq \mu_2 ... \geq \mu_N$ and $\bar{\mu}_1 \geq \bar{\mu}_2 \cdots \geq \bar{\mu}_P$. Defining A_i and $\bar{A}_i$ to be the rain attenuation of G_i and $\bar{\mathsf{G}}_i$, respectively, we obtain $A_1 \leq A_2 \leq \cdots \leq A_N$ and $\bar{A}_1 \leq \bar{A}_2 \leq \cdots \leq \bar{A}_P$ by exploiting the relation between the channel gain and rain attenuation.
- **Pairing**: After the sorting step, NCC initiates pairing the active $\mathsf{G}_{k'}$ and idle $\bar{\mathsf{G}}_k$ GWs, where $k = 1, ..., P$ and $k' = N - k + 1$. Thus, P switching pairs will be formed such that the weakest active GW, G_N, will have the best chance to switch to the strongest idle GW, $\bar{\mathsf{G}}_1$.
- **Switching**: The switching between the pairs will take place based on MSSC scheme introduced for two GWs in [37]. Based on this switching method, if $\mu_{k'}$ is lower than γ_{th} and $\bar{\mu}_k$ is higher than γ_{th}, switching occurs between two GWs. Here, γ_{th} is the outage threshold.

Note that, in each time slot, the state of the GWs (active or idle) can change due to switching. However, this will not impact the ensuing statistical analysis since the SNR associated with different GWs have independent and identical distribution.

Complexity: Regarding the complexity of the switching algorithm, it should be noted that the switching process involves the sorting and comparison operations where sorting operation has a complexity of $\mathcal{O}(n \log n)$ in worst case [96].

It is assumed that the NCC handles traffic rerouting when a decision to switch is undertaken. This process could involve higher layers which could have a bearing on the performance. For example, packet-loss during the switching process is an issue studied in [29]. The analysis of such issues is pertinent; however, the current work focuses on analyzing physical layer performance and higher layer issues like traffic rerouting (switching) are left for further investigation. As such, our contribution

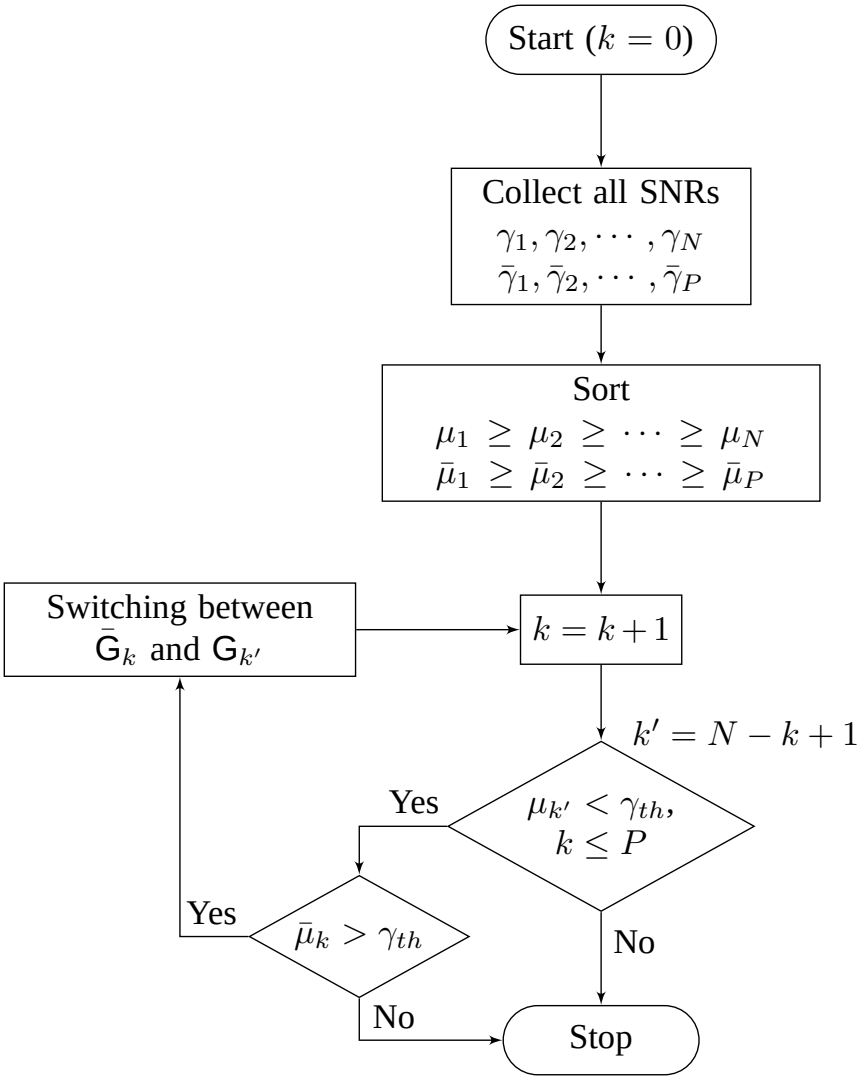

Figure 4.2. Flowchart of $N + P$ Gateway Switching scheme

should be construed as only a building block that needs to be combined with other higher layer tools for carrying out cross-layer system optimization.

4.3.2 Average Outage Probability

In this subsection, we will study the performance of the proposed $N+P$ scheme for the feeder link in terms of average outage probability when switching is considered for every sample. We define the $N+P$ average outage probability of the feeder link as,

$$\bar{P}_{FL}(\gamma_{\text{th}}) = \frac{1}{N}\left(\sum_{m=1}^{N-P}\bar{Q}_m + \sum_{k=1}^{P}\bar{P}_{1+1,k}\right). \tag{4.19}$$

Here $\bar{Q}_m$, $1 \le m \le N-P$, is the average outage probability of each of the $N-P$ GWs that are not involved in the switching process. Further, $\bar{P}_{1+1,k}$ [2] is the average outage probability of kth pair from the P switching pairs.

We now evaluate $\bar{P}_{1+1,k}$ and $\bar{Q}_m$. The methodology used in Section 4.2.2 is applicable to the current scenario in a straight forward manner, but with additional book keeping. Omitting the additional details for ease of comprehension, the average outage probabilities of the switching pairs, $\mathsf{G}_{k'}$ and $\bar{\mathsf{G}}_k$, can be calculated as,

$$\begin{aligned}\bar{P}_{1+1,k}(\gamma_{\text{th}}) &= \Pr\{\mu_{k'} \le \gamma_{\text{th}}\}\Pr\{\bar{\mu}_k \le \gamma_{\text{th}}\}\\ &= \Pr\{A_{k'} > \alpha_{\text{th}}\}\Pr\{\bar{A}_k > \alpha_{\text{th}}\}\\ &= \left(1 - P_{A_{k'}}(\alpha_{\text{th}})\right)\left(1 - P_{\bar{A}_k}(\alpha_{\text{th}})\right)\end{aligned} \tag{4.20}$$

The outage probability of the remaining $N-P$ active GWs, that are not involved in the switching process can be calculated as

$$\bar{Q}_m(\gamma_{\text{th}}) = \Pr\{\mu_m \le \gamma_{\text{th}}\} = 1 - P_{A_m}(\alpha_{\text{th}}). \tag{4.21}$$

In (4.20) and (4.21), $P_{A_m}(\cdot)$ and $P_{\bar{A}_k}(\cdot)$ are the Cumulative Distribution Function (CDF) of mth and kth order statistics of A and $\bar{A}$, respectively. These CDFs can be obtained from [97] as,

$$P_{A_{k'}}(\alpha_{\text{th}}) = \sum_{t=k'}^{N}\binom{N}{t}\left[P_A(\alpha_{\text{th}})\right]^t\left(1 - P_A(\alpha_{\text{th}})\right)^{N-t}, \tag{4.22}$$

$$P_{A_k}(\alpha_{\text{th}}) = \sum_{t=k}^{P}\binom{P}{t}\left[P_A(\alpha_{\text{th}})\right]^t\left(1 - P_A(\alpha_{\text{th}})\right)^{P-t}. \tag{4.23}$$

Towards obtaining (4.19), it now remains to evaluate $P_A(\alpha_{\text{th}})$. Since rain attenuation follows the log-normal distribution in (2.4), $P_A(\alpha_{\text{th}})$ can be obtained as,

$$P_A(\alpha_{\text{th}}) = 1 - 0.5\ \text{erfc}\left(\frac{\ln\alpha_{\text{th}} - m_L}{\sqrt{2}\sigma_L}\right). \tag{4.24}$$

[2] We slightly abuse the notation $\bar{P}_{1+1}$ of (4.5) to incorporate the kth pair; each pair employs ordered SNR and hence the average outage probability would be different.

Finally, by substituting (4.20) and (4.21) in (4.19), we get an expression for the feeder link average outage probability of the system as,

$$\bar{P}_{FL}(\gamma_{\rm th}) = \frac{1}{N}\sum_{m=1}^{N-P}\left(1 - P_{A_m}(\alpha_{\rm th})\right) + \frac{1}{N}\sum_{k=1}^{P}\left(1 - P_{A_{k'}}(\alpha_{\rm th})\right)\left(1 - P_{\bar{A}_k}(\alpha_{\rm th})\right). \tag{4.25}$$

To illustrate the generalization of the derived expressions, it can be easily shown that the result in (4.10) can be obtained from (4.25) by using $N = P = 1$. Note that, similar to the expression in (4.10), equation (4.25) will be independent of the temporal correlation when $n_{\rm sw} = 1$. It should be noted that (4.25) is similar to the result of [7]; however, the current work employs a bottom-up approach where the switching strategy is defined and the resulting outage is then calculated.

Remark 3. *While the earlier discussion focused on $n_{sw} = 1$, the ideas of Section 4.2.3 on $n_{sw} > 1$ can be extended to the $N + P$ configuration. Fortunately, the computation of $\boldsymbol{E}\{n_{out}(k)\}$ does not involve ordered SNRs.*

4.3.3 End-to-End Outage Analysis

Given that the user link (link between the satellite and user) will operate in a band (like Ka) lower than the feeder link, it is interesting to investigate the improvement of the end-to-end link due to $N + P$ scheme. The vast majority of SatCom systems are transparent − the satellite repeater only downconverts the signal received on the feeder link and amplifies it before re-transmitting onto the user link.

To study the end-to-end performance of the system, we assume that each active GW serves a single user in each time slot considering time division multiple access (TDMA) channel. Therefore, we can assume that there are N end-to-end links (GW to the user terminal). The average outage probability of $N + P$ scheme will be the average of these N end-to-end links.

Following a similar approach used in (12) of [37], we can find the outage probability of the lth end-to-end link as,

$$\bar{P}_{E2E,l}(\gamma_{\rm th}) = \bar{P}_{FL,l}(\gamma_{\rm th}) + \int_{\gamma_{\rm th}}^{\infty} \bar{P}_{FL,l}(z) f_{\gamma_g}(\gamma_g) d\gamma_g \tag{4.26}$$

where $1 \leq l \leq N$ and

$$z = \gamma_{\rm th}(\gamma_g + 1)/(\gamma_g - \gamma_{\rm th}). \tag{4.27}$$

γ_g is the SNR of a Ka-band user link which is assumed to have a log-normal PDF ($f_{\gamma_g}(\cdot)$) and $\bar{P}_{FL,l}(\cdot)$ is the outage probability of the feeder link in each of the N end-to-end links. For the active GWs involved in the switching process, $\bar{P}_{FL,l}(\cdot)$

can be found using (4.20) and for those not involved in the switching process it can be found from (4.21).

Therefore, average end-to-end outage performance of a transparent satellite with $N+P$ GWs can be found as,

$$\begin{aligned}\bar{P}_{E2E}(\gamma_{\text{th}}) &= \frac{1}{N}\sum_{l=1}^{N}\bar{P}_{E2E,l}(\gamma_{\text{th}}) \\ &= \bar{P}_{FL}(\gamma_{\text{th}}) + \int_{\gamma_{\text{th}}}^{\infty}\bar{P}_{FL}(z)f_{\gamma_g}(\gamma_g)d\gamma_g \end{aligned} \tag{4.28}$$

where $\bar{P}_{FL}(\gamma_{\text{th}})$ is defined in (4.25). Here, we assumed that SNRs of all user links are i.i.d with the same PDF, $f_{\gamma_g}(.)$.

4.3.4 Average Switching Rate

When GW switching is used, the switching rate is an important issue since a high switching rate results in large overhead and can make the system unstable. Let the number of switching instances be denoted by N_{sw} and the total number of the SNR (rain attenuation) samples by N_r. We also assume that the investigation for switching is done for every sample, e. g. $T_{\text{sw}} = \Delta t$ since $n_{\text{sw}} = 1$. Then, the switching probability can be expressed as $\frac{N_{\text{sw}}}{N_r}$ and switching rate as *Switching Probability* $/\Delta t$. Note that, the switching rate is actually defined as the ratio of number of switching instances over the total time, e.g. $N_{\text{sw}}/(N_r\Delta t)$. For a fixed value of N_r and based on this definition, the lower the time interval between the samples (Δt), the lower will be the switching probability. This is because, for small values of Δt, the rain attenuation samples are highly correlated. As Δt increases, correlation between the samples decreases and results in a higher switching probability.

In this subsection, for the ease of mathematical analysis, we consider the i.i.d samples (large Δt) which leads to the upper bound of the switching probability. In Section 4.4, we will study the effect of different Δt on the switching probability by numerical simulation.

As explained in Section 4.3, switching will occur between $\mu_{k'}$ and $\bar{\mu}_k$ based on MSSC scheme. Hence, similar to the approach used in [37] for i.i.d random variables, it is possible to define a six state Markov chain model for each switching pair. The transitional probability matrix $\mathbf{P}$ of the Markov chain can be obtained as (for details kindly refer to [37]),

$$\mathbf{P} = \begin{bmatrix} \rho_{k'} & p_k & 1-\rho_{k'}-p_k & 0 & 0 & 0 \\ \rho_{k'} & p_k & 1-\rho_{k'}-p_k & 0 & 0 & 0 \\ 0 & 0 & 0 & \varrho_k & p_k & 1-\varrho_k-p_k \\ 0 & 0 & 0 & \varrho_k & p_k & 1-\varrho_k-p_k \\ 0 & 0 & 0 & \varrho_k & p_k & 1-\varrho_k-p_k \\ \rho_{k'} & p_k & 1-\rho_{k'}-p_k & 0 & 0 & 0 \end{bmatrix}, \tag{4.29}$$

where,

$$\rho_{k'} = P_{A_{k'}}(\gamma_{\text{th}}), \tag{4.30}$$

$$p_k = (1 - P_{A_{k'}}(\gamma_{\text{th}}))(1 - P_{A_k}(\gamma_{\text{th}})), \tag{4.31}$$

$$\varrho_k = P_{\bar{A}_k}(\gamma_{\text{th}}). \tag{4.32}$$

We define $\pi_{i,k}$ as the probability that kth switching pair is in state i. By using the facts that $\overrightarrow{\pi} = \overrightarrow{\pi}\mathbf{P}$ and $\sum_{i=1}^{6} \pi_{i,k} = 1$, where $\overrightarrow{\pi} = [\pi_{1,k}, \pi_{2,k}, ..., \pi_{6,k}]$, the switching probability of kth pair can be calculated as

$$\pi_k(\gamma_{\text{th}}) = \frac{2(1 - \rho_{k'} - p_k)(1 - \varrho_k - p_k)}{2 - \rho_{k'} - \varrho_k - 2p_k}, \tag{4.33}$$

Now, we can define the average switching probability as

$$P_{\text{sw}} = \frac{1}{P} \sum_{k=1}^{P} \pi_k(\gamma_{\text{th}}). \tag{4.34}$$

The switching rate can be easily calculated as $P_{\text{sw}}/\Delta t$ where Δt is the interval between switching instants. In Section 4.4, we will see that how Δt affects the switching rate.

4.4 Numerical Results and Discussion

Tables 4.1 and 4.2 respectively detail the propagation parameters and the link budget parameters for typical Central-European climate that were used as input to the empirical rain attenuation prediction model included in ITU-R Recommendation P.618. For simulation purposes, we consider a dynamic rain attenuation model based on [19] wherever Δt is used. More details about the rain attenuation time series are provided in Section 2.1. In this method, the rain attenuation samples are synthesized from a discrete white Gaussian noise process. In the first step, the white Gaussian noise is low-pass filtered and then transformed from a normal distribution to a log-normal distribution. Finally, it is calibrated to match the desired rain attenuation statistics.

Figure 4.3 presents the average availability ($1 - \bar{P}_{FL}$ in percentage) of the large scale GW diversity scheme versus unavailability of a single GW ($1 - P_A(\alpha_{\text{th}})$ in percentage). For the case of $4 + 1$ and $7 + 1$, it can be seen that if availability of each GW is 99%, the average availability of the whole GW network will be around 99.97% and 99.96%, respectively. This figure is obtained from (4.25).

Figure 4.4 illustrates the feeder-link outage performance of the proposed scheme for different configurations. It is aimed at providing some insights about the effect of N, P on performance and aid in system design. We can see that, with the number of idle GWs fixed ($P = 1$), the outage probability degrades gracefully with increasing number of active GWs. This means that if we assign only one idle GW

Table 4.1. propagation and link budget assumptions

Q/V band Feeder Up-Link	**Value**
Carrier frequency	50 GHz
Elevation angle	32°
Polarization	Circular
EIRP_{GW} including back-off	76.5 dBW
UL free space loss	218.3 dB
$(\text{G/T})_{Sat}$	31.45 dB
γ_{CS}	28.3 dB

for 10 active GWs, this scheme could still provide acceptable outage performance. Also, it can be seen that for a fixed number of active GWs ($N = 10$), if we increase the number of idle GWs from 1 to 2 outage probability decreases considerably. It is worth mentioning that all results are theoretical evaluations.

Figure 4.5 presents the average outage probability of different configurations when $\frac{N}{P} = 4$. It can be inferred from the figure that for a fixed ratio of $\frac{N}{P}$, if the number of GWs increases, the system will have a better outage performance. This means that, for example, if there are 8 active GWs and 2 idle GWs, the $8 + 2$ architecture will result in better overall performance than two $4 + 1$ clusters.

Figure 4.6 illustrates the performance of the $1+1$ system when switching is done based on the predicted value of the rain attenuation. As it can be seen, increasing t_d degrades the outage performance of the system. For the availability of 99.9% ($\bar{P}_{out} = 10^{-3}$), performing switching based on the prediction results in 0.25 dB and 0.4 dB degradation in the outage performance for $t_d = 5$ seconds and $t_d = 10$ seconds, respectively.

Figure 4.7 shows the effect of setting different n_{sw} (recall that n_{sw} is the number of SNR samples between two switching check instances) on the outage probability of the $1 + 1$ system. In this case, we assume that NCC checks the switching possibility every n_{sw} samples and switching is performed instantaneously. As expected, increasing the n_{sw} degrades the system performance because switching is not done on time to cope with the outages. For the considered operating point of $\bar{P}_{out} = 10^{-3}$, it can be seen that the performance is affected considerably. For very high values of n_{sw}, the performance curve converges to that of the single GW system. In $N+P$ scheme, n_{sw} will have the similar effect. We can derive the similar conclusions from Figure 4.8 for the end-to-end average outage probability.

Figure 4.9 presents the switching probability of the $1+1$ scheme for different Δt. As it was discussed in subsection 4.3.4, larger Δt increases the switching probability. It can be seen that as $\Delta t \to \infty$, switching probability converges to the upper bound described by (4.34).

Figure 4.10 shows the influence of different switching thresholds on the switching

Table 4.2. propagation and link budget assumptions

Ka-band User Down-Link	**Value**
Carrier frequency	20 GHz
Elevation angle	35°
Polarization	Circular
EIRP_{sat} including back-off	72.5 dBW
DL free space loss	210.5 dB
$(\text{G/T})_{UT}$	20.3 dB
γ_{CS}	21.3 dB

probability, average outage probability and the spectral efficiency of the system. In fact, γ_{th} is chosen correspond to the minimum SNR required to support a certain Modcod in DVB-S2. It can be seen that the improvements in spectral efficiency are negligible while the switching rate is sensitive to the threshold. As expected, by increasing γ_{th}, the switching probability of the system increases and so does the spectral efficiency.

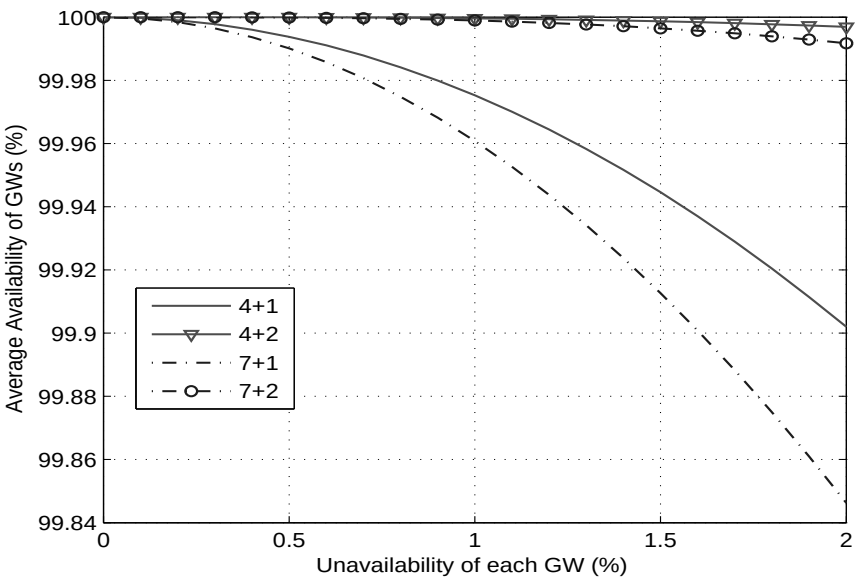

Figure 4.3. Average availability of the GWs versus unavailability of a single GW

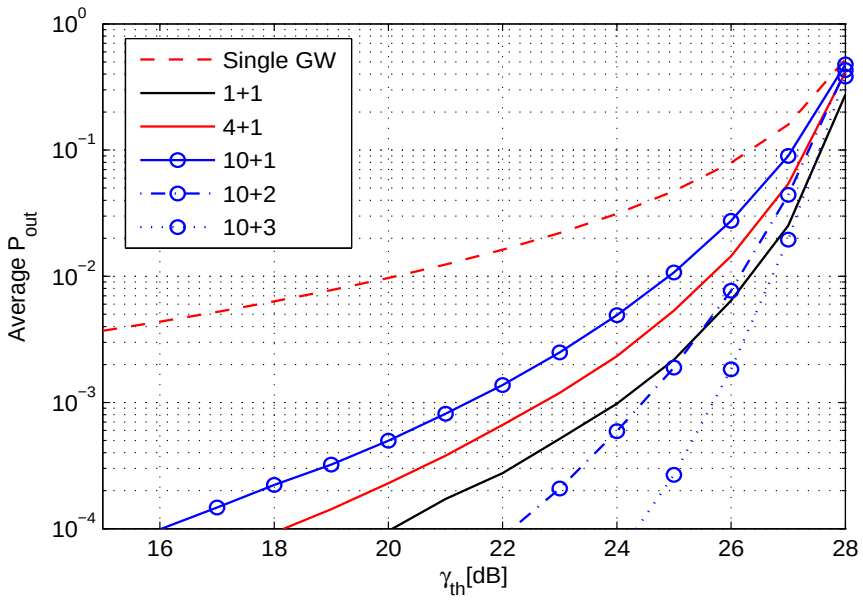

Figure 4.4. Average outage probability for different $N + P$ configurations

4.5 Summary

In this chapter, we have devised a practical switching scheme to exploit multiple GW transmit diversity when moving the feeder link of a multibeam broadband satellite network to Q/V band. The novel aspect of the proposed scheme are the association of GWs into switching pairs based on ordered SNR and the use of the robust MSSC strategy. Also, considering a dynamic rain attenuation model, we have studied the effect of performing switching based on the predicted rain attenuation values. Expressions for key performance indicators − average outage probability and switching rate− have been derived analytically providing insights into system sizing especially on the relative effect of the number of idle and active GWs. An interesting result is that larger clusters yield better performance for a given ratio of idle and active GWs. It is further seen that an increase in switching threshold, enhances achieved spectral efficiency, but at the cost of higher switching probability.

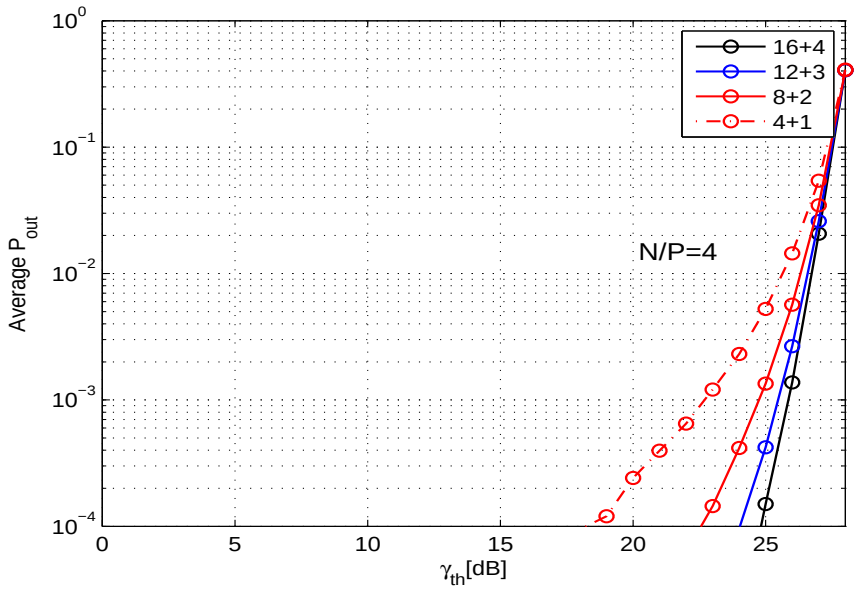

Figure 4.5. Average outage probability for $\frac{N}{P} = 4$ and different $N + P$ schemes

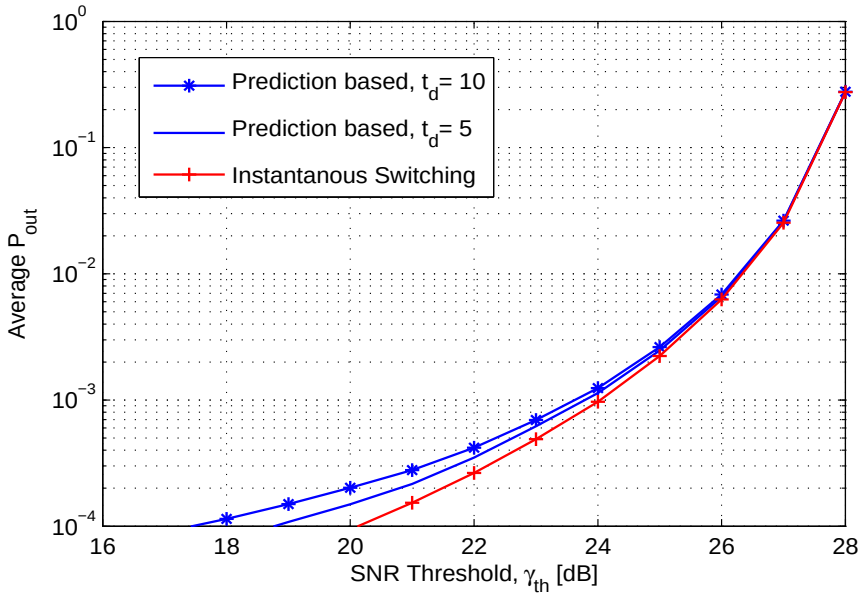

Figure 4.6. Average outage probability of $1 + 1$ case for different estimation lags and $\Delta t = 1$

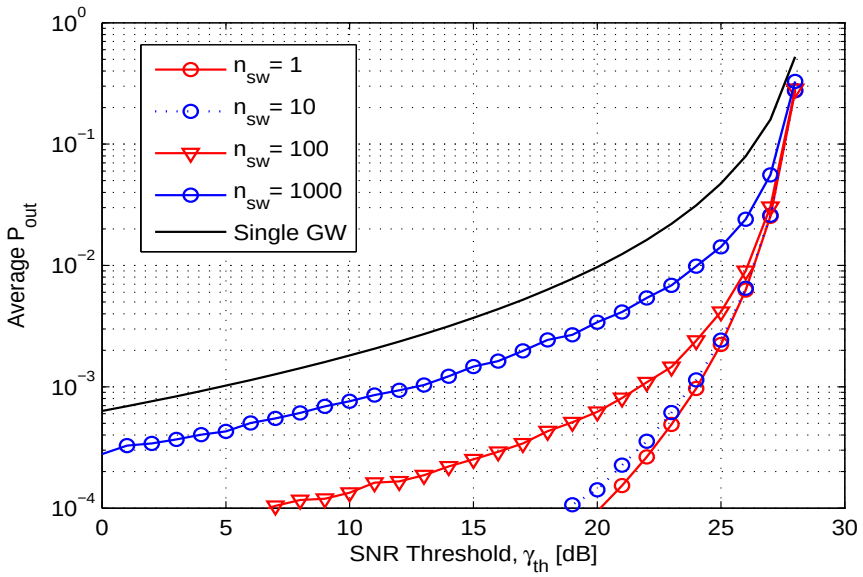

Figure 4.7. Feeder Link average outage probability of $1+1$ case for different n_{sw} and $\Delta t = 1$

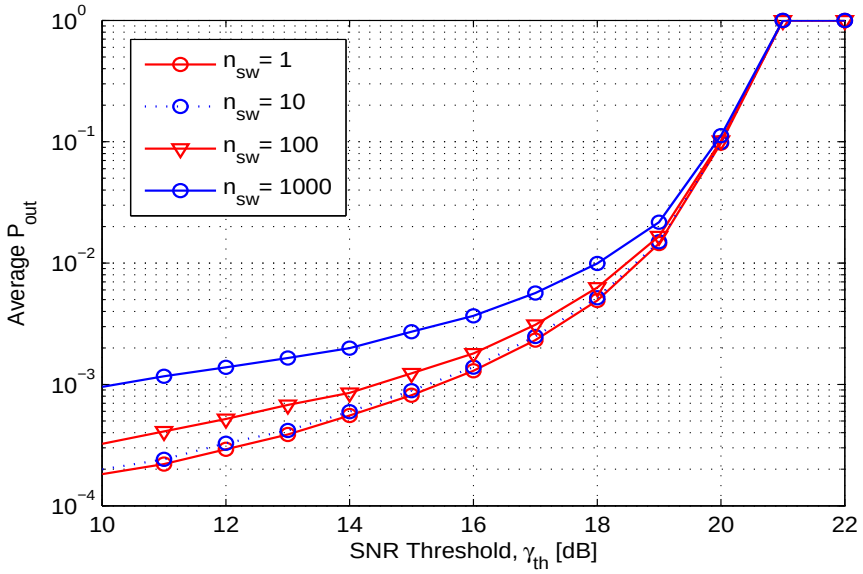

Figure 4.8. End-to-end average outage probability of $1+1$ case for different n_{sw} and $\Delta t = 1$

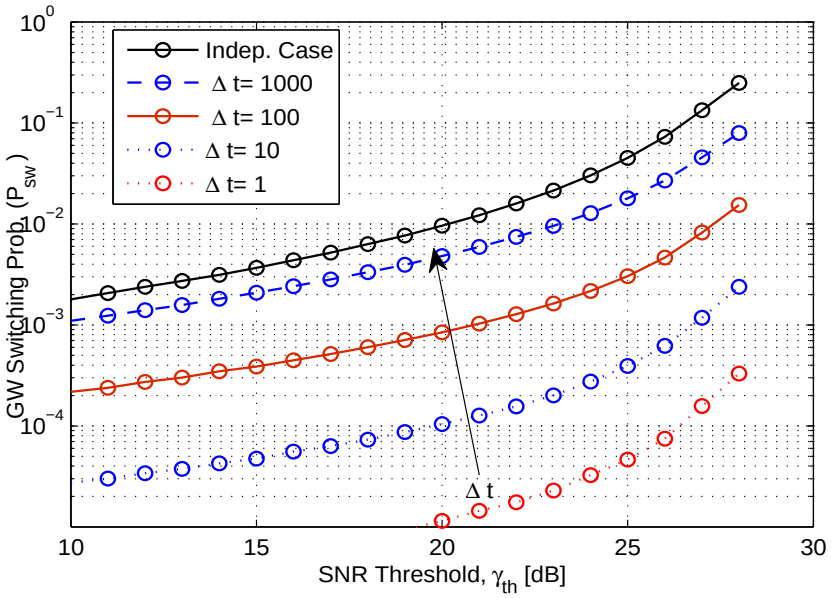

Figure 4.9. GW Switching Probability for $1 + 1$ scheme and different Δt and $n_{\mathrm{sw}} = 1$

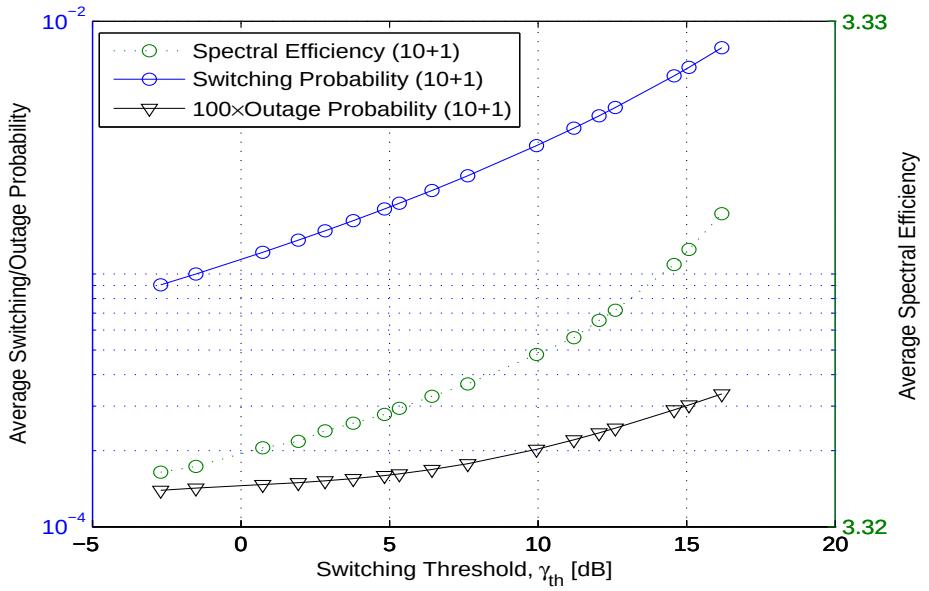

Figure 4.10. Average Switching probability and Spectral Efficiency for different switching thresholds

Chapter 5

Phase Uncertainty in Multibeam Satellite Channels: Modeling and Robust Precoder Design

> Essentially, all models are wrong, but some are useful.
>
> *George E. P. Box*
> 1913-2013

5.1 Introduction

In this chapter, the precoder design on the user downlink channel of a multibeam satellite system is studied. Due to fluctuations of the phase components, the channel is time-varying resulting in outdated channel state information at the transmitter because of the long round trip delay. In Section 5.2, a model for the phase uncertainty is proposed and a robust precoder design framework is studied considering requirements on availability and average SINR. Probabilistic and expectation based approaches are employed in Section 5.3 to formulate the design criteria which are solved using convex optimization tools. The performance of the resulting precoder is evaluated through extensive simulations. Although a satellite channel is considered in this chapter, the presented analysis is valid for any vector channel with phase uncertainty.

5.2 Phase Uncertainty Model

Similar to terrestrial communication channels, satellite based communication channels are time-varying and for typical precoding applications, the transmitter needs

to know the CSI of the downlink channel. In the satellite context the UT estimates the amplitude and the phase of each of the sub-channels and feeds them back to the GW. In Chapter 2, the multibeam satellite channel is described and channel model is given in (2.13). Based on this model, the baseband time-varying sub-channel in the forward-link between antenna j and user i at time t can be denoted by $h_{ij}(t) = |h_{ij}|e^{\mathrm{j}\theta_{ij}(t)}$. As mentioned, the amplitude variation of this channel is dominated by the rain attenuation whose variations are negligible during the RTD interval. Therefore, the temporal variations of the amplitude are considered to be negligible over the intervals of interest and hence the time dependency is omitted from $|h_{ij}|$.

On the other hand, the phase of the sub-channels can be affected by different time varying components. For example, each feed will contribute a continuously time varying random phase component to the sub-channels. This random phase component corresponds to the phase noise of the LO and is the main contributor to the phase uncertainty. Since satellite antenna spacing is very small compared to communication distance and that a line of sight environment is considered, all the sub-channels are usually assumed to be identical [23]. While this is acceptable for the amplitude of the sub-channels, the same might not be valid for the phase of the sub-channels. Phase is sensitive to minor channel geometrical differences and, therefore, each sub-channel can have different time varying phase components. Tropospheric effects such as rain and cloud attenuation and scintillations (with fast variations in the order of milliseconds) can introduce additional time varying phase variations to each sub-channel [38]. Finally, the imperfections and the channel nature result in time varying phase components which are independent across the sub-channels and are incorporated in the channel model as $\theta_{ij}(t)$.

Note that, there are also other components that are identical for all the sub-channels of the i^{th} user and hence do not affect the received SINR. An example of such a component can be phase noise of the LO at receiver front end at UT. Hence, we do not consider such variations in our work. The interested reader is referred to [34, 98] for further details on the various contributors to the time varying phase.

Assume that channel is estimated by the terminals at t_0 and sent back to the GW. At $t_1 \approx t_0 + 250ms$ precoder is designed by the GW and applied to the channel at $t_2 \approx t_1 + 250$. Due to the long RTD in GEO satellite systems and the time varying phase components, the phase of the channel when precoding is applied at $t_2 \approx t_0 + 500ms$ will be different than the phase at t_0, $\boldsymbol{\theta}_i(t_0)$. Since $\theta_{ij}(t_2)$ is the actual phase for the sub-channel $h_{i,j}(t_2)$ and further using $\boldsymbol{\theta}_i(t_2)$, we model the temporal variations as,

$$\boldsymbol{\theta}_i(t_2) = \boldsymbol{\theta}_i(t_0) + \mathbf{e}_i, \tag{5.1}$$

where $\mathbf{e}_i \triangleq [\mathrm{e}_{i1}, \mathrm{e}_{i2}, \ldots, \mathrm{e}_{iK}]^T$ is the phase error, or phase uncertainty, vector with independent identically distributed (i.i.d) Gaussian random entries, $\mathbf{e}_i \sim \mathcal{N}(\mathbf{0}, \delta_i^2\mathbf{I})$. Here, δ_i^2 is the variance of the phase error for the i^{th} user. Note that, in principle,

e_{ik} is zero mean variable and,

$$-(2\pi n+\pi) < \mathrm{e}_{ik} \leq 2\pi n+\pi,\ \forall i,k \in [K],\ n \in \{\mathbb{Z} \geq 0\}, \tag{5.2}$$

This type of variables have *wrapped Gaussian (normal) distribution* [99]. However, in practice, the variance of e_{ik} is very small compared to π, so we can assume that $-\pi << \mathrm{e}_{ik} << \pi$. Therefore, it is acceptable to assume that $\mathbf{e}_i \sim \mathcal{N}(\mathbf{0}, \delta_i^2\mathbf{I})$.

For ease of notation, we define the corresponding channel at t_2 and t_0, respectively as,

$$\mathbf{h}_i \triangleq [|h_{i1}|e^{\mathrm{j}\theta_{i1}(t_2)}, \ldots, |h_{iK}|e^{\mathrm{j}\theta_{iK}(t_2)}]^T, \tag{5.3}$$

$$\widehat{\mathbf{h}}_i \triangleq [|h_{i1}|e^{\mathrm{j}\theta_{i1}(t_0)}, \ldots, |h_{iK}|e^{\mathrm{j}\theta_{iK}(t_0)}]^T. \tag{5.4}$$

Under these notations and assuming that the channel amplitudes are identical at t_2 and t_0, the $K \times 1$ channel fading coefficients from all antenna feeds towards the i^{th} UT at instance t_2 are then given by,

$$\mathbf{h}_i = \widehat{\mathbf{h}}_i \odot \mathbf{q}_i, \tag{5.5}$$

where $\mathbf{q}_i = e^{\mathrm{j}\mathbf{e}_i}$. In (5.5), $\widehat{\mathbf{h}}_i$ is a known channel vector at t_0, but $\mathbf{q}_i$ is a random vector arising out of the phase uncertainty of $\mathbf{e}_i$. The correlation matrix of $\mathbf{q}_i$, denoted by $\mathbf{C}_i$, is assumed to be known and takes the form,

$$\mathbf{C}_i \triangleq \mathbf{E}\{\mathbf{q}_i\mathbf{q}_i^H\} = \mathbf{E}\{\mathbf{Q}_i\}, \tag{5.6}$$

where $\mathbf{Q}_i \triangleq \mathbf{q}_i\mathbf{q}_i^H$. The diagonal elements of $\mathbf{C}_i$ are unity and off-diagonal entries can be found by using the moment generating function of the Gaussian random variable as follows,

$$\begin{aligned}[\mathbf{C}_i]_{lm} &= \mathbf{E}\{[\mathbf{Q}_i]_{lm}\} \\ &= \mathbf{E}\{e^{\mathrm{j}\mathrm{e}_{i,l}}\}\,\mathbf{E}\{e^{-\mathrm{j}\mathrm{e}_{i,m}}\} = e^{-\delta_i^2} \triangleq \rho_i.\end{aligned} \tag{5.7}$$

Having introduced a model for phase uncertainty, we investigate different approaches for robust precoder design.

5.3 Robust Precoder Design

Typical designs assume perfect CSI and design $\mathbf{w}_i$ to optimize a function of SINR_i. However, in the presence of channel uncertainty, SINR_i is a random variable, which cannot be computed at the transmitter for designing $\mathbf{w}_i$. This motivates the robust design approaches considered.

As it was mentioned in Section 5.1, we investigate two approaches, probabilistic and expectation based, to achieve the robustness. In general, precoder design problem can be formulated differently to achieve the different objectives. Power

minimization subject to QoS constraints and fairness among the user are two main objectives for precoder design. In the following sections, considering different robust approaches and objectives, we study robust precoder designs for the channel with phase uncertainty.

Remark 4. *While the current work considers phase uncertainty in the satellite channel, the ensuing analysis can be applied to any downlink channel with phase uncertainty if it can be modeled as* (5.5).

5.3.1 Probabilistic Approach: Power Minimization

An approach to achieve robustness against the channel uncertainty is to design the precoder that can satisfy the QoS requirement on link/service availability. In this case, the precoder ensures that the SINR of each user is greater than a specific chosen threshold, γ_{th}, with probability of α_i. Mathematically, it can be expressed by the constraint $\Pr\{\text{SINR}_i \geq \gamma_{\text{th}}\} \geq \alpha_i$. Considering this approach, a meaningful formulation of the forward-link precoding problem leads to,

$$\begin{aligned} \mathcal{P}: \underset{\mathbf{W}}{\text{minimize}} \quad & \sum_{i=1}^{K} \text{Tr}\left(\mathbf{W}_i\right) \\ \underset{\forall i \in [K]}{\text{subject to}} \quad & \Pr\Big\{ \text{SINR}_i \geq \gamma_{\text{th}} \Big\} \geq \alpha_i, \\ & \Big[\sum_{j=1}^{K} \mathbf{W}_j \Big]_{i,i} \leq P_i, \\ & \mathbf{W}_i \succcurlyeq 0, \, \text{rank}(\mathbf{W}_i) = 1, \end{aligned}$$

where α_i is the required availability for i^{th} user. The objective of this formulation is to minimize the total transmit power while enforcing the constraints on the availability for each user considering the per-antenna power constraints. In the considered full frequency reuse, each antenna has a dedicated amplifier and hence it is meaningful to impose per-antenna power constraint. Here, P_i denotes the maximum transmit power of the i^{th} antenna serving the i^{th} user located in the i^{th} beam.

Equations (7.41) and (2.22) indicate that SINR_i is a random variable due to $\mathbf{q}_i$. A probabilistic approach is then pursued towards evaluating the availability over these random variables. In general, the first constraint is difficult to tackle and we will now study it in more detail.

Let us denote the availability of i^{th} user by $f_i(\mathbf{W})$. Using (7.41) we have,

$$\begin{aligned} f_i(\mathbf{W}) &\triangleq \Pr\Big\{ \text{SINR}_i \geq \gamma_{\text{th}} \Big\}, \\ &= \Pr\Big\{ \text{Tr}(\mathbf{R}_i \mathbf{W}_i) - \gamma_{\text{th}} \sum_{j \neq i} \text{Tr}(\mathbf{R}_i \mathbf{W}_j) \geq \gamma_{\text{th}} N_0 \Big\}. \end{aligned} \tag{5.8}$$

By defining $\mathbf{Z}_i \triangleq \mathbf{W}_i - \gamma_{\text{th}} \sum_{j \neq i} \mathbf{W}_j$, we can write,

$$f_i(\mathbf{W}) = \Pr\Big\{ \operatorname{Tr}(\mathbf{R}_i \mathbf{Z}_i) \geq \gamma_{\text{th}} N_0 \Big\}. \tag{5.9}$$

It is interesting to have an insight on what (5.9) denotes. $\operatorname{Tr}(\mathbf{R}_i \mathbf{Z}_i)$ can be interpreted as the *effective received power*, since it is the difference between a scaled version of the received interference power, $\gamma_{\text{th}} \sum_{j \neq i} \operatorname{Tr}(\mathbf{R}_i \mathbf{W}_j)$, and the useful received power, $\operatorname{Tr}(\mathbf{R}_i \mathbf{W}_i)$. The coefficient γ_{th} in the interference term can be interpreted as the price of having a specific SINR threshold of γ_{th}. This means that for a fixed $\mathbf{W}$, the higher the threshold chosen, the higher will the interference perceived by users be. This results in a lower effective received power. These two competing measures, will affect the feasibility of the problem at high γ_{th}.

For simplicity, let us denote the effective received power by $y_i \triangleq \operatorname{Tr}(\mathbf{R}_i \mathbf{Z}_i)$. Using (2.22) and the fact that $\operatorname{Tr}(\mathbf{XY}) = \operatorname{Tr}(\mathbf{YX})$ [100], we have,

$$y_i = \operatorname{Tr}\Big(\operatorname{diag}(\widehat{\mathbf{h}}_i) \mathbf{Q}_i \operatorname{diag}(\widehat{\mathbf{h}}_i^H) \mathbf{Z}_i \Big) = \operatorname{Tr}(\mathbf{A}_i \mathbf{Q}_i), \tag{5.10}$$

where

$$\mathbf{A}_i = \operatorname{diag}(\widehat{\mathbf{h}}_i^H) \mathbf{Z}_i . \operatorname{diag}(\widehat{\mathbf{h}}_i) \tag{5.11}$$

The following lemma provides the mean and variance of the random variable y_i.

Lemma 1: With $\mathbf{Q}_i$ defined in (5.6) and for any Hermitian matrix $\mathbf{A}_i \in \mathcal{C}^{K \times K}$, the mean and variance of $y_i = \operatorname{Tr}(\mathbf{A}_i \mathbf{Q}_i)$ can be found as

$$\mu_i = \operatorname{Tr}(\mathbf{A}_i \mathbf{C}_i) \tag{5.12}$$

$$\sigma_i^2 = \operatorname{vec}(\mathbf{A}_i^T)^T \mathbf{G}_i \operatorname{vec}(\mathbf{A}_i) \tag{5.13}$$

where

$$\mathbf{G}_i = \mathbf{G}_i' - \operatorname{vec}(\mathbf{C}_i) \operatorname{vec}(\mathbf{C}_i^T)^T$$

with $\mathbf{G}_i' = \mathbf{E}\{\mathbf{Q}_i \otimes \mathbf{Q}_i\}$ and is calculated in Appendix B.

Proof. The mean and variance of y_i can be calculated respectively as follows,

$$\mu_i = \mathbf{E}\{y_i\} = \operatorname{Tr}(\mathbf{A}_i \, \mathbf{E}\{\mathbf{Q}_i\}) = \operatorname{Tr}(\mathbf{A}_i \mathbf{C}_i), \tag{5.14}$$

$$\sigma_i^2 = \mathbf{E}\{(y_i - \mu_i)^2\} = \mathbf{E}\{\operatorname{Tr}(\mathbf{A}_i \mathbf{Q}_i) \operatorname{Tr}(\mathbf{A}_i \mathbf{Q}_i)\} - \mu_i^2. \tag{5.15}$$

The first term in (5.15) can be rewritten as,

$$\mathbf{E}\{\operatorname{Tr}(\mathbf{q}_i^H \mathbf{A}_i \mathbf{q}_i) \operatorname{Tr}(\mathbf{q}_i^H \mathbf{A}_i \mathbf{q}_i)\} = \mathbf{E}\{\mathbf{q}_i^H \mathbf{A}_i \mathbf{q}_i \mathbf{q}_i^H \mathbf{A}_i \mathbf{q}_i\} \tag{5.16}$$

$$= \mathbf{E}\{\operatorname{Tr}(\mathbf{q}_i^H \mathbf{A}_i \mathbf{q}_i \mathbf{q}_i^H \mathbf{A}_i \mathbf{q}_i)\} \tag{5.17}$$

$$= \mathbf{E}\{\operatorname{Tr}(\mathbf{A}_i \mathbf{Q}_i \mathbf{A}_i \mathbf{Q}_i)\} \tag{5.18}$$

$$= \operatorname{vec}(\mathbf{A}_i^H)^H \, \mathbf{E}\{\mathbf{Q}_i^T \otimes \mathbf{Q}_i\} \operatorname{vec}(\mathbf{A}_i). \tag{5.19}$$

We define the $K^2 \times K^2$ matrix $\mathbf{G}'_i = \mathbf{E}\{\mathbf{Q}_i^T \otimes \mathbf{Q}_i\}$. This matrix can be computed using (5.7) and statistical independence of the elements of $\mathbf{q}_i$. More details are provided in Appendix B regarding the calculation of the matrix $\mathbf{G}'_i$.

Now, the variance of y_i can be expressed as,

$$\sigma_i^2 = \mathrm{vec}(\mathbf{A}_i^H)^H \mathbf{G}'_i \,\mathrm{vec}(\mathbf{A}_i) - \mathrm{Tr}(\mathbf{A}_i \mathbf{C}_i)^2 \tag{5.20}$$

Knowing that $\mathrm{Tr}(\mathbf{XY}) = \mathrm{vec}(\mathbf{X}^T)^T \,\mathrm{vec}(\mathbf{Y})$, the second term in (5.20) can be expanded and finally we have,

$$\sigma_i^2 = \mathrm{vec}(\mathbf{A}_i^H)^H \mathbf{G}_i \,\mathrm{vec}(\mathbf{A}_i) \tag{5.21}$$

where

$$\mathbf{G}_i = \mathbf{G}'_i - \mathrm{vec}(\mathbf{C}_i)\,\mathrm{vec}(\mathbf{C}_i^T)^T. \tag{5.22}$$

Since for any $\mathbf{A}_i$, we have $\sigma_i^2 \geq 0$, we can conclude that $\mathbf{G}_i \succeq 0$. □

Writing $y_i = \mathbf{q}_i^{Hger} \mathbf{A}_i \mathbf{q}_i$, it can be shown that y_i is a sum of K dependent random variables, so it is difficult to find its exact PDF. Knowing only the mean and variance of y_i, we need to find an approximation for $\Pr\{y_i \geq \gamma_{\mathrm{th}} N_0\}$. Our approach is to approximate the distribution of y_i by a Gaussian distribution, then evaluate the availability of users. We use a Gaussian approximation for tractability. It is observed that the PDF of y_i has a left hand-side (LHS) tail. Since practically we are interested in a LHS tail, PDF of y_i can be approximated by a Gaussian distribution where both y_i and its Gaussian approximation have LHS tails. The impact of this approximation will be discussed in Section 5.4.

With the Gaussian approximation for y_i and knowing μ_i and σ_i^2, we can evaluate $f_i(\mathbf{W})$ in (5.8). It can be shown that,

$$f_i(\mathbf{W}) \approx \begin{cases} \dfrac{1}{2} + \dfrac{1}{2}\,\mathrm{erf}\left(\dfrac{\mu_i - \gamma_{\mathrm{th}}\, N_0}{\sqrt{2}\sigma_i}\right), & \mu_i \geq \gamma_{\mathrm{th}} N_0 \quad (5.23) \\ \dfrac{1}{2} - \dfrac{1}{2}\,\mathrm{erf}\left(\dfrac{\gamma_{\mathrm{th}}\, N_0 - \mu_i}{\sqrt{2}\sigma_i}\right), & \mu_i < \gamma_{\mathrm{th}} N_0\,. \quad (5.24) \end{cases}$$

Here $\mathrm{erf}(\cdot)$ is the error function. Since user's acceptable availability requirement is at least $\alpha_i > 0.5$ [41], we need $f_i(\mathbf{W}) \geq \alpha_i > 0.5$, and hence only (5.23) will be considered. Clearly, $f_i(\mathbf{W}) \geq \alpha_i$ subsumes $\mu_i \geq \gamma_{\mathrm{th}} N_0$ when $\alpha_i > 0.5$. Then by considering $f_i(\mathbf{W}) \geq \alpha_i$, we can rewrite the availability constraint as,

$$0.5 + 0.5\,\mathrm{erf}\left(\frac{\mu_i - \gamma_{\mathrm{th}} N_0}{\sqrt{2}\sigma_i}\right) \geq \alpha_i. \tag{5.25}$$

After straightforward algebra and using μ_i and σ_i^2 defined in (5.14) and (5.20), the constraint in (5.25) can be expressed as,

$$b_i \sqrt{\mathrm{vec}(\mathbf{A}_i^T)^T \mathbf{G}_i \,\mathrm{vec}(\mathbf{A}_i)} \leq \mu_i - \gamma_{\mathrm{th}} N_0, \tag{5.26}$$

where $b_i = \sqrt{2}\,\mathrm{erf}^{-1}(2\alpha_i - 1)$ and $b_i > 0$. Finally, (5.26) can be rewritten as,

$$b_i \|\mathbf{G}_i^{\frac{1}{2}} \mathrm{vec}(\mathbf{A}_i)\| \leq \mathrm{Tr}(\mathbf{A}_i\mathbf{C}_i) - \gamma_{\mathrm{th}} N_0, \tag{5.27}$$

We can show that (5.27) is a convex constraint, since it is an inverse image of the second-order cone,

$$S = \{(\mathbf{x}, z) |\ \|\mathbf{x}\| \leq z,\ z \geq 0\}, \tag{5.28}$$

under the affine transformation $\mathbf{x} = \sqrt{b_i}\mathbf{G}_i^{\frac{1}{2}} \mathrm{vec}(\mathbf{A}_i)$ and $z = \mathrm{Tr}(\mathbf{A}_i\mathbf{C}_i) - \gamma_{\mathrm{th}} N_0$. Note that from (5.23) where $\alpha_i > 0.5$, we have $z \geq 0$. Hence, in $\mathcal{P}$, the only non-convex constraint is $\mathrm{rank}(\mathbf{W}_i) = 1$. However, this can be relaxed by retaining only the semidefiniteness constraint, $\mathbf{W}_i \succcurlyeq 0$, which is convex [47]. Under this relaxation, the variables of the optimization problem would be $\{\mathbf{W}_i\}_1^K$. Then per-antenna power constraints will also be convex. By replacing the availability constraint in $\mathcal{P}$ with the one in (5.27), the resulting optimization problem can be written as,

$$\begin{aligned}
\mathcal{P}_1 :\ \underset{\mathbf{W}}{\text{minimize}}\ & \sum_{i=1}^{K} \mathrm{Tr}(\mathbf{W}_i) \\
\underset{\forall i \in [K]}{\text{subject to}}\ & b_i \|\mathbf{G}_i^{\frac{1}{2}} \mathrm{vec}(\mathbf{A}_i)\| \leq \mathrm{Tr}(\mathbf{A}_i\mathbf{C}_i) - \gamma_{\mathrm{th}} N_0 \\
& \Big[\sum_{j=1}^{K} \mathbf{W}_j\Big]_{i,i} \leq P_i\,,\ \mathbf{W}_i \succcurlyeq 0.
\end{aligned}$$

This optimization problem can be solved by using convex solvers like CVX [59,73].

We denote the resulting precoding matrix of $\mathcal{P}_1$ by $\mathbf{W}^\star = [\mathbf{w}_1^\star, \cdots, \mathbf{w}_K^\star]$ where $\mathbf{w}_i^\star$ is the precoding vector for the i^{th} user. Note that the solution to $\mathcal{P}_1$ can yield high rank $\{\mathbf{W}_i\}_1^K$. In such situations, rank-one approximation techniques [54] need to be employed. Additional details are provided in Section 5.4 regarding the solution of the optimization problem and rank-one approximation techniques. It should be noted that the rank-one relaxed problem, $\mathcal{P}_1$, is equivalent to $\mathcal{P}$ if it is possible to find a rank-one solution for $\mathcal{P}_1$.

5.3.2 Probabilistic Approach: Max-Min Fairness

In this part, unlike the previous section, the goal is to maximize a utility function $f(\mathbf{W})$ which should be a strictly increasing function of $\{f_i(\mathbf{W})\}_1^K$. Recall that $f_i(\mathbf{W})$ is defined in (5.8). A function that considers the fairness in the sense of availability among the users is $f(\cdot) = \min(\cdot)$. By defining this function, the objective is to maximize the minimum of the availabilities subject to per-antenna power constraints. This formulation is also known as max-min fairness problem. The motivation behind this formulation can be the need for having the highest possible

QoS, considering the fairness among the users and per antenna power constraints. The optimization problem can be written as,

$$\begin{aligned} \mathcal{F}: \underset{\mathbf{W}}{\text{maximize}} \quad & \min\{f_1(\mathbf{W}), \ldots, f_K(\mathbf{W})\} \\ \underset{\forall i \in [K]}{\text{subject to}} \quad & \left[\sum_{j=1}^{K} \mathbf{W}_j\right]_{i,i} \leq P_i, \\ & \mathbf{W}_i \succcurlyeq 0, \, \text{rank}(\mathbf{W}_i) = 1. \end{aligned}$$

A first step towards solving $\mathcal{F}$ is to characterize the objective function and the same is undertaken in the following Lemma.

Lemma 2: With the Gaussian approximation for y_i, $f(\mathbf{W})$ is a quasiconcave function of $\mathbf{W}$.

Proof. Under the Gaussian assumption on y_i, we can show that $f_i(\mathbf{W})$ is a quasiconcave function, since its superlevel set $\{(\mathbf{x}, z) \,|\, f_i(\mathbf{W}) \geq \tau\}$ is convex as was shown in (5.27) and (5.28) (with α_i being replaced by τ). Also, we observe that the minimum of quasiconcave functions, is quasiconcave [59]. Therefore,

$$f(\mathbf{W}) = \min\{f_1(\mathbf{W}), f_2(\mathbf{W}), \ldots, f_K(\mathbf{W})\}$$

is a quasiconcave function. □

Hence, we can find the solution of the optimization problem $\mathcal{F}$ by solving the following feasibility problem,

$$\begin{aligned} \mathcal{F}_1(\tau): \quad & \text{find} \quad \mathbf{W} \\ \underset{\forall i \in [K]}{\text{subject to}} \quad & f(\mathbf{W}) \geq \tau, \\ & \left[\sum_{j=1}^{K} \mathbf{W}_j\right]_{i,i} \leq P_i, \\ & \mathbf{W}_i \succcurlyeq 0, \, \text{rank}(\mathbf{W}_i) = 1, \end{aligned}$$

where τ is a constant and a procedure for finding its optimal value will be discussed later. It is straightforward to show that the first constraint in $\mathcal{F}_1(\tau)$ is equivalent to $f_i(\mathbf{W}) \geq \tau$, $\forall\, i \in [K]$. Then, $f_i(\mathbf{W}) \geq \tau$ can be written similar to (5.27). Finally, by dropping the rank-one constraint, the relaxed optimization problem can be written as,

$$\begin{aligned} \mathcal{F}_2(\tau): \text{find} \quad & \mathbf{W} \\ \underset{\forall i \in [K]}{\text{subject to}} \quad & b_i \|\mathbf{G}_i^{\frac{1}{2}} \text{vec}(\mathbf{A}_i)\| \leq \text{Tr}(\mathbf{A}_i \mathbf{C}_i) - \gamma_{\text{th}} N_0, \\ & \left[\sum_{j=1}^{K} \mathbf{W}_j\right]_{i,i} \leq P_i, \; \mathbf{W}_i \succcurlyeq 0. \end{aligned}$$

Algorithm 1: Bisection Method for the quasiconcave optimization problem $\mathcal{F}_2(\tau)$

initialize l, u, tolerance $\epsilon > 0$;
while $l - u > \epsilon$ **do**
  $t \leftarrow (u + l)/2$;
  Solve the feasibility problem $\mathcal{F}_2(\tau)$ using CVX ;
  if $\mathcal{F}_2(\tau)$*is feasible* **then**
    $l \leftarrow \tau$;
  else
    $u \leftarrow \tau$;
  end
end
$\tau^\star \leftarrow l$ and $\mathbf{W}^\star = \mathcal{F}_2(\tau^\star)$

where $b_i = \sqrt{2}\,\mathrm{erf}^{-1}(2\tau - 1)$. This is a feasibility problem and the optimal solution can be found by using the bisection method [59] and CVX tool [73]. Again, it is possible that $\mathcal{F}_2(\tau)$ yields non unity rank solutions. In Section 5.4, we will discuss how to extract a rank-one solution from a high rank solution.

Remark 5. *Problems $\mathcal{F}_1(\tau)$ and $\mathcal{F}_2(\tau)$ are dependant on τ. However, by iteratively solving $\mathcal{F}_2(\tau)$ to obtain the highest feasible τ, using the bisection method, we can find the solution of $\mathcal{F}(\tau)$.*

It only remains to find the optimal value of τ to solve $\mathcal{F}_2(\tau)$. Towards this, we assume that the optimal value of τ is in the interval of $[l, u]$ and is denoted by $\tau^\star$ while the corresponding optimal precoding matrices are denoted by $\mathbf{W}^\star = \mathcal{F}_2(\tau^\star)$. In Algorithm 1, the bisection method for finding the optimal value, $\tau^\star$, is explained. As was indicated in Section 5.3.1, an acceptable value for user's availability is greater than 0.5. Therefore, we can assume $1 > \tau^\star > 0.5$. Then, the appropriate values for l and u would be 0.5 and 1, respectively. The idea of Algorithm 1 is to search for the optimal point by iteratively bisecting the interval $[l, u]$. At each iteration, the midpoint of the interval is checked for feasibility. If $\mathcal{F}_2(\tau)$ is feasible, the optimal point is in the upper half of the interval, else it is in the lower half. Then the values of u and l are updated to search in an appropriate interval. This process is repeated until the searching interval gets small enough, $u - l < \epsilon$.

5.3.3 Expectation Based Approach: Power Minimization

In this section, an expectation based approach will be discussed where the robustness is achieved by defining the required QoS goals based on the average performance of the system. Since the average SINR of the users is closely related to the average performance of the system, it defines another QoS measure. To this end, the precoder is designed to satisfy the requirement on the average SINR, with $\mathbf{E}\{\mathrm{SINR}_i\} \geq \gamma_{\mathrm{th}}$, where expectation is over the random $\mathbf{q}_i$.

Following this robust approach, the power minimization precoding formulation can be written as,

$$\begin{aligned}\mathcal{G}: \underset{\mathbf{W}}{\text{minimize}} \quad & \sum_{i=1}^{K} \text{Tr}(\mathbf{W}_i) \\ \underset{\forall i \in [K]}{\text{subject to}} \quad & \mathbf{E}\{\text{SINR}_i\} \geq \gamma_{\text{th}}, \\ & \left[\sum_{j=1}^{K} \mathbf{W}_j\right]_{i,i} \leq P_i, \\ & \mathbf{W}_i \succcurlyeq 0, \, \text{rank}(\mathbf{W}_i) = 1.\end{aligned}$$

The objective of this optimization problem is to minimize the total transmit power subject to satisfying the required average SINR for each user considering the per-antenna power constraint for each antenna feed.

In general, it is difficult to evaluate the exact value of $\mathbf{E}\{\text{SINR}_i\}$, since the expectation of SINR_i over $\mathbf{q}_i$ is intractable We use an approximation for SINR_i denoted by SINR'_i where the received signal and interference power are replaced by their expected values [101, 102]. Then, SINR'_i can be expressed as,

$$\text{SINR}'_i \triangleq \frac{\mathbf{E}\left\{\text{Tr}(\mathbf{R}_i \mathbf{W}_i)\right\}}{\mathbf{E}\left\{\sum_{j \neq i} \text{Tr}(\mathbf{R}_i \mathbf{W}_j)\right\} + N_0}. \tag{5.29}$$

However, further exploitation of the results in [101,102] is difficult due to the differences in the modeling assumptions. Fortunately, numerical evaluations show that SINR'_i is a tight lower bound on $\mathbf{E}\{\text{SINR}_i\}$. Therefore, if the precoding matrices satisfy the constraint $\text{SINR}'_i \geq \gamma_{\text{th}}$, then they can also satisfy the constraint $\mathbf{E}\{\text{SINR}_i\} \geq \gamma_{\text{th}}$. So, we can replace the constraint on the average SINR in $\mathcal{G}$ by the stricter constraint $\text{SINR}'_i \geq \gamma_{\text{th}}$.

Remark 6. *Note that the constraint in* (5.29) *can also be interpreted as the result of using long-term (averaging over phase noise) channel correlation matrix,* $\boldsymbol{E}\{\mathbf{R}_i\}$*, instead of instantaneous* $\mathbf{R}_i$ *to achieve the robustness.*

After the expectation operation, the constraint $\text{SINR}'_i \geq \gamma_{\text{th}}$ can be rewritten as,

$$\text{Tr}(\mathbf{A}_i \mathbf{C}_i) - \gamma_{\text{th}} N_0 \geq 0, \tag{5.30}$$

where $\mathbf{A}_i$ and $\mathbf{C}_i$ are defined in (5.10) and (5.6), respectively. This is a convex (affine in $\mathbf{W}_i$) constraint and the effect of the phase uncertainty is reflected in $\mathbf{C}_i$.

It is interesting to relate the probabilistic and expectation based approaches.

Remark 7. *The constraint in* (5.30) *can be obtained directly from the availability constraint in* (5.27) *by assuming* $b_i = 0$.

This happens when $\alpha_i = 0.5$. In this case, by using (5.25) we can show that the constraint,

$$\Pr\{\text{SINR}_i \ \geq \ \gamma_{\text{th}}\} \geq 0.5, \tag{5.31}$$

is equivalent to the constraint $\text{SINR}_i' \geq \gamma_{\text{th}}$. We can rewrite the constraint in (5.27) as,

$$\text{Tr}(\mathbf{A}_i\mathbf{C}_i) - \gamma_{\text{th}}N_0 \geq b_i\sigma_i \geq 0. \tag{5.32}$$

From this expression, we can observe that for $\alpha_i > 0.5$, the availability constraint (5.32) is stricter than (5.30).

As discussed in Section 5.3.2, the rank-one constraint can be relaxed towards reducing $\mathcal{G}$ to a convex optimization problem. Finally, the expectation based robust optimization problem can be written as,

$$\begin{aligned} \mathcal{G}_1 : \underset{\mathbf{W}}{\text{minimize}} \quad & \sum_{i=1}^{K} \text{Tr}(\mathbf{W}_i) \\ \underset{\forall i \in [K]}{\text{subject to}} \quad & \text{Tr}(\mathbf{A}_i\mathbf{C}_i) - \gamma_{\text{th}}N_0 \geq 0, \\ & \Big[\sum_{j=1}^{K} \mathbf{W}_j\Big]_{i,i} \leq P_i,\ \mathbf{W}_i \succcurlyeq 0. \end{aligned}$$

This is a convex optimization problem and can be solved by using standard convex solvers like CVX [73]. Let us denote the optimal solutions by $\mathbf{W}_i^\star$. We provide more details about the rank of the solutions of $\mathcal{G}_1$.

Remark 8. *We can write the optimization problem $\mathcal{G}_1$ as a separable SDP problem [103].*

Using the results of [103] for separable SDP problems, we can show that for optimal solution of $\mathcal{G}_1$, the following bound holds,

$$\sum_{i=1}^{K} \text{rank}^2(\mathbf{W}_i^\star) \leq 2K, \tag{5.33}$$

where $2K$ is the number of constraints in $\mathcal{G}_1$. If we denote the number of rank-one solutions by η, then at least the following should hold,

$$\eta + 4(K - \eta) \leq 2K, \tag{5.34}$$

which results in $\eta \geq \frac{2K}{3}$. This means that at least $\frac{2K}{3}$ of $\{\mathbf{W}_i^\star\}$ will be rank-one for $\mathcal{G}_1$. Also note that since the total power is minimized in $\mathcal{G}_1$, in practice some of the per-antenna power constraints will not be active. Therefore, based on (5.33), the fewer the number of active constraints, the higher the number of rank one solutions.

5.3.4 Expectation Based Approach: Max-Min Fairness

This section briefly studies the problem of maximizing the minimum of SINR'_is subject to per-antenna power constraints where the fairness among the users is considered. To this end, similar to the formulation used in Section 5.3.2, we take advantage of the max-min formulation and form the robust design problem as,

$$\begin{aligned} \mathcal{E}: \ \underset{\mathbf{W}}{\text{maximize}} \quad & \min\{\text{SINR}'_1, \ldots, \text{SINR}'_K\} \\ \underset{\forall i \in [K]}{\text{subject to}} \quad & \left[\sum_{j=1}^{K} \mathbf{W}_j\right]_{i,i} \leq P_i, \\ & \mathbf{W}_i \succcurlyeq 0, \ \text{rank}(\mathbf{W}_i) = 1. \end{aligned}$$

We can show that SINR'_i is a quasiconcave function of $\mathbf{W}$ since $\text{SINR}'_i \geq \upsilon$ is a convex constraint for any constant υ as was seen in (5.30). Similar to the approach used in Section 5.3.2, corresponding feasibility problem can be deduced as,

$$\begin{aligned} \mathcal{E}_1(\upsilon): \ \text{find} \quad & \mathbf{W} \\ \underset{\forall i \in [K]}{\text{subject to}} \quad & \text{SINR}' \geq \upsilon, \\ & \left[\sum_{j=1}^{K} \mathbf{W}_j\right]_{i,i} \leq P_i, \\ & \mathbf{W}_i \succcurlyeq 0, \text{rank}(\mathbf{W}_i) = 1, \end{aligned}$$

where

$$\text{SINR}' = \min\{\text{SINR}'_1, \ldots, \text{SINR}'_K\}. \tag{5.35}$$

The constraint $\text{SINR}' \geq \upsilon$ is equivalent to $\text{SINR}'_i \geq \upsilon$, $\forall i \in [K]$. Then, by using (5.30) and relaxing the rank constraint, $\mathcal{E}_1(\upsilon)$ can be rewritten as,

$$\begin{aligned} \mathcal{E}_2(\upsilon): \ \text{find} \quad & \mathbf{W} \\ \underset{\forall i \in [K]}{\text{subject to}} \quad & \text{Tr}(\mathbf{A}_i \mathbf{C}_i) - \upsilon N_0 \geq 0, \\ & \left[\sum_{j=1}^{K} \mathbf{W}_j\right]_{i,i} \leq P_i, \mathbf{W}_i \succcurlyeq 0. \end{aligned}$$

The optimal value of υ in the feasibility problem $\mathcal{E}_2(\upsilon)$ can be found by using the Algorithm 1 and CVX. For this purpose, τ and $\mathcal{F}_2$ in Algorithm 1 should be replaced by υ and $\mathcal{E}_2$, respectively.

A summary of the different formulations and approaches has been provided in Table 5.1 in order to have a better overview.

Table 5.1. Summary of different Formulations and Approaches

	Power Minimization	Max-Min Fairness
Probabilistic	$\mathcal{P}_1$	$\mathcal{F}_2(\tau)$
Expectation Based	$\mathcal{G}_1$	$\mathcal{E}_2(\upsilon)$

Table 5.2. Ratio of rank-one solutions to feasible solutions in 1000 realizations

Uncertainty	$\sigma_i = 5^\circ$		$\sigma_i = 10^\circ$	
γ_{th}	4dB	7dB	4dB	7dB
$\mathcal{P}_1$ ($\alpha_i = 90\%$)	841/841	396/396	627/627	129/129
$\mathcal{F}_2(\tau)$	82/866	184/465	265/772	228/268
$\mathcal{G}_1$	872/872	494/494	791/791	291/291
$\mathcal{E}_2(\upsilon)$	827/1000		719/998	

5.4 Numerical Results and Discussion

In this section, we investigate the performance of the proposed robust precoders through numerical evaluations. We generate 1000 random realizations of the user locations within each of the 7 beams, where users are uniformly distributed within the beam, each having a diameter of 500km. Then, we find the corresponding channel vector for each user based on the model described in Section 2. The link budget and system parameters are given in Table 2.2. As it was shown in Figure 2.3, the first tier of 7 beams is considered.

We assume that a single user per beam is served in each transmission slot; therefore in total 7 users are targeted in each precoded signal. Here, it is assumed that a single user is selected *randomly* from each beam to make a group of 7 users, and the precoding matrix is subsequently designed; the impact of user scheduling is left for future work.

After generating the channel realizations, all the optimization problems discussed in Section 5.3 are solved. For optimization problems $\mathcal{F}_2$ and $\mathcal{E}$, parameters l and u are chosen equal to the SNRs corresponding to the lowest and the highest supported ModCods, respectively. Therefore, based on DVB-S2 ModCods [104], we have $l = -2.72$dB and $u = 16.2$dB and DVB-S2x has extended both these limits [35].

Let $\mathbf{W}^\star = \{\mathbf{W}_1^\star, \ldots, \mathbf{W}_K^\star\}$ denote the solution of the rank-one relaxed optimization problem. If $\mathbf{W}_i^\star$ is rank-one, then we can write $\mathbf{W}_i^\star = \mathbf{w}_i^\star \mathbf{w}_i^{\star H}$ where $\mathbf{w}_i^\star$ is the optimal solution. On the other hand, if the rank of $\mathbf{W}_i^\star$ is larger than one,

then we have to extract a rank-one solution from $\mathbf{W}_i^\star$ [54]. Let

$$r_i = \text{rank}(\mathbf{W}_i^\star), \tag{5.36}$$

$$\mathbf{W}_i^\star = \sum_{j=1}^{r_i} \lambda_{ij} \boldsymbol{\omega}_{ij} \boldsymbol{\omega}_{ij}^H, \tag{5.37}$$

where $\lambda_{i1} \geq \lambda_{i2} \geq \dots \lambda_{ir_i}$ are the eigenvalues of $\mathbf{W}_i^\star$ and $\boldsymbol{\omega}_{ij}$ are the corresponding eigenvectors. We define a rank merit for matrix $\mathbf{W}_i^\star$ by

$$\text{RM}_i = \frac{\lambda_{i1}}{\sum_{j=1}^{r_i} \lambda_{ij}}. \tag{5.38}$$

Numerically, we declare that $\{\mathbf{W}_i^\star\}$ is rank-one if it satisfies the following condition [43],

$$\text{RM}_i \geq 0.9999, \quad \forall i \in [K]. \tag{5.39}$$

Table 5.2 shows the ratio of rank-one solutions for different formulations. In this table, the numerators of the fractions are the number of the rank-one solutions and the denominators are the number of feasible solution obtained using CVX for 1000 sample runs. Interestingly, it can be observed that the power minimization approaches, $\mathcal{P}_1$ and $\mathcal{G}_1$, yield rank-one solutions for all feasible instances in 1000 realizations. Hence, associated rank-one solutions can be simply found as $\mathbf{w}_i^\star = \sqrt{\lambda_{i1}}\boldsymbol{\omega}_{i1}$.

For the max-min problems, $\mathcal{F}_2(\tau)$ and $\mathcal{E}_2(\upsilon)$, it can be observed in Table 5.2 that the solutions are not always rank-one considering the condition in (5.39). However, in all non rank-one examples the rank merit of the $\mathbf{W}_i^\star$ was greater than 0.989. Hence, $\sqrt{\lambda_{i1}}\boldsymbol{\omega}_{i1}$ was used as a suboptimal solution while the SINR_i' constraints were never violated by more than 0.29%. Note that $\lambda_i \boldsymbol{\omega}_{i1} \boldsymbol{\omega}_{i1}^{Hger}$ is the best rank-one approximation of $\mathbf{W}_i^\star$ in the least two-norm sense [54].

Fig. 5.1 shows the feasibility rate of the different optimization problems for 1000 channel realizations. The feasibility rate is the number of the feasible realizations (solvable instances of the optimization problem) divided by the total number of realizations. For the power minimization probabilistic approach (problem $\mathcal{P}_1$) the feasibility rate is calculated for the availability of 90%. As an example, consider the problem $\mathcal{P}_1$ where $\sigma = 5^\circ$. For $\gamma_{\text{th}} = 6$dB, it can be seen that the designed robust precoder can guarantee for almost 60% of the realization (users), it can provide SINR greater than 6dB for 90% of times (or with probability of 0.9). As expected, by increasing the phase uncertainty to $\sigma = 10^\circ$, the feasibility rate decreases. As it can be seen, for the same γ_{th}, the feasibility rate of $\mathcal{F}_2$ is higher than $\mathcal{P}_1$. This is because of the fact that the availability of users in $\mathcal{F}_2$ is not forced to be higher than 90% as in $\mathcal{P}_1$.

Also, the feasibility rate of the problem $\mathcal{G}_1$ is shown. It can be seen that among the two power minimization approaches, $\mathcal{G}_1$ and $\mathcal{P}_1$, the former has a higher feasibility rate. This is because of the fact that the availability constraint in $\mathcal{P}_1$ is stricter than constraint $\text{SINR}_i' \geq \gamma_{\text{th}}$, as it was discussed in Section 5.3.3.

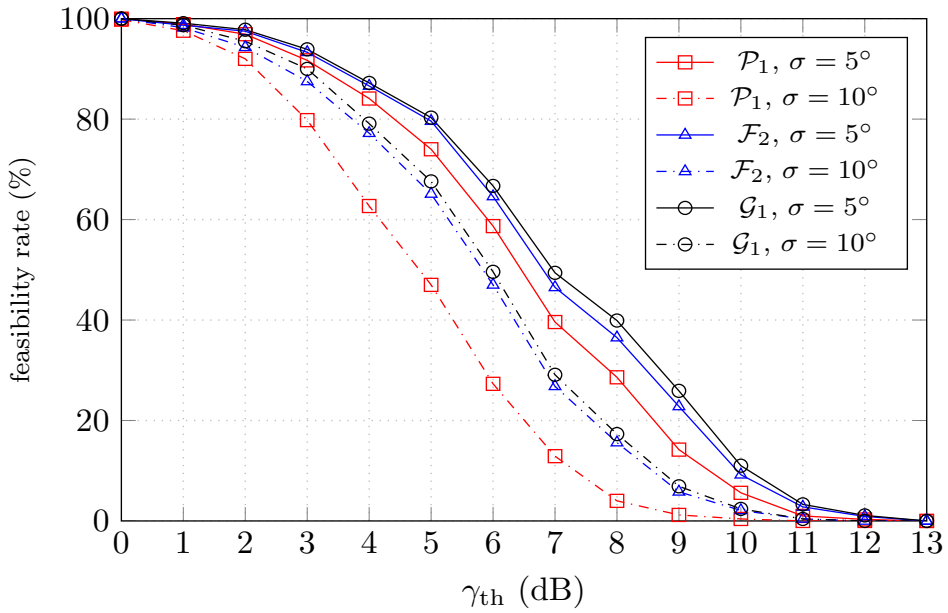

Figure 5.1. Feasibility rate of different optimization problems for 1000 channel realizations

We denote the number of feasible realizations by N_f and availability of users in n^{th} feasible realization by $f_i^{(n)}(\mathbf{W})$. Then we define the average system availability as

$$\bar{f}(\mathbf{W}) = \frac{1}{KN_f} \sum_{n=1}^{N_f} \sum_{i=1}^{K} f_i^{(n)}(\mathbf{W}) \tag{5.40}$$

where K is number of co-channel users in one transmission slot (number of beams). Fig. 5.2 shows the average availability of all users for 1000 realizations. It can been seen that for the problem $\mathcal{P}_1$, the average availability for different γ_{th} is close to the required availability of $\alpha_i = 90\%$. Note that, due to the approximation, the obtained solution differs slightly from the desired availability. On the other hand, the formulation $\mathcal{F}_2$ provides higher availability at lower SINRs. As expected, the achieved average availability decreases, as γ_{th} increases.

Fig. 5.3 shows the average (over feasible realizations) total transmitted power for the different formulation. It is observed that the formulation $\mathcal{P}_1$ is efficient in the sense of transmitted power and by increasing γ_{th}, the average transmitted power increases. In $\mathcal{P}_1$, a higher phase uncertainty leads to higher transmitted power to achieve 90% availability. As it can be seen, the formulation $\mathcal{F}_2$ requires more power than $\mathcal{P}_1$. An important observation is that, for the high γ_{th}, although $\mathcal{F}_2$ is using

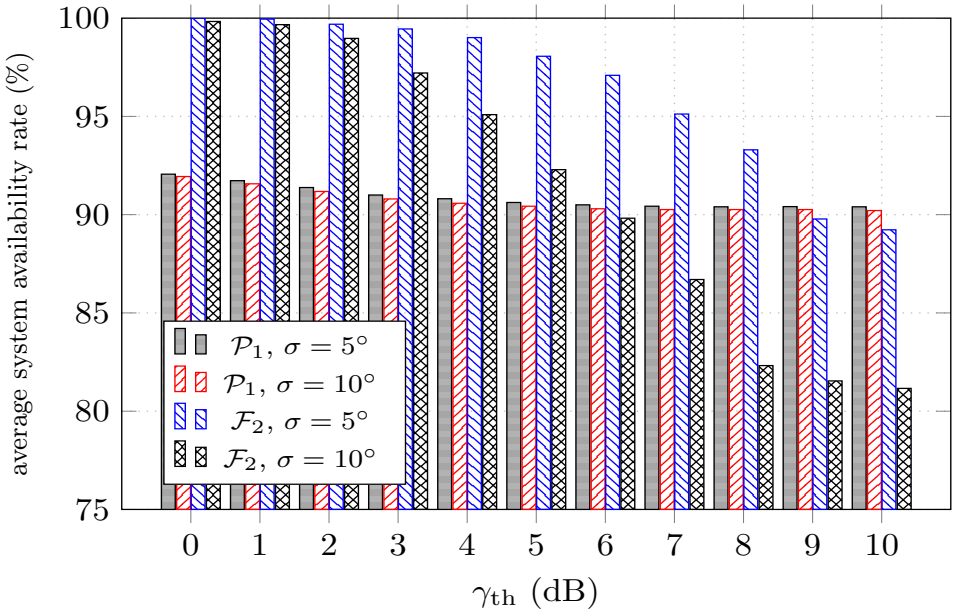

Figure 5.2. Average Availability of users for different optimization problems

more power than $\mathcal{P}_1$ but its average availability is lesser than that for $\mathcal{P}_1$ (kindly refer to Fig. 5.2). The reason is that in $\mathcal{F}_2$, we do not have a constraint to satisfy availability of 90%, so users with bad channel condition will be considered for being served. These users will require high power but will still have low availability which affects the average performance of the system. This also explains the observation in Fig. 5.3 that for $\mathcal{F}_2$ in high γ_{th} regime, $\sigma_i = 5°$ needs more power than the case $\sigma_i = 10°$. It can also be observed that for the same γ_{th}, both $\mathcal{P}_1$ and $\mathcal{G}_1$ require almost the same average total transmit power.

Fig. 5.4 and Fig. 5.5 show the results for formulation $\mathcal{E}_2(\upsilon)$. Fig. 5.4 depicts the distribution of υ for $\sigma_i = 5°$ and $\sigma_i = 10°$. It can be seen that by decreasing the amount of the uncertainty, distribution of υ is shifted to the right, which means that probability of having a higher υ is increased. For $\sigma_i = 10°$ and $\sigma_i = 5°$, the average υ are 4.3dB and 5.8dB, respectively. Fig. 5.5 shows the distribution of the total transmit power. It is observed that when $\sigma_i = 5°$, more power is transmitted compared to the case of $\sigma_i = 10°$. This can be explained by having look at Fig. 5.4. When there is less uncertainty, the transmitter can use more power in order to provide higher υ.

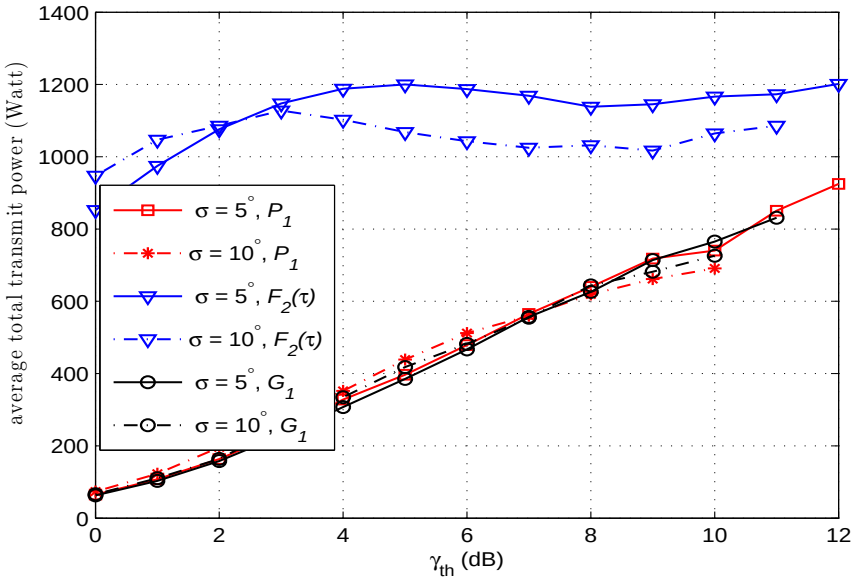

Figure 5.3. Dependence of Average Total Transmit power on the Threshold γ_{th} for availability of $\alpha_i = 90\%$.

5.5 Summary

While multibeam satellite systems with full frequency reuse provide an ideal application for introducing and exploiting precoding techniques, the precoder design must take practical limitations into account. This chapter considers the impact of phase uncertainty resulting from time-varying phase components and long RTD on precoding. This uncertainty is modeled as a random process and constraints are imposed on the availability and average SINR of the users to render the precoder robust to phase variations. For each of these QoS requirements, probabilistic and expectation based approaches to the design of the precoder are pursued leading to 4 different precoder designs. The choice of different QoS requirements and different approaches provide flexibility to the system designer. The resulting optimization problems are formulated and solved using convex optimization techniques. Numerical evaluations illustrate the detrimental effect of phase uncertainty and vindicate the need for robust designs by showing that the pursued designs achieve the required QoS requirements. This would further accelerate the proliferation of precoding in the satellite community.

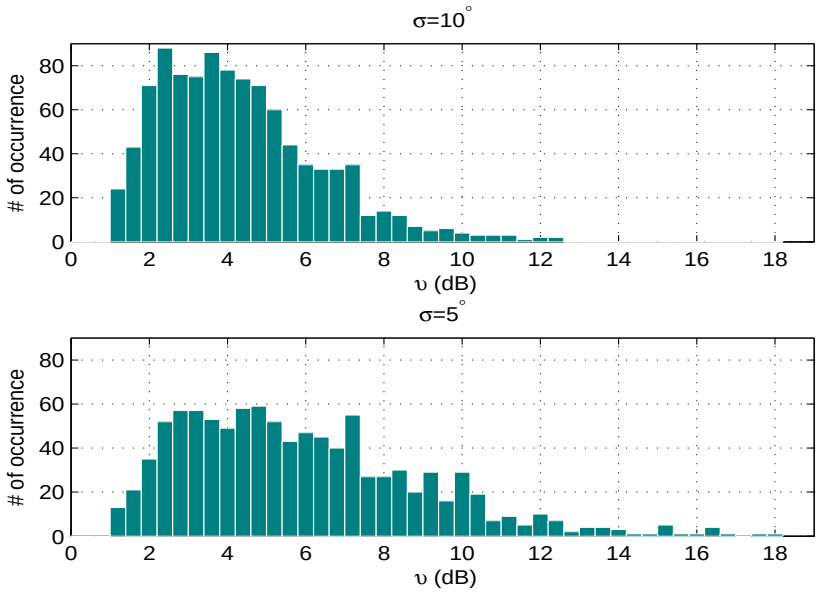

Figure 5.4. Distribution of υ(i.e. the solution of $\mathcal{E}_2(\upsilon)$) in 1000 iterations.

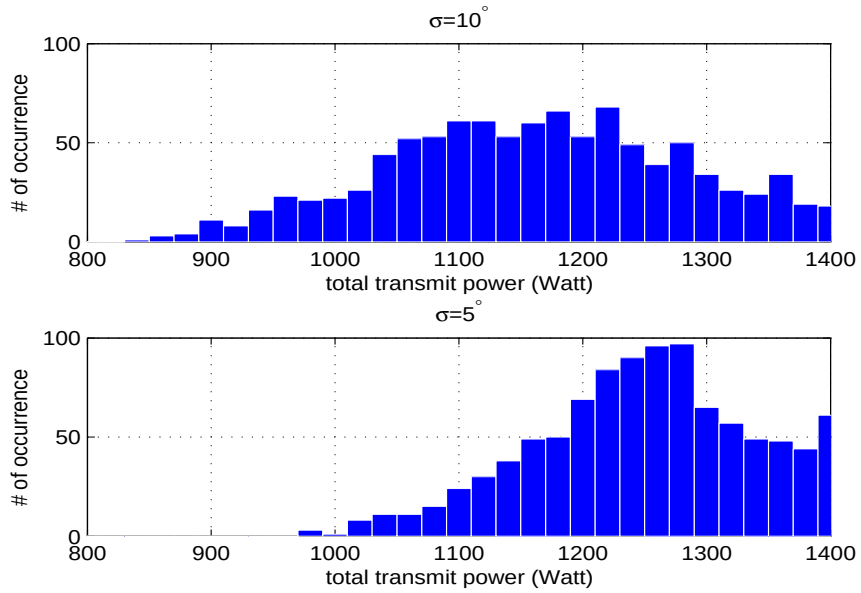

Figure 5.5. Distribution of the total transmit power for $\mathcal{E}_2(\upsilon)$ in 1000 iterations.

Chapter 6

An Iterative Approach to Nonconvex QCQP with Applications in Signal Processing

6.1 Introduction

Nonconvex QCQP is an important class of optimization problems that can be formulated as,

$$\begin{aligned} \mathcal{P}: \min_{\mathbf{x}\in\mathbb{C}^N} \quad & \mathbf{x}^H\mathbf{A}_0\mathbf{x} \\ \text{s. t.} \quad & \mathbf{x}^H\mathbf{A}_i\mathbf{x} \leq c_i, \quad \forall i \in [M], \end{aligned} \tag{6.1}$$

where $\mathbf{A}_0$ and $\mathbf{A}_i$ are Hermitian matrices for all $i \in [M]$, M denotes the number of quadratic constraints, and $c_i \in \mathbb{R}$.

Herein, we are interested in *a subclass of nonconvex* QCQP problems with *convex* objective and *nonconvex* constraints, $\mathbf{A}_0$ is a positive definite (PD) matrix and $\mathbf{A}_i$ are Hermitian matrices with at least one negative eigenvalues [46]. This class of nonconvex QCQP problems captures many problems that are of interest to the signal processing and communications community such as beamforming design [47–49], radar optimal code design [50–53], multiple-input multiple-output (MIMO) and multiuser estimation and detection [54], as well as phase retrieval [55, 56]. The application is also extended to other domains such as portfolio risk management in financial engineering [57]. Nonconvex QCQP is known to be an NP-hard problem, i.e. at least as hard NP-complete problems which are particularly deemed by optimization community to be difficult [58].

Due to its wide area of application, the nonconvex QCQP problem has been studied extensively in the optimization and signal processing literature. The NP-hardness of the problem has motivated the search for various efficient approaches to solve $\mathcal{P}$ including those based on the *semidefinite relaxation* (SDR) [54, 59], the *reformulation linearization technique* (RLT) [60, 61], and the *successive convex approximation* (SCA) [62–64]. Recently a variant of SCA known as *feasible point pursuit-successive convex approximation (FPP-SCA)* has also been proposed in [65].

To the best of our knowledge, SDR is yet the most prominent and widely–used technique employed for tackling nonconvex QCQP.

Note that $\mathcal{P}$ in (6.1) includes several class of widely known optimization problems including *binary quadratic programming* (BQP) where,

$$\mathbf{A}_i = \mathbf{e}_i\mathbf{e}_i^T, \quad \mathbf{x} \in \mathbb{R}^N, \tag{6.2}$$

and *unimodular quadratic programming* (UQP) [105] where

$$\mathbf{A}_i = \mathbf{e}_i\mathbf{e}_i^T, \quad \mathbf{x} \in \mathbb{C}^N. \tag{6.3}$$

6.2 Problem Reformulation

We begin our reformulation by rewriting $\mathcal{P}$ in an equivalent form. We can assume, without loss of generality, that $c_i \neq 0$; otherwise $\mathcal{P}$ will have a trivial solution of $\mathbf{x} = 0$ or it will be infeasible. Since $\mathbf{A}_0$ is a PD matrix, using the change of parameters by

$$\mathbf{A}_i \;\leftarrow\; \left(\mathbf{A}_0^{-\frac{1}{2}}\mathbf{A}_i\mathbf{A}_0^{-\frac{1}{2}}\right)/c_i, \tag{6.4}$$

and $\mathbf{x} \leftarrow \mathbf{A}_0^{\frac{1}{2}}\mathbf{x}$, the nonconvex QCQP of interest may be recast as,

$$\begin{aligned} \mathcal{P}_1 : \min_{\mathbf{x}\in\mathbb{C}^N} \quad & \|\mathbf{x}\|^2 \\ \text{s. t.} \quad & \mathbf{x}^H\mathbf{A}_i\mathbf{x} \lhd_i 1, \quad \forall i \in [M], \end{aligned} \tag{6.5}$$

with $\mathbf{A}_i$ being Hermitian matrices. Here " $\lhd_i$ " can represent any of " $\geq$ ", " $\leq$ " or " $=$ " for each i.

Now, let us define $\mathbf{x} = \sqrt{p}\,\mathbf{u}$, where $p \in \mathbb{R}^+$ and $\mathbf{u} \in \mathbb{C}^N$ is a unit norm vector. Then, (6.5) can be written as,

$$\begin{aligned} \mathcal{P}_1 : \min_{\mathbf{u},p} \quad & p \\ \text{s. t.} \quad & \mathbf{u}^H\mathbf{A}_i\mathbf{u} \lhd_i \frac{1}{p}, \quad \forall i \in [M], \\ & \|\mathbf{u}\|^2 = 1. \end{aligned} \tag{6.6}$$

Let us define $q = 1/p$, then $\mathcal{P}_1$ can be rewritten as,

$$\begin{aligned} \mathcal{P}_1 : \max_{\mathbf{u},q} \quad & q \\ \text{s. t.} \quad & \mathbf{u}^H\mathbf{A}_i\mathbf{u} \lhd_i q, \quad \forall i \in [M], \\ & \|\mathbf{u}\|^2 = 1. \end{aligned} \tag{6.7}$$

By introducing slack variables $\{t_i\}$, we transform all inequality constraints to equality constraints, viz.

$$\mathbf{u}^H \mathbf{A}_i \mathbf{u} + t_i = q, \quad \forall i \in [M], \tag{6.8}$$

$$0 \lhd_i t_i, \quad \forall i \in [M]. \tag{6.9}$$

where $t_i \in \mathbb{R}$. Therefore, $\mathcal{P}_1$ can be reformulated as,

$$\begin{aligned} \mathcal{P}_2 : \underset{\mathbf{u},q,\{t_i\}}{\text{max.}} \quad & q \\ \text{s. t.} \quad & \mathbf{u}^H \left(\mathbf{A}_i + t_i \mathbf{I}\right) \mathbf{u} = q, \quad \forall i \in [M], \\ & \|\mathbf{u}\|^2 = 1, \quad 0 \lhd_i t_i, \quad \forall i \in [M]. \end{aligned} \tag{6.10}$$

Any Hermitian matrix can be decomposed as a difference of two PSD matrices simply by partitioning the matrix into parts comprising only non-positive and non-negative eigenvalues. In particular, we consider,

$$\mathbf{A}_i = \mathbf{A}_i^+ - \mathbf{A}_i^-, \quad \mathbf{A}_i^+, \mathbf{A}_i^- \succeq 0, \forall i \in [M]. \tag{6.11}$$

We can also decompose t_i as $t_i = t_i^+ - t_i^-, \forall i \in [M]$ where

$$t_i^+ = \begin{cases} t_i & \text{if} \quad t_i > 0 \\ 0 & \text{if} \quad t_i \leq 0 \end{cases}, \tag{6.12}$$

and

$$t_i^- = \begin{cases} 0 & \text{if} \quad t_i > 0 \\ |t_i| & \text{if} \quad t_i \leq 0 \end{cases}. \tag{6.13}$$

Consequently, the constraint in $\mathcal{P}_2$ can be written as,

$$\mathbf{u}^H \left(\mathbf{A}_i^+ + t_i^+ \mathbf{I}\right) \mathbf{u} = \mathbf{u}^H \left(\mathbf{A}_i^- + (q + t_i^-)\mathbf{I}\right) \mathbf{u} \tag{6.14}$$

For notational simplicity, we define

$$\mathbf{C}_i = \mathbf{A}_i^- + (q + t_i^-)\mathbf{I}, \tag{6.15}$$

$$\mathbf{B}_i = \mathbf{A}_i^+ + t_i^+ \mathbf{I}, \tag{6.16}$$

where both matrices are PSD. Note that (6.14) holds if and only if $\|\mathbf{B}_i^{\frac{1}{2}} \mathbf{u}\| = \|\mathbf{C}_i^{\frac{1}{2}} \mathbf{u}\|$. In particular, the left-hand side of (6.14) is close to the right-hand side of (6.14) if and only if $\|\mathbf{B}_i^{\frac{1}{2}} \mathbf{u}\|$ is *close to* $\|\mathbf{C}_i^{\frac{1}{2}} \mathbf{u}\|$. Therefore, one can consider the following optimization problem as a penalized reformulation of $\mathcal{P}_2$

$$\begin{aligned} \mathcal{P}_3 : \underset{\mathbf{u},q,\{t_i\}}{\text{max.}} \quad & q - \eta \sum_{i=1}^{M} \left(\|\mathbf{B}_i^{\frac{1}{2}} \mathbf{u}\| - \|\mathbf{C}_i^{\frac{1}{2}} \mathbf{u}\| \right)^2 \\ \text{s. t.} \quad & \|\mathbf{u}\|^2 = 1, \quad 0 \lhd_i t_i, \ \forall i \in [M], \end{aligned} \tag{6.17}$$

in which $\eta > 0$ determines the weight of the penalty-term added to the original objective of $\mathcal{P}_2$; and where $\mathcal{P}_3$ and $\mathcal{P}_2$ coincide as $\eta \to +\infty$. Note that optimizing $\mathcal{P}_3$ with respect to (w. r. t.) $\mathbf{u}$ may require rewriting $\mathcal{P}_3$ as a quartic objective in $\mathbf{u}$. To avoid this, we introduce another alternative objective:

$$\begin{aligned} \mathcal{P}_4 : \max_{\mathbf{u},q,\{t_i\},\{\mathbf{Q}_i\}} \quad & q - \eta \sum_{i=1}^{M} \|\mathbf{B}_i^{\frac{1}{2}}\mathbf{u} - \mathbf{Q}_i\mathbf{C}_i^{\frac{1}{2}}\mathbf{u}\|^2 \\ \text{s. t.} \quad & \|\mathbf{Q}_i\|_F \leq 1, \quad 0 \lhd_i t_i, \quad \forall i \in [M], \\ & \|\mathbf{u}\|^2 = 1. \end{aligned} \tag{6.18}$$

In contrast to $\mathcal{P}_3$, the optimization problem $\mathcal{P}_4$ w. r. t. $\mathbf{u}$ can be easily cast as a problem of finding the largest eigenvalue of a PSD matrix—more on this later. To establish the equivalence of $\mathcal{P}_3$ and $\mathcal{P}_4$, observe that the minimizer $\mathbf{Q}_i$ of $\mathcal{P}_4$ should be a matrix with Frobenius norm less than or equal to 1 that satisfies the following condition,

$$\mathbf{Q}_i\mathbf{C}_i^{\frac{1}{2}}\mathbf{u} = \left(\frac{\|\mathbf{C}_i^{\frac{1}{2}}\mathbf{u}\|}{\|\mathbf{B}_i^{\frac{1}{2}}\mathbf{u}\|}\right)\mathbf{B}_i^{\frac{1}{2}}\mathbf{u}. \tag{6.19}$$

In this case, it will be straightforward to verify that,

$$\begin{aligned} \sum_{i=1}^{M} \|\mathbf{B}_i^{\frac{1}{2}}\mathbf{u} - \mathbf{Q}_i\mathbf{C}_i^{\frac{1}{2}}\mathbf{u}\|^2 &= \sum_{i=1}^{M} \left\| \mathbf{B}_i^{\frac{1}{2}}\mathbf{u} - \left(\frac{\|\mathbf{C}_i^{\frac{1}{2}}\mathbf{u}\|}{\|\mathbf{B}_i^{\frac{1}{2}}\mathbf{u}\|}\right)\mathbf{B}_i^{\frac{1}{2}}\mathbf{u} \right\|^2 \\ &= \sum_{i=1}^{M} \left(\|\mathbf{B}_i^{\frac{1}{2}}\mathbf{u}\|_2 - \|\mathbf{C}_i^{\frac{1}{2}}\mathbf{u}\|_2 \right)^2. \end{aligned} \tag{6.20}$$

In Section 6.3, we present an analytical approach for the derivation of $\{\mathbf{Q}_i\}$.

6.3 Proposed Optimization Framework

We now propose an efficient iterative optimization framework based on a separate optimization of the objective of $\mathcal{P}_4$ and $\mathcal{P}_3$ over its partitions of variables $\mathbf{u}$, $\{\mathbf{Q}_i\}$, q, and $\{t_i\}$, at each iteration where the iterations can be initiated from any arbitrary setting.

6.3.1 Optimization w. r. t. u

Consider q, $\{\mathbf{Q}_i\}$ and $\{t_i\}$ are fixed, then one can optimize $\mathcal{P}_4$ w. r. t. $\mathbf{u}$ via maximizing the criterion:

$$-\sum_{i=1}^{K} \|\mathbf{B}_i^{\frac{1}{2}}\mathbf{u} - \mathbf{Q}_i\mathbf{C}_i^{\frac{1}{2}}\mathbf{u}\|^2 = -\mathbf{u}^H\mathbf{R}\mathbf{u} \tag{6.21}$$

where

$$\mathbf{R} = \sum_{i=1}^{K} \left\{ (\mathbf{B}_i + \mathbf{C}_i) - (\mathbf{B}_i^{\frac{1}{2}} \mathbf{Q}_i \mathbf{C}_i^{\frac{1}{2}} + \mathbf{C}_i^{\frac{1}{2}} \mathbf{Q}_i^H \mathbf{B}_i^{\frac{1}{2}}) \right\}.$$

In general, matrix $-\mathbf{R}$ is not PSD. However by diagonal loading (DL), one can make it PSD. Let us define diagonally loaded PD matrix $\widehat{\mathbf{R}} \triangleq -\mathbf{R} + \mu\mathbf{I}$ with $\mu > 0$ being larger than the minimum eigenvalue of $-\mathbf{R}$. One choice for μ can be Frobenius norm of matrix $\mathbf{R}$, $\mu = \|\mathbf{R}\|_F$. Due to the fact that $\|\mathbf{u}\|^2 = 1$, DL will not change the solution of the optimization problem since it only adds a constant to the objective function:

$$\mathbf{u}^H \widehat{\mathbf{R}} \mathbf{u} = -\mathbf{u}^H \mathbf{R} \mathbf{u} + \mu \tag{6.22}$$

in which μ is constant. Consequently, one can minimize (or decrease monotonically) the criterion in (6.21) by maximizing (or increasing monotonically) the objective of the following optimization problem:

$$\max_{\|\mathbf{u}\|^2=1} \quad \mathbf{u}^H \widehat{\mathbf{R}} \mathbf{u} \,. \tag{6.23}$$

Problem (6.23) is very well-known in that its solution is given by the unit-norm eigenvector corresponding to the largest eigenvalue of $\widehat{\mathbf{R}}$, which can be found efficiently using power method iterations [106].

6.3.2 Tightening the Upper-Bound: Optimization w. r. t. $\{\mathbf{Q}_i\}$

We define $\mathbf{w}_i$ and $\mathbf{v}_i$ for notational simplicity as,

$$\begin{aligned} \mathbf{w}_i &= \mathbf{B}_i^{\frac{1}{2}} \mathbf{u}, \\ \mathbf{v}_i &= \mathbf{C}_i^{\frac{1}{2}} \mathbf{u}, \end{aligned} \tag{6.24}$$

Then, the penalty term in $\mathcal{P}_3$ can be rewritten as

$$\sum_{i=1}^{M} \left(\|\mathbf{w}_i\| - \|\mathbf{v}_i\| \right)^2 . \tag{6.25}$$

Using the following Lemma, we provide an upper-bound for this penalty term.

Lemma 1. *For any* $\mathbf{w}_i \in \mathbb{C}^N$, $\mathbf{v}_i \in \mathbb{C}^N$ *and* $\mathbf{Q}_i \in \mathbb{C}^{N \times N}$ *with* $\|\mathbf{Q}_i\|_F \leq 1$, *we have*

$$\|\mathbf{w}_i\| - \|\mathbf{v}_i\| \leq \|\mathbf{w}_i - \mathbf{Q}_i \mathbf{v}_i\|. \tag{6.26}$$

Proof. We prove it in two steps:

1. We first show that $\|\mathbf{w}_i\| - \|\mathbf{v}_i\| \leq \|\mathbf{w}_i\| - \|\mathbf{Q}_i \mathbf{v}_i\|$.

2. Then we show that $\|\mathbf{w}_i\| - \|\mathbf{Q}_i\mathbf{v}_i\| \leq \|\mathbf{w}_i - \mathbf{Q}_i\mathbf{v}_i\|$

Note that the second step is a direct result of *backward triangle inequality* and does not need to be proved. Note that we can extend $\|\mathbf{Q}_i\mathbf{v}_i\|^2$ as,

$$\|\mathbf{Q}_i\mathbf{v}_i\|^2 = \mathbf{v}_i^H\mathbf{Q}_i^H\mathbf{Q}_i\mathbf{v}_i = \mathrm{Tr}(\mathbf{Q}_i^H\mathbf{Q}_i\mathbf{v}_i\mathbf{v}_i^H). \tag{6.27}$$

As $\mathbf{Q}_i^H\mathbf{Q}_i$ and $\mathbf{v}_i\mathbf{v}_i^H$ are PSD, we have,

$$\mathrm{Tr}(\mathbf{Q}_i^H\mathbf{Q}_i\mathbf{v}_i\mathbf{v}_i^H) \leq \mathrm{Tr}(\mathbf{Q}_i^H\mathbf{Q}_i)\,\mathrm{Tr}(\mathbf{v}_i\mathbf{v}_i^H) \leq \mathrm{Tr}(\mathbf{v}_i\mathbf{v}_i^H). \tag{6.28}$$

The last inequality in (6.28) is result of the fact that $\|\mathbf{Q}_i\|_F \leq 1$ is equivalent to $\mathrm{Tr}(\mathbf{Q}_i^H\mathbf{Q}_i) \leq 1$. From (6.28), we conclude that $\|\mathbf{Q}_i\mathbf{v}_i\|^2 \leq \|\mathbf{v}_i\|^2$ or equivalently $\|\mathbf{Q}_i\mathbf{v}_i\| \leq \|\mathbf{v}_i\|$. Finally, this leads to

$$\|\mathbf{w}_i\| - \|\mathbf{v}_i\| \leq \|\mathbf{w}_i\| - \|\mathbf{Q}_i\mathbf{v}_i\|, \tag{6.29}$$

which concludes the proof. □

Considering above lemma, it is straightforward to verify that

$$\sum_{i=1}^{M} \left(\|\mathbf{w}_i\| - \|\mathbf{v}_i\|\right)^2 \leq \sum_{i=1}^{M} \|\mathbf{w}_i - \mathbf{Q}_i\mathbf{v}_i\|^2. \tag{6.30}$$

As mentioned in Section 6.2, optimal $\{\mathbf{Q}_i\}$ should satisfy (6.30) with equality. Hence, given $\mathbf{u}$, p and $\{t_i\}$, we must have

$$\|\mathbf{w}_i\| - \|\mathbf{v}_i\| = \begin{cases} + \min\limits_{\|\mathbf{Q}_i\|_F \leq 1} \|\mathbf{w}_i - \mathbf{Q}_i\mathbf{v}_i\| & \text{if} \quad \|\mathbf{w}_i\| \geq \|\mathbf{v}_i\| \\ - \min\limits_{\|\mathbf{Q}_i\|_F \leq 1} \|\mathbf{w}_i - \mathbf{Q}_i\mathbf{v}_i\| & \text{if} \quad \|\mathbf{w}_i\| < \|\mathbf{v}_i\| \end{cases} \tag{6.31}$$

Now, the question to be addressed is finding optimal $\{\mathbf{Q}_i\}$. The typical method to find $\mathbf{Q}_i$ is to solve the optimization problem stated in (6.31). Interestingly, we show that in fact it is not necessary to numerically tackle such an optimization problem to find optimal $\{\mathbf{Q}_i\}$. Recall the optimality condition of $\mathbf{Q}_i$ in (7.12), which may be written as,

$$\mathbf{Q}_i\mathbf{v}_i = \Big(\frac{\|\mathbf{v}_i\|}{\|\mathbf{w}_i\|}\Big)\mathbf{w}_i \ . \tag{6.32}$$

Note that (6.32) can be recast as,

$$\mathbf{Q}_i\mathbf{v}_i = \frac{\mathbf{w}_i\|\mathbf{v}_i\|^2}{\|\mathbf{w}_i\|\|\mathbf{v}_i\|} = \frac{\mathbf{w}_i\mathbf{v}_i^H}{\|\mathbf{w}_i\|\|\mathbf{v}_i\|}\mathbf{v}_i \ . \tag{6.33}$$

Thus, the optimal $\mathbf{Q}_i = \mathbf{Q}_i^\star$ of $\mathcal{P}_4$ is immediately given by

$$\mathbf{Q}_i^\star = \frac{\mathbf{w}_i \mathbf{v}_i^H}{\|\mathbf{w}_i\| \|\mathbf{v}_i\|} \,. \tag{6.34}$$

It is straightforward to verify that $\mathbf{Q}_i^\star$ of (6.34) satisfies (6.31) and $\|\mathbf{Q}_i^\star\|_F = 1$. Note that given $\mathbf{u}$, q and $\{t_i\}$, calculation of $\mathbf{Q}_i^\star$ is not demanding from a computational point of view.

6.3.3 Optimization w. r. t. q

Now, assume that $\mathbf{u}$, $\{\mathbf{Q}_i\}$ and $\{t_i\}$ are given. Considering $\mathcal{P}_3$, the minimization w. r. t. q can be handled by the following optimization problem:

$$\max_{q} \quad q - \eta \sum_{i=1}^{M} \left(\alpha_i - \|\mathbf{C}_i^{\frac{1}{2}} \mathbf{u}\| \right)^2 , \tag{6.35}$$

where $\alpha_i = \|\mathbf{B}_i^{\frac{1}{2}} \mathbf{u}\|$ is given for $i \in [M]$. We recall form (6.14) that

$$\mathbf{C}_i \;=\; \mathbf{A}_i^- + (q + t_i^-)\mathbf{I} \tag{6.36}$$

is a function of q. Since $\mathbf{A}_i^-$ is a PSD matrix, it may be characterized by its eigen-value decomposition $\mathbf{A}_i^- = \mathbf{V}_i \mathbf{\Lambda}_i \mathbf{V}_i^H$ where $\mathbf{V}_i$ is a unitary matrix and Λ_i is a diagonal matrix formed from the eigenvalues of $\mathbf{A}_i^-$. As a result, $\mathbf{C}_i^{\frac{1}{2}}$ can be written as,

$$\mathbf{C}_i^{\frac{1}{2}} = \mathbf{V}_i \left(\mathbf{\Lambda}_i + (q + t_i^-)\mathbf{I} \right)^{\frac{1}{2}} \mathbf{V}_i^H. \tag{6.37}$$

Since multiplication with a unitary matrix does not change the ℓ_2-norm, we have that

$$\begin{aligned} \|\mathbf{C}_i^{\frac{1}{2}} \mathbf{u}\| &= \| \left(\mathbf{\Lambda}_i + (q + t_i^-)\mathbf{I} \right)^{\frac{1}{2}} \mathbf{V}_i^H \mathbf{u}\| && (6.38) \\ &= \left(\sum_{k=1}^{M} |\mathbf{a}_i(k)|^2 \left(\boldsymbol{\lambda}_i(k) + q + t_i^- \right) \right)^{\frac{1}{2}} && (6.39) \\ &= \left(b_i + q + t_i^- \right)^{\frac{1}{2}} , \end{aligned}$$

where $\mathbf{a}_i = \mathbf{V}_i^H \mathbf{u}$, $\boldsymbol{\lambda}_i$ is a vector formed from diagonal elements of $\mathbf{\Lambda}_i$ ($\boldsymbol{\lambda}_i = \mathrm{diag}(\mathbf{\Lambda}_i)$) or equivalently from the eigenvalues of $\mathbf{A}_i^-$, and

$$b_i = \sum_{k=1}^{M} |\mathbf{a}_i(k)|^2 \boldsymbol{\lambda}_i(k). \tag{6.40}$$

In (6.42), we have used the fact that

$$\sum_{k=1}^{M} |\mathbf{a}_i(k)|^2 = \|\mathbf{a}_i\|^2 = 1. \tag{6.41}$$

The objective function of (6.35) now can be expanded as

$$f(q) = q - \eta \sum_{i=1}^{M} \left(\alpha_i^2 + b_i + q + t_i^- - 2\alpha_i \left(b_i + q + t_i^- \right)^{\frac{1}{2}} \right). \tag{6.42}$$

By looking over its second derivative of $f(p)$, one can readily observe that $f(q)$ is a concave function. The first and the second derivative of $f(q)$ is given by

$$f'(q) = 1 - \eta \sum_{i=1}^{M} \left(1 - \alpha_i \left(b_i + q + t_i^- \right)^{-\frac{1}{2}} \right), \tag{6.43}$$

$$f''(q) = -\eta \sum_{i=1}^{M} \frac{\alpha_i}{2} \left(b_i + q + t_i^- \right)^{-\frac{3}{2}}. \tag{6.44}$$

Since q, α_i, b_i and η have positive values, we can conclude that $f''(q) < 0$. This means that $-f(q)$ is a convex function and we can use numerical methods like gradient descent algorithm to find the global optimum $q^\star$.

6.3.4 Optimization w. r. t. t_i

Assuming $\mathbf{u}$ and q are known, the values of $\{t_i\}$ minimizing $\mathcal{P}_3$ and $\mathcal{P}_4$ can be calculated by using (6.8), that implies

$$t_i = q - \mathbf{u}^H \mathbf{A}_i \mathbf{u}. \tag{6.45}$$

However, it should be noted that at the optimal point, following conditions need to be satisfied for all $i \in [M]$,

$$0 \lhd_i t_i \tag{6.46}$$

otherwise it means that constraint in (6.6) is not satisfied and optimization problem $\mathcal{P}_1$ is not feasible. When the constraints (6.46) is imposed, the *optimal feasible* solution in each iteration can be found by,

$$t_i = \begin{cases} t_i & \text{if (6.46) is satisfied} \\ 0 & \text{if (6.46) is not satisfied} \end{cases} \tag{6.47}$$

6.4 Application to Multigroup Multicast Beamforming

Consider the general *multigroup multicast beamforming* problem [48] for a downlink channel, with a n_{Tx}-antenna transmitter and K single-antenna users assigned to $G \leq K$ multicast groups. We denote the subset of user indices in the k^{th} group by $\mathcal{G}_k$ for any $k \in [G]$. Let $\mathbf{h}_i \in \mathbb{C}^{n_{\mathrm{Tx}}}$ denote the channel between the transmit antennas and the i^{th} user. Also let $\mathbf{w}_k \in \mathbb{C}^{n_{\mathrm{Tx}}}$ denote the beamforming vector corresponding to the k^{th} group, $k \in [G]$, multicast group of users. The beamformed vector to k^{th} group takes the form $\mathbf{w}_k s_k$ with $\mathbf{E}[|s_k|^2] = 1$ where s_k is the symbol to be transmitted. The beamforming vectors are to be designed in order to enhance the network performance. In particular, the SINR value for any user $i \in \mathcal{G}_k$ (and any $k \in [G]$) is given by [48],

$$\mathrm{SINR}_i = \frac{\mathbf{w}_k^H \mathbf{R}_i \mathbf{w}_k}{\left(\sum_{j \in [G] \setminus \{k\}} \mathbf{w}_j^H \mathbf{R}_i \mathbf{w}_j\right) + \sigma_i^2}, \tag{6.48}$$

where $\mathbf{R}_i = \mathbf{E}\{\mathbf{h}_i \mathbf{h}_i^H\}$ is the covariance matrix of the i^{th} channel, σ_i^2 denotes the variance of the zero-mean additive white Gaussian noise (AWGN).

Consequently, the problem of minimizing total transmit power subject to constraints on user SINR performance in the network can be formulated as [47, 48],

$$\begin{aligned} \min_{\{\mathbf{w}_k\}_{k=1}^G} \quad & \sum_{k=1}^{G} \|\mathbf{w}_k\|_2^2 \\ \text{s. t.} \quad & \mathrm{SINR}_i \geq \gamma_i \, , i \in [K] \end{aligned} \tag{6.49}$$

Note that by a specific reformulation, the SINR metric in (7.41) can be rewritten as a quadratic criterion. To see this, define the *stacked* beamforming vector $\mathbf{w} \in \mathbb{C}^N$ (with $N = n_{\mathrm{Tx}} G$) as,

$$\mathbf{w} \triangleq \mathrm{vec}([\mathbf{w}_1 \ \mathbf{w}_2 \ \cdots \ \mathbf{w}_G]), \tag{6.50}$$

and $\widehat{\mathbf{R}}_i$ and $\widetilde{\mathbf{R}}_i$ as

$$\widehat{\mathbf{R}}_i \triangleq \mathrm{diag}\,(\mathbf{e}_j) \otimes \mathbf{R}_i, \qquad \forall\, i \in [K], i \in \mathcal{G}_j \tag{6.51}$$

$$\widetilde{\mathbf{R}}_i \triangleq (\mathbf{I}_G - \mathrm{diag}\,(\mathbf{e}_j)) \otimes \mathbf{R}_i, \qquad \forall\, i \in [K], i \in \mathcal{G}_j \tag{6.52}$$

in which $\{\widehat{\mathbf{R}}_i\}$ and $\{\widetilde{\mathbf{R}}_i\}$ are PSD matrices. It can be easily verified that

$$\mathrm{SINR}_i = \frac{\mathbf{w}^H \widehat{\mathbf{R}}_i \mathbf{w}}{\mathbf{w}^H \widetilde{\mathbf{R}}_i \mathbf{w} + \sigma_i^2}, \quad \forall\, i \in [K]. \tag{6.53}$$

As a result, the SINR constraint in (7.42) can be rewritten as,

$$\mathbf{w}^H \widehat{\mathbf{R}}_i \mathbf{w} - \gamma_i \mathbf{w}^H \widetilde{\mathbf{R}}_i \mathbf{w} \geq \gamma_i \sigma_i^2, \tag{6.54}$$

or equivalently as $\mathbf{w}^H\mathbf{R}_i\mathbf{w} \geq 1$, where $\mathbf{R}_i$ is given by,

$$\mathbf{R}_i = \frac{1}{\gamma_i\sigma_i^2}\left(\widehat{\mathbf{R}}_i - \gamma_i\widetilde{\mathbf{R}}_i\right). \tag{6.55}$$

The beamforming design problem for minimizing total transmit power with SINR constraint can thus be formulated as,

$$\begin{aligned} \min_{\mathbf{w}}. \quad & \|\mathbf{w}\|^2, \\ \text{s. t.} \quad & \mathbf{w}^H\mathbf{R}_i\mathbf{w} \geq 1, \quad \forall i \in [K]. \end{aligned} \tag{6.56}$$

Note that this formulation can also be used to solve physical-layer multicasting and traditional multiuser transmit beamforming problems; see [49] and [47] for details.

6.5 Numerical Results and Discussion

In this section, a brief numerical example is provided to investigate the performance of the proposed method. To this end, we consider a multigroup multicast beamforming scenario with $G = 3$, $n_{\text{Tx}} = 4$ and $K = 15$ single-antenna users. We assume $\gamma_i = 1$ for all users. The entries of the channel vectors $\mathbf{h}_i$ are drawn from an i. i. d. complex Gaussian distribution with zero mean, with a variance set to 10. The Gaussian noise components received at each user antenna are assumed to have unit variance, i.e. $\sigma_i^2 = 1$ for all $i \in [K]$. We stop the optimization iterations whenever the objective decrease becomes bounded by 10^{-5} or number of iterations goes beyond 1000. Figure 6.1 shows the transition of objective function of $\mathcal{P}_3$ (equivalent to $\mathcal{P}_4$), with $\eta = 10$ in different iterations. It also shows the values of p in different iterations. It can be observed that objective function is monotonically decreasing. The difference between p and the objective of $\mathcal{P}_3$ denotes the penalty term of $\mathcal{P}_3$. Since $\eta = 10$ the penalty term might not be exactly zero, therefore resulted SINR for users, $\hat{\gamma}_i$, might be slightly less than targeted γ_i. In this case, one can readily find the feasible beamforming vector $\mathbf{w}$ by simply scaling it. The results leading to Figure 6.1 was obtained in 2.5 seconds on a standard PC, while SDR followed by a randomization step (with 1000 realizations) took 3.5 seconds. Also our approach resulted in $p^\star = 1.22$ while SDR achieved $p^\star_{\text{SDR}} = 1.37$. Note that the lower bound for $p^\star$ achieved by SDR (corresponding to high-rank solution) was $p^\star_{\text{LB}} = 1.16$.

6.6 Summary

An iterative approach is proposed to solve the nonconvex QCQP. Each iteration of the proposed method requires solving the subproblems which are accomplished by computationally efficient steps. The multigroup multicast beamforming problem is formulated as nonconvex QCQP and solved using the proposed method. Numerical results showed the proposed approach is computationally efficient and has good performance

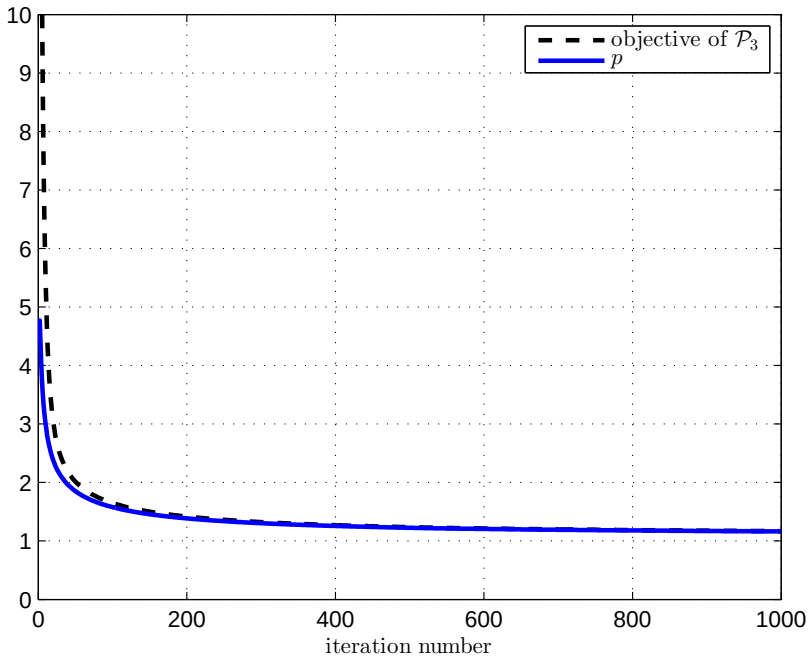

Figure 6.1. Transition of the objective function $\mathcal{P}_3$ and parameter p vs. iteration number when weights of the penalty-term, η, is set to 10.

Chapter 7

A Max-Min Fractional Quadratic Programming Framework with Applications in Signal Processing

7.1 Introduction

Maximizing the minimal performance is a widely used proactive approach to achieve *fairness* [48, 49, 66–72], or *robustness* [45, 107–112] in systems requiring advanced signal processing. On the other hand, many of such applications share a similar structure of the performance metric; namely, a variety of quality metrics for signal design, including e.g. signal-to-noise (plus interference) ratio (SINR) and mean-square error (MSE), can be represented as a fraction of quadratic functions of the signal to be designed—several examples will be presented shortly in Section 7.4. The goal of this chapter is therefore to study and propose an efficient approach to signal design dealing with the following NP-hard [48, 49] optimization problem:

$$\begin{aligned} \mathcal{P}_1 : \max_{\mathbf{w}} \quad & \min_{i\in[K]} \left\{ \frac{\mathbf{w}^H \mathbf{A}_i \mathbf{w}}{\mathbf{w}^H \mathbf{B}_i \mathbf{w}} \right\} \\ \text{s. t.} \quad & \mathbf{w} \in \Omega \end{aligned} \tag{7.1}$$

where $\mathbf{w} \in \mathbb{C}^N$ is the signal to be designed, $\mathbf{A}_i \in \mathbb{C}^{N\times N}$ and $\mathbf{B}_i \in \mathbb{C}^{N\times N}$ are positive semidefinite (PSD) matrices and Ω is the feasible set of the problem which is determined by the constraint on the signal $\mathbf{w}$.

7.1.1 Preliminaries and Related Problems

In order to study $\mathcal{P}_1$ the following preliminaries appear to be necessary:

1. The objective of $\mathcal{P}_1$ and its optima (values) are independent to a scaling of $\mathbf{w}$. As a result, we can readily assume that $\mathbf{w}$ has a given l_2-norm. More

precisely, in the sequel we assume that $\|\mathbf{w}\|_2^2 = P$. Such an assumption can be used conveniently along with other signal constraints used in practice—see the discussion on signal constraints below (7.18).

2. The objective of $\mathcal{P}_1$ is upper bounded via the generalized eigenvalue bound, viz.

$$\frac{\mathbf{w}^H \mathbf{A}_i \mathbf{w}}{\mathbf{w}^H \mathbf{B}_i \mathbf{w}} \leq \sigma_{max} \left\{ \mathbf{B}_i^{-1} \mathbf{A}_i \right\}, \quad \forall\ \mathbf{w} \neq 0, \tag{7.2}$$

which due to *max-min inequality* [59] implies

$$\begin{aligned} &\max_{\mathbf{w}} \left\{ \min_{i \in [K]} \left\{ \frac{\mathbf{w}^H \mathbf{A}_i \mathbf{w}}{\mathbf{w}^H \mathbf{B}_i \mathbf{w}} \right\} \right\} \\ \leq &\min_{i \in [K]} \left\{ \max_{\mathbf{w}} \left\{ \frac{\mathbf{w}^H \mathbf{A}_i \mathbf{w}}{\mathbf{w}^H \mathbf{B}_i \mathbf{w}} \right\} \right\} \\ \leq &\min_{i \in [K]} \left\{ \sigma_{max} \left\{ \mathbf{B}_i^{-1} \mathbf{A}_i \right\} \right\}. \end{aligned} \tag{7.3}$$

As a consequence of (7.3), any optimization approach that can yield a monotonically increasing sequence of the objective of $\mathcal{P}_1$ is *convergent*.

There are several interesting problems that have strong connections to $\mathcal{P}_1$; and thus tackling $\mathcal{P}_1$ may hold the key to approaching them. We discuss these problems below.

- Min-Max problems:
  Proposed algorithm can also be used to solve min-max problem,

$$\begin{aligned} \min_{\mathbf{w}} \quad & \max_{i \in [K]} \left\{ \frac{\mathbf{w}^H \mathbf{A}_i \mathbf{w}}{\mathbf{w}^H \mathbf{B}_i \mathbf{w}} \right\} \\ \text{s. t.} \quad & \mathbf{w} \in \mathbf{\Omega}. \end{aligned} \tag{7.4}$$

  Equivalently, this problem can be written as a max-min formulation as

$$\begin{aligned} \max_{\mathbf{w}} \quad & \min_{i \in [K]} \left\{ \frac{\mathbf{w}^H \mathbf{B}_i \mathbf{w}}{\mathbf{w}^H \mathbf{A}_i \mathbf{w}} \right\} \\ \text{s. t.} \quad & \mathbf{w} \in \mathbf{\Omega}. \end{aligned} \tag{7.5}$$

- Quadratic form problems:
  Another related optimization problem is quadratic form problems as,

$$\begin{aligned} \max_{\mathbf{w}} \quad & \min_{i \in [K]} \left\{ \mathbf{w}^H \mathbf{A}_i \mathbf{w} \right\} \\ \text{s. t.} \quad & \mathbf{w} \in \mathbf{\Omega}, \end{aligned} \tag{7.6}$$

7.2 The Max-Min Optimization Framework

We begin by considering a reformulated version of $\mathcal{P}_1$; namely,

$$\begin{aligned} \mathcal{P}_2: \quad \max_{\mathbf{w}} \quad & \min_{i\in[K]} \{\lambda_i\} \\ \text{s. t.} \quad & \mathbf{w} \in \Omega\,, \qquad (7.7) \\ & \lambda_i = \frac{\mathbf{w}^H \mathbf{A}_i \mathbf{w}}{\mathbf{w}^H \mathbf{B}_i \mathbf{w}},\ \forall\, i \in [K]. \qquad (7.8) \end{aligned}$$

Note that (7.8) holds if and only if $\|\mathbf{A}_i^{\frac{1}{2}}\mathbf{w}\|_2^2 = \lambda_i \|\mathbf{B}_i^{\frac{1}{2}}\mathbf{w}\|_2^2$, or equivalently $\|\mathbf{A}_i^{\frac{1}{2}}\mathbf{w}\|_2 = \sqrt{\lambda_i}\|\mathbf{B}_i^{\frac{1}{2}}\mathbf{w}\|_2$. In particular, the LHS of (7.8) is *close* to the RHS of (7.8) if and only if $\|\mathbf{A}_i^{\frac{1}{2}}\mathbf{w}\|_2$ is *close* to $\sqrt{\lambda_i}\|\mathbf{B}_i^{\frac{1}{2}}\mathbf{w}\|_2$. Therefore, by employing the auxiliary variables $\{\lambda_i\}$, one can consider the following optimization problem as an alternative to $\mathcal{P}_2$ (and $\mathcal{P}_1$):

$$\begin{aligned} \mathcal{P}_3: \max_{\mathbf{w},\{\lambda_i\}} \ & \min_{i\in[K]} \{\lambda_i\} - \eta \sum_{i=1}^{K} (\|\mathbf{A}_i^{\frac{1}{2}}\mathbf{w}\|_2 - \sqrt{\lambda_i}\|\mathbf{B}_i^{\frac{1}{2}}\mathbf{w}\|_2)^2 \\ \text{s. t.} \quad & \mathbf{w} \in \Omega\ ;\ \lambda_i \geq 0,\ \forall\, i \in [K]; \qquad (7.9) \end{aligned}$$

in which $\eta > 0$ determines the weight of the penalty-term added to the original objective of $\mathcal{P}_2$; and where $\mathcal{P}_3$ and $\mathcal{P}_2$ coincide as $\eta \to +\infty$. Note that optimizing $\mathcal{P}_3$ w. r. t. $\mathbf{w}$ may require rewriting $\mathcal{P}_3$ as a quartic objective in $\mathbf{w}$. To circumvent this, we continue by introducing $\mathcal{P}_4$—yet another alternative objective:

$$\begin{aligned} \mathcal{P}_4: \max_{\mathbf{w},\{\lambda_i\},\{\mathbf{Q}_i\}} \ & \min_{i\in[K]} \{\lambda_i\} - \eta \sum_{i=1}^{K} \|\mathbf{A}_i^{\frac{1}{2}}\mathbf{w} - \sqrt{\lambda_i}\mathbf{Q}_i\mathbf{B}_i^{\frac{1}{2}}\mathbf{w}\|_2^2 \\ \text{s. t.} \quad & \mathbf{w} \in \Omega\ ,\ \lambda_i \geq 0,\ \forall\, i \in [K]; \qquad (7.10) \\ & \|\mathbf{Q}_i\|_F \leq 1,\ \forall\, i \in [K]. \qquad (7.11) \end{aligned}$$

To see why $\mathcal{P}_4$ and $\mathcal{P}_3$ are equivalent, observe that the minimizer $\mathbf{Q}_i$ of $\mathcal{P}_4$ (satisfying (7.11), also known as Steifel manifold [113–115]) is a similar matrix to the one introduced in Chapter 6. More precisely, at the minimizer $\mathbf{Q}_i$ of $\mathcal{P}_4$, we have that

$$\mathbf{Q}_i\mathbf{B}_i^{\frac{1}{2}}\mathbf{w} = \left(\frac{\mathbf{A}_i^{\frac{1}{2}}\mathbf{w}}{\|\mathbf{A}_i^{\frac{1}{2}}\mathbf{w}\|_2}\right)\|\mathbf{B}_i^{\frac{1}{2}}\mathbf{w}\|_2. \qquad (7.12)$$

Using (7.12), it is straightforward to verify that

$$\begin{aligned} & \sum_{i=1}^{K} \|\mathbf{A}_i^{\frac{1}{2}}\mathbf{w} - \sqrt{\lambda_i}\mathbf{Q}_i\mathbf{B}_i^{\frac{1}{2}}\mathbf{w}\|_2^2 \qquad (7.13) \\ = & \sum_{i=1}^{K} \left\| \mathbf{A}_i^{\frac{1}{2}}\mathbf{w} - \sqrt{\lambda_i}\left(\frac{\mathbf{A}_i^{\frac{1}{2}}\mathbf{w}}{\|\mathbf{A}_i^{\frac{1}{2}}\mathbf{w}\|_2}\right)\|\mathbf{B}_i^{\frac{1}{2}}\mathbf{w}\|_2 \right\|_2^2 \\ = & \sum_{i=1}^{K} \left(\left\|\mathbf{A}_i^{\frac{1}{2}}\mathbf{w}\right\|_2 - \sqrt{\lambda_i}\left\|\mathbf{B}_i^{\frac{1}{2}}\mathbf{w}\right\|_2 \right)^2 \end{aligned}$$

which concludes the proof.

In contrast to $\mathcal{P}_3$, the optimization problem $\mathcal{P}_4$ can be easily rewritten as a quadratic program (QP) in $\mathbf{w}$; a widely studied type of program that facilitates the usage of power method-like iterations, and thus employing different signal constraints Ω—more on this later. Note that, until now, we have shown that

- $\mathcal{P}_1$ and $\mathcal{P}_2$ are equivalent.
- $\mathcal{P}_3$ and $\mathcal{P}_4$ are equivalent.
- $\mathcal{P}_3$ and $\mathcal{P}_4$ can be used as alternatives to the original problem, i.e. $\mathcal{P}_1$.

In the following, our goal is to

- propose an efficient iterative optimization framework based on a separate optimization of the objective of $\mathcal{P}_4$ over its three partition of variables, viz. $\mathbf{w}$, $\{\mathbf{Q}_i\}$, and $\{\lambda_i\}$, and in particular,
- study the properties of $\mathcal{P}_4$ to pave the way for an effective usage of our proposed framework in tackling fractional quadratic programs.

We note that considering $\mathcal{P}_3$ can also be useful in such a study, as $\mathcal{P}_3$ may be viewed as a simplified version of $\mathcal{P}_4$, in which the objective is already optimized w. r. t. $\{\mathbf{Q}_i\}$.

7.2.1 Power Method-Like Iterations (Optimization w. r. t. w)

For fixed $\{\mathbf{Q}_i\}$ and $\{\lambda_i\}$, one can optimize $\mathcal{P}_4$ w. r. t . $\mathbf{w}$ via minimizing the criterion:

$$\sum_{i=1}^{K} \|\mathbf{A}_i^{\frac{1}{2}}\mathbf{w} - \sqrt{\lambda_i}\mathbf{Q}_i\mathbf{B}_i^{\frac{1}{2}}\mathbf{w}\|_2^2 = \mathbf{w}^H\mathbf{R}\mathbf{w} \qquad (7.14)$$

where

$$\mathbf{R} = \sum_{i=1}^{K} \left\{ (\mathbf{A}_i + \lambda_i \mathbf{B}_i) - \sqrt{\lambda_i} (\mathbf{A}_i^{\frac{1}{2}} \mathbf{Q}_i \mathbf{B}_i^{\frac{1}{2}} + \mathbf{B}_i^{\frac{1}{2}} \mathbf{Q}_i^H \mathbf{A}_i^{\frac{1}{2}}) \right\}. \tag{7.15}$$

Due to the fact that Ω enforces a fixed ℓ_2-norm on $\mathbf{w}$ (i.e. $\|\mathbf{w}\|_2^2 = N$), by defining $\hat{\mathbf{R}} \triangleq \mu \mathbf{I} - \mathbf{R}$ (in which $\mu > 0$ is larger than the maximum eigenvalue of $\mathbf{R}$), we have that

$$\mathbf{w}^H \mathbf{R} \mathbf{w} = -\mathbf{w}^H \hat{\mathbf{R}} \mathbf{w} + \underbrace{\mu N}_{const.}. \tag{7.16}$$

Consequently, one can minimize (or decrease monotonically) the criterion in (7.14) by maximizing (or increasing monotonically) the objective of the following optimization problem:

$$\begin{aligned} \max_{\mathbf{w}} \quad & \mathbf{w}^H \hat{\mathbf{R}} \mathbf{w} \\ \text{s. t.} \quad & \mathbf{w} \in \Omega. \end{aligned} \tag{7.17}$$

Although (7.17) is NP-hard for a general signal constraint set [74, 105], a monotonically increasing objective of (7.17) can be obtained using *power method-like* iterations developed in [105], and [120]; namely, we update $\mathbf{w}$ iteratively by solving the following *nearest-vector* problem at each iteration:

$$\begin{aligned} \min_{\mathbf{w}^{(s+1)}} \quad & \left\| \mathbf{w}^{(s+1)} - \hat{\mathbf{R}} \mathbf{w}^{(s)} \right\|_2 \\ \text{s. t.} \quad & \mathbf{w}^{(s+1)} \in \Omega, \end{aligned} \tag{7.18}$$

where s denotes the internal iteration number, and $\mathbf{w}^{(0)}$ is the current value of $\mathbf{w}$. Note that we can continue updating $\mathbf{w}$ until convergence in the objective of (7.17), or for a fixed number of steps, say S.

Now, we take a deeper look at various signal constraints Ω typically used in practice, as well as their associated constrained solutions to (7.18):

• *Total-power constraint:* Note that the energy of designed signals should always be upper bounded in practice, which can be formulated as a total-power constraint, viz.

$$\Omega = \{\mathbf{w} \,:\, \|\mathbf{w}\|_2^2 = P\}, \quad P > 0. \tag{7.19}$$

In this case, the set of power method-like iterations in (7.18) boils down to a typical power method aiming to find the dominant eigenvector of $\hat{\mathbf{R}}$, however with an additional scaling to attain a power of P.

• *Per-antenna power constraint:* Power management per antenna avoids an uneven (and most likely hazardous) distribution of power over the antenna array,

and is shown to be more effective than total-power constraint in some applications; see e.g. [122]. We consider K antennas each with a power of P_{ant}, and assume that $M = N/K$ entries of $\mathbf{w}$ are devoted to each antenna. As a result, we can solve (7.18) by considering the nearest-vector problem for sub-vectors associated with each antenna separately—i.e., K nearest-vector problems all with vector arguments of length M.

• *Unimodular signal design:* Unimodular codes are widely used in many radar and communication applications due to their low peak-to-average-power ratio [105, 123]. The set of unimodular codes is defined as

$$\Omega = \left\{e^{j\varphi} \,:\, \varphi \in [0, 2\pi)\right\}^N. \tag{7.20}$$

Moreover, the unimodular solution to (7.18) is simply given by

$$\mathbf{w}^{(s+1)} = \exp\left(j \arg\left(\hat{\mathbf{R}}\mathbf{w}^{(s)}\right)\right). \tag{7.21}$$

• *Discrete-phase signal design:* Such signals share the low peak-to-average-power ratio property of unimodular signals, and at the same time, offer a reduced implementation complexity due to their discrete/finite nature [123,124]. We define the set of discrete-phase signals as

$$\Omega = \left\{e^{j\frac{2\pi}{Q}q} :\; q = 0, 1, \cdots, Q-1\right\}^N \tag{7.22}$$

where Q denotes the phase *quantization* level. The discrete-phase solution to (7.18) is given by

$$\mathbf{w}^{(s+1)} = \exp\left(j\mu_Q\left(\arg\left(\hat{\mathbf{R}}\mathbf{w}^{(s)}\right)\right)\right) \tag{7.23}$$

where $\mu_Q(.)$ yields (for each entry of the vector argument) the closest element in the Q-ary alphabet described in (7.22).

We refer the interested reader to find more details on the properties of power method-like iterations in [105]- [121].

7.2.2 Optimization w. r. t. $\{\mathbf{Q}_i\}$

Suppose $\mathbf{w}$ and $\{\lambda_i\}$ are fixed. As mentioned earlier, the minimizer $\mathbf{Q}_i$ of $\mathcal{P}_4$ can be calculated by the method discussed in Section 6.3.2. Let

$$\begin{cases} \mathbf{x}_i = \mathbf{A}_i^{\frac{1}{2}}\mathbf{w} \,/\, \|\mathbf{A}_i^{\frac{1}{2}}\mathbf{w}\|_2, \\ \mathbf{y}_i = \mathbf{B}_i^{\frac{1}{2}}\mathbf{w} \,/\, \|\mathbf{B}_i^{\frac{1}{2}}\mathbf{w}\|_2. \end{cases} \tag{7.24}$$

Then the optimal $\mathbf{Q}_i$ can be found as,

$$\mathbf{Q}_i^\star = \frac{\mathbf{x}_i\mathbf{y}_i^H}{\|\mathbf{x}_i\|\|\mathbf{y}_i\|}. \tag{7.25}$$

Please refer to Section 6.3.2 for more details.

7.2.3 Grab-n-Pull (Optimization w. r. t. $\{\lambda_i\}$)

Note that according to (7.13), once the optimal $\{\mathbf{Q}_i\}$ is used, the objectives of $\mathcal{P}_3$ and $\mathcal{P}_4$ can be considered interchangeably. We assume that optimal $\mathbf{w}$ and $\{\mathbf{Q}_i\}$ are obtained according to the ideas described in sub-sections (7.2.1) and (7.2.2), respectively, and are fixed. Therefore, to find $\{\lambda_i\}$, we can equivalently focus on obtaining the maximizer $\{\lambda_i\}$ of $\mathcal{P}_3$ via the optimization problem:

$$\begin{aligned}\Lambda: \quad \max_{\{\lambda_i\}} \ \min_{i\in[K]} \{\lambda_i\} - \eta \sum_{i=1}^{K} \left(\|\mathbf{A}_i^{\frac{1}{2}}\mathbf{w}\|_2 - \sqrt{\lambda_i}\|\mathbf{B}_i^{\frac{1}{2}}\mathbf{w}\|_2\right)^2 \\ \text{s. t.} \quad \lambda_i \geq 0, \ \forall\, i \in [K].\end{aligned} \tag{7.26}$$

Definition 1. *Let $\{\lambda_i^\star\}$ denote the optimal $\{\lambda_i\}$ of Λ, and $\lambda^\star \triangleq \min_{i\in[K]}\{\lambda_i^\star\}$. We let Υ to denote the set of all indices m for which $\lambda_m^\star$ takes the minimal value among all $\{\lambda_i^\star\}$, i.e.*

$$\Upsilon = \{m \in [K] \ : \ \lambda_m^\star = \lambda^\star\}. \tag{7.27}$$

*Moreover, we refer to $\gamma_i^2 \triangleq \|\mathbf{A}_i^{\frac{1}{2}}\mathbf{w}\|_2^2 \,/\, \|\mathbf{B}_i^{\frac{1}{2}}\mathbf{w}\|_2^2$ as the **shadow value** of $\lambda_i^\star$, for all $i \in [K]$.*

It is straightforward to verify from the objective of (7.26) that if $\lambda_i^\star > \lambda^\star \in \Upsilon$, then $\lambda_i^\star = \gamma_i^2$. On the other hand, to obtain $\lambda^\star$, we need to maximize the criterion:

$$f(\lambda) = \lambda - \eta \sum_{k\in\Upsilon} \left(\|\mathbf{A}_k^{\frac{1}{2}}\mathbf{w}\|_2 - \sqrt{\lambda}\,\|\mathbf{B}_k^{\frac{1}{2}}\mathbf{w}\|_2\right)^2. \tag{7.28}$$

Provided that η is large *enough* (see Section 7.3), the optimal $\lambda^\star$ of the quadratic criterion in (7.28) is given by

$$\sqrt{\lambda^\star} = \frac{\eta \sum_{k\in\Upsilon} \alpha_k\beta_k}{\eta \sum_{k\in\Upsilon} \beta_k^2 - 1} \tag{7.29}$$

in which $\alpha_k \triangleq \|\mathbf{A}_k^{\frac{1}{2}}\mathbf{w}\|_2$, and $\beta_k \triangleq \|\mathbf{B}_k^{\frac{1}{2}}\mathbf{w}\|_2$. It is interesting to have some insight into what $\sqrt{\lambda^\star}$ represents: Note that (7.29) can be rewritten as

$$\sqrt{\lambda^\star} = \frac{\sum_{k\in\Upsilon} \gamma_k\beta_k^2}{\sum_{k\in\Upsilon} \beta_k^2 - 1/\eta}. \tag{7.30}$$

As a result, $\sqrt{\lambda^\star}$ can be viewed as a weighted average of γ_k for $k \in \Upsilon$—except that the term $-1/\eta$ in the denominator of (7.30) makes $\sqrt{\lambda^\star}$ *a bit* larger than the actual weighted average. However, for an increasing η, $\sqrt{\lambda^\star}$ converges to the exact value of the weighted average specified above.

Hereafter, we propose a recursive *Grab-n-Pull* procedure to fully determine Υ, while we can obtain $\sqrt{\lambda^\star}$ via (7.29). The proposed approach will make use of the following observation:

Table 7.1. Recursive Grab-n-Pull Procedure to Determine Υ

Step 0: Set $\Upsilon = \varnothing$.

Step 1: Include 1 in Υ.

Remark: Based on Lemma 2, the primitive index 1 *belongs to* Υ*, as* $\sqrt{\lambda^\star}$ *is always larger than* γ_1*.*

Step 2: Given the current index set of minimal variables Υ, obtain $\sqrt{\lambda^\star}$ using (7.29).

Remark: Note that if $\sqrt{\lambda^\star}$ *is smaller than* γ_k *for all* $k \in [K]\backslash\Upsilon$ *then the obtained* Υ *is optimal, as all* λ_k *with* $k \in [K]\backslash\Upsilon$ *have chosen their values freely to maximize the objective of (7.26); as a result, adding other indices to* Υ *will lead to a decreased objective of (7.26).*

Step 3: Let $\{h\} \subset [K]$ denote the indices for which $h \notin \Upsilon$. If $\gamma_h \leq \sqrt{\lambda^\star}$, include h in Υ. Goto Step 2.

Remark: This is a direct consequence of Lemma 2, particularly considering that $\sqrt{\lambda^\star}$ *is only increasing with growing* $|\Upsilon|$*, which corresponds to adding larger* γ_i*s to the weighted sum in (7.30).*

Lemma 2. *if* $\gamma_i^2 < \lambda^\star \in \Upsilon$ *for any* $i \in [K]$*, then* $i \in \Upsilon$*.*

Proof. The inequality $\gamma_i^2 < \lambda^\star$ implies that $\lambda_i^\star \neq \gamma_i^2$. Considering the discussion above (7.28), one can conclude that $\lambda_i^\star \leq \lambda^\star$, which due to the definition of $\lambda^\star$ yields $\lambda_i^\star = \lambda^\star$. Hence, the proof is complete. □

Without loss of generality, and for the sake of simplicity, we assume in the sequel that the matrix pairs $\{(\mathbf{A}_i, \mathbf{B}_i)\}$ are sorted in such a way to form the ascending order:

$$\gamma_1 \leq \gamma_2 \leq \cdots \leq \gamma_K. \tag{7.31}$$

The Grab-n-Pull approach is described in Table 7.1. Moreover, an illustration of the method is depicted in Fig. 1. The name of the method, i.e. *Grab-n-Pull*, comes from the intuition that the method grabs and pulls the lowest values of $\{\lambda_i\}$ to a level which is suitable for optimization of the alternative objectives, while achieving *equality*, at least for the *lowest* λ_is.

Finally, our optimization framework based on maximizing the objective of $\mathcal{P}_4$ over $\mathbf{w}$, $\{\mathbf{Q}_i\}$, and $\{\lambda_i\}$ is summarized using a flowchart in Fig. 2. Note that, due to the key role of Grab-n-Pull procedure in the proposed optimization framework, we also use the term Grab-n-Pull when referring to the general framework. In the following section, we study different criteria in choosing a suitable η, as well as, various interesting aspects tied to the proposed framework.

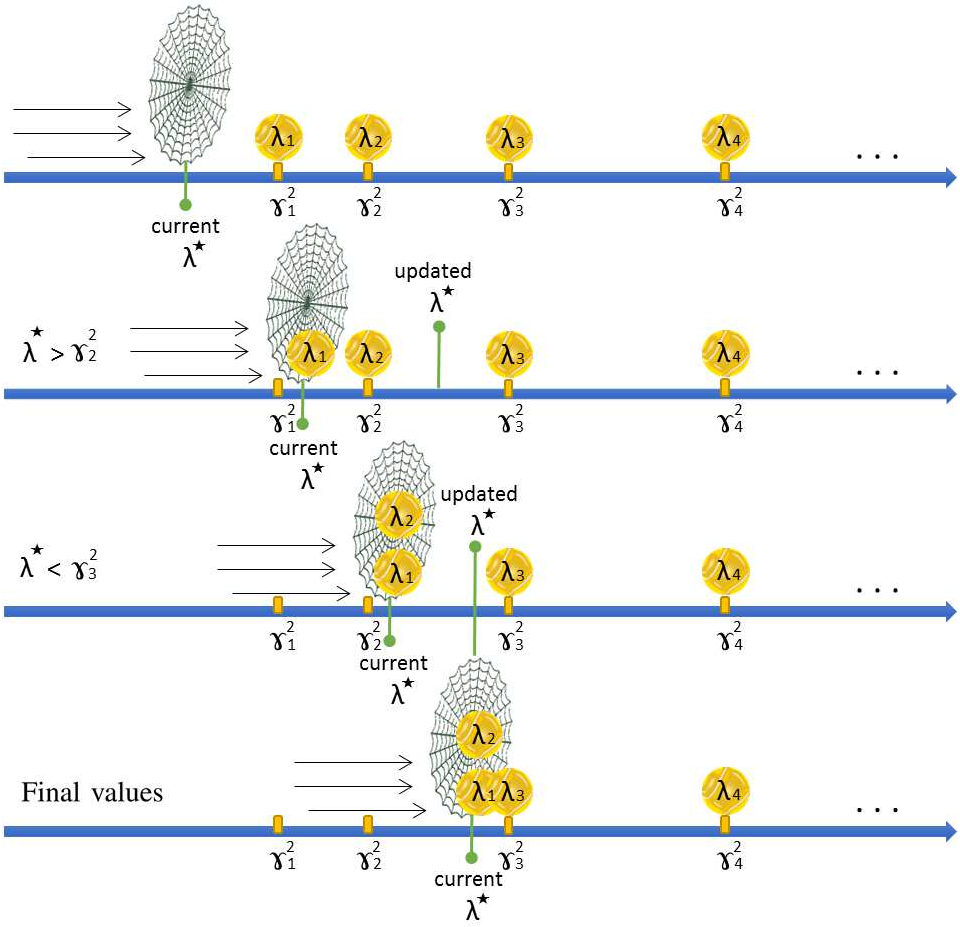

Figure 7.1. An illustration of the Grab-n-Pull procedure. The approach reaches the optimal values of $\{\lambda_i\}$ when $\lambda^\star < \gamma_3^2$, which sets $\Upsilon = \{1, 2\}$.

7.3 Grab-n-Pull: Settings and Discussions

To perform a suitable selection of η, one should note that unlike the objective of the original problem $\mathcal{P}_1$, choosing η may be sensitive not only to $\{\mathbf{A}_k\}$ and $\{\mathbf{B}_k\}$, but also to the power, or a scaling of the signal $\mathbf{w}$. This can be observed easily from the penalty terms in $\mathcal{P}_3$ and $\mathcal{P}_4$ where a scaling of $\mathbf{w}$ can be fully compensated via a corresponding scaling in η.

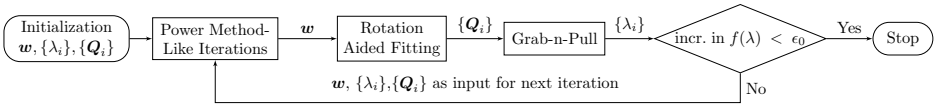

Figure 7.2. Flowchart of the proposed algorithm

7.3.1 Lower Bound on η—with Connections to Convergence

We begin our study from $f(\lambda)$ in (7.28). In particular, by defining α_k and β_k as in (7.29), $f(\lambda)$ can be written as

$$f(\lambda) = \lambda - \eta \sum_{k\in\Upsilon} \left(\alpha_k^2 + \lambda\beta_k^2 - 2\sqrt{\lambda}\alpha_k\beta_k\right) \tag{7.32}$$
$$= \lambda\left(1 - \eta\sum_{k\in\Upsilon}\beta_k^2\right) + 2\sqrt{\lambda}\eta\left(\sum_{k\in\Upsilon}\alpha_k\beta_k\right) - \eta\sum_{k\in\Upsilon}\alpha_k^2.$$

Note that the above quadratic function of $\sqrt{\lambda}$ can be meaningfully maximized (with a bounded solution) if and only if $1 - \eta\sum_{k\in\Upsilon}\beta_k^2 < 0$, or equivalently,

$$\eta > \left(\sum_{k\in\Upsilon}\beta_k^2\right)^{-1} = \left(\mathbf{w}^H\left(\sum_{k\in\Upsilon}\mathbf{B}_k\right)\mathbf{w}\right)^{-1}. \tag{7.33}$$

In order to ensure the satisfaction of (7.33), one can choose the following conservative lower bound for η:

$$\eta > \eta_{lb} \triangleq \frac{1}{P}\left(\max_{i\in[K]}\left\{\sigma_{\min}^{-1}(\mathbf{B}_k)\right\}\right). \tag{7.34}$$

To see why Lemma 3 implies the convergence of our algorithm, observe that different steps of the proposed framework lead to an increasing objective of $\mathcal{P}_4$ (and $\mathcal{P}_3$). To guarantee convergence in terms of the objective value, we only need to show that the objective is bounded from above—a condition which will be met by satisfying (7.34).

7.3.2 On the Penalty Coefficient: the Larger, the Better?

Although with a larger η one may expect a lower value of the penalty functions in $\mathcal{P}_3$ and $\mathcal{P}_4$, a lower η can play a useful role in speeding up the algorithm. Remember that, given the index set Υ, the maximizer of $f(\lambda)$ is given by

$$\sqrt{\lambda^\star} = \frac{\sum_{k\in\Upsilon}\gamma_k\beta_k^2}{\sum_{k\in\Upsilon}\beta_k^2 - 1/\eta}. \tag{7.35}$$

As discussed earlier, for a finite $\eta > 0$, $\sqrt{\lambda^\star}$ is larger than the below wighted sum of $\{\gamma_k\}_{k\in[K]}$:

$$\left(\sum_{k\in\Upsilon}\gamma_k\beta_k^2\right) / \left(\sum_{k\in\Upsilon}\beta_k^2\right), \tag{7.36}$$

which leads to the following *bootstrapping effect*.

Remark 2 (Bootstrapping Effect): For the sake of simplicity, assume Υ has a cardinality of one (including solely a generic index k), and consider the associated objective function of Λ:

$$f(\lambda) = \lambda - \eta\left(\alpha_k - \sqrt{\lambda}\beta_k\right)^2 \tag{7.37}$$

The goal of employing the penalty function in (7.37) is for λ to be as close as possible to its shadow value $\gamma_k^2 = \alpha_k^2/\beta_k^2 = (\mathbf{w}^H\mathbf{A}_k\mathbf{w})/(\mathbf{w}^H\mathbf{B}_k\mathbf{w})$. Note that:

(a) For a finite $\eta > 0$, the maximizer $\lambda^\star$ of $f(\lambda)$ is larger than γ_k^2:

$$\lambda^\star = \left(\beta_k^2 \,/\, \left(\beta_k^2 - 1/\eta\right)\right)\gamma_k^2. \tag{7.38}$$

(b) Only the penalty term of (7.37) is variable with $\mathbf{w}$. In particular, for a fixed λ, optimization w. r. t. $\mathbf{w}$ will be performed to achieve a γ_k^2 as close as possible to $\lambda^\star$.

(c) Then, thanks to (a), $\lambda^\star$ will be chosen to be larger than the current value of γ_k^2, and the same phenomenon persists by continuing with (b).

In sum, *an increased γ_k^2 will lead to an increased $\lambda^\star$, and an increased $\lambda^\star$ will lead to an increased γ_k^2, until convergence.* It is worth noting that a similar behavior occurs for $|\Upsilon| > 1$. ■

Now observe that while the bootstrapping effect occurs for any finite $\eta > 0$ satisfying (7.34), the penalty coefficient η can be viewed as a tuning parameter for the speed of the algorithm. Specifically, one can easily see that if η is large, $\lambda^\star$ will be slightly greater than the weighted average of $\{\gamma_k^2\}_{k\in\Upsilon}$, whereas for smaller values of η, the bounces from the weighted average are much larger—and the bootstrapping process can occur much quicker. In a related observation, one can also verify that the choice of η affects the cardinality of Υ. By evaluating $f(\lambda)$ at its maximizer $\lambda^\star$

(see (7.35)) we obtain

$$f(\lambda^\star) = \eta \left(\frac{\eta \left(\sum_{k\in\Upsilon} \alpha_k \beta_k \right)^2}{\eta \sum_{k\in\Upsilon} \beta_k^2 - 1} - \sum_{k\in\Upsilon} \alpha_k^2 \right) \tag{7.39}$$

$$= \left(\left(\sum_{k\in\Upsilon} \beta_k^2 \right) - 1/\eta \right)^{-1} \times \tag{7.40}$$

$$\left(\sum_{k\in\Upsilon} \alpha_k^2 + \eta \left[\underbrace{\left(\sum_{k\in\Upsilon} \alpha_k \beta_k \right)^2 - \left(\sum_{k\in\Upsilon} \beta_k^2 \right) \left(\sum_{k\in\Upsilon} \alpha_k^2 \right)}_{(*)} \right] \right).$$

Note that, according to the Cauchy-Schwarz inequality, $(*)$ is always less than or equal to zero. Also, the equality is attained only if all $\{\gamma_k\}_{k\in\Upsilon}$ are identical, or $|\Upsilon| = 1$. As a result, we can conclude that for *sufficiently large* values of η, a pair $(\Upsilon, \lambda^\star)$ can serve as a solution to Λ only if $|\Upsilon|$ is kept to its minimum, given by the number of minimal $\{\gamma_k\}$ which are also identical. This implies that at the initial iterations of the method when $\{\gamma_k\}$ are most likely to be distinct, we should have $|\Upsilon| = 1$; this can cause difficulty combined with the fact that a large η requires $\lambda^\star$ to take many small steps while moving away from γ_1^2 and reaching other $\{\gamma_k\}$, and thus increasing $|\Upsilon|$ (assuming the ordering in (7.31)). We should add that the Grab-n-Pull procedure is most useful when $|\Upsilon| > 1$, or equivalently when η is not very large.

We conclude this section by discussing the trade-off originated from the selection of η, namely the question of a higher convergence speed vs. a smaller value of the penalty functions in $\mathcal{P}_3$ and $\mathcal{P}_4$. To devise a reasonable approach to this trade-off, we consider the following insight: While we can tackle $\mathcal{P}_1$ by blindly increasing all the fractions in the $\max - \min$ structure, $\mathcal{P}_3$ and $\mathcal{P}_4$ suggest an alternative approach by employing the auxiliary variables $\{\lambda_i\}$. The role of $\{\lambda_i\}$ is to *determine* the *increasing* levels $\{(\mathbf{w}^H \mathbf{A}_k \mathbf{w})/(\mathbf{w}^H \mathbf{B}_k \mathbf{w})\}$ should converge to, and the optimization w. r. t. $\mathbf{w}$ will be performed such that $\{(\mathbf{w}^H \mathbf{A}_k \mathbf{w})/(\mathbf{w}^H \mathbf{B}_k \mathbf{w})\}$ can get close to those levels. Consequently, putting less focus on small values of the penalty functions specified above, only makes the proposed method closer to the blind approach—while leaving us with the interesting advantages of the proposed framework including the quadratic nature of the objective, efficiency, and possibility of working with various signal constraints.

7.4 Application: Precoding for Fairness-Achieving Networks:

In this part, an examples from signal processing applications id described that require tackling $\mathcal{P}_1$.

A common interpretation of fairness in the networks entails allocating the available resources in order to maximize the minimal user performance [48,49,66–72]. In such scenarios, a judicious design of the *precoding* signals for different users can be viewed as a vital part of the network configuration. We consider the general *multi-group multicast* precoding problem [48] for a downlink channel, with a n_{Tx}-antenna transmitter and K single-antenna users assigned to $G \leq K$ multicast groups. We denote the subset of user indices in the k^{th} group by $\mathcal{G}_k$ for any $k \in [G]$. Let $\mathbf{h}_i \in \mathbb{C}^{n_{\mathrm{Tx}}}$ denote the channel between the transmit antennas and the i^{th} user. Also let $\mathbf{w}_k \in \mathbb{C}^{n_{\mathrm{Tx}}}$ denote the *precoding* vector corresponding to the k^{th}, $k \in [G]$, multicast group of users. To form the data stream to the users, any complex symbol to be transmitted, will be modulated by the precoding vector of the intended group of users. The precoding vectors are to be designed in order to enhance the network performance. In particular, the SINR value for any user $i \in \mathcal{G}_k$ (and any $k \in [G]$) is given by [47, 48]

$$\mathrm{SINR}_i = \frac{\mathbf{w}_k^H \mathbf{R}_i \mathbf{w}_k}{\left(\sum_{j \in [G]\setminus\{k\}} \mathbf{w}_j^H \mathbf{R}_i \mathbf{w}_j\right) + \sigma_i^2}, \tag{7.41}$$

where $\mathbf{R}_i = \mathbf{E}\{\mathbf{h}_i \mathbf{h}_i^H\}$ is the covariance matrix of the i^{th} channel, σ_i^2 denotes the variance of the zero-mean additive white Gaussian noise (AWGN).

Consequently, the problem of maximizing the minimal user SINR performance in the network can be formulated as [48],

$$\begin{aligned} \max_{\{\mathbf{w}_k\}_{k=1}^G} \quad & \min_{k \in [G]} \left\{ \min_{i \in \mathcal{G}_k} \left\{ \frac{\mathbf{w}_k^H \mathbf{R}_i \mathbf{w}_k}{\left(\sum_{j \in [G]\setminus\{k\}} \mathbf{w}_j^H \mathbf{R}_i \mathbf{w}_j\right) + \sigma_i^2} \right\} \right\} \\ \text{s. t.} \quad & \sum_{k=1}^{G} \|\mathbf{w}_k\|_2^2 \leq P. \end{aligned} \tag{7.42}$$

Note that by a specific reformulation, the SINR metric in (7.41) can be rewritten as a fractional quadratic criterion. To see this, define the *stacked* precoding vector $\mathbf{w} \in \mathbb{C}^N$ (with $N = n_{\mathrm{Tx}} G$) as

$$\mathbf{w} \triangleq \mathrm{vec}([\mathbf{w}_1 \ \mathbf{w}_2 \ \cdots \ \mathbf{w}_G]), \tag{7.43}$$

and observe that (7.41) will increase for any increased scaling of $\mathbf{w}$. As a result, any finite-energy constraint on $\mathbf{w}$ while maximizing $\{\mathrm{SINR}_i\}$ will be *active*, i.e. it will be satisfied with equality. Accordingly, we have $\|\mathbf{w}\|_2^2 = P$, and let

$$\mathbf{A}_i \triangleq \mathbf{R}_i \otimes \mathrm{diag}\left(\mathbf{e}_i\right), \qquad \forall\, i \in [K], \tag{7.44}$$

$$\mathbf{B}_i \triangleq \mathbf{R}_i \otimes \left(\mathbf{I}_K - \mathrm{diag}\left(\mathbf{e}_i\right)\right) + \frac{\sigma_i^2}{P}\mathbf{I}_N, \qquad \forall\, i \in [K], \tag{7.45}$$

where diag (.) denotes the diagonal matrix formed by the entries of the vector argument, $\otimes$ stands for the Kronecker product of matrices, and $\mathbf{e}_i$ is the the i^{th} standard basis vector in $\mathbb{C}^K$. Now, it is not difficult to verify that

$$\text{SINR}_i = \frac{\mathbf{w}^H \mathbf{A}_i \mathbf{w}}{\mathbf{w}^H \mathbf{B}_i \mathbf{w}}, \quad \forall\, i \in [K], \tag{7.46}$$

in which $\{\mathbf{A}_i\}$ are positive semidefinite (PSD) and $\{\mathbf{B}_i\}$ are positive definite (PD). As a result, the precoding design problem for maximizing the minimal user SINR performance can be formulated as $\mathcal{P}_1$. Note that $\mathcal{P}_1$ may also be used to formulate the weighted SINR optimization problems; see [48, 66, 67] for details.

7.5 Numerical Examples

In this section, we provide several numerical examples to investigate the performance of the proposed method (performing the optimization w. r. t. all variables at each iteration). We first study the impact of choosing η on the performance of the proposed algorithm. We then compare GnP with SDR in terms of run-time and accuracy of approximate solutions. At the end, we provide an application-driven example where the GnP algorithm is used to tackle a network beamforming problem.

In all examples, we stop the optimization iterations whenever the increase in the objective becomes smaller than $\epsilon_0 = 10^{-6}$. Recall from Definition 1 that, at the optimal point, $\lambda^\star = \min\{\lambda_i\}, \forall i \in [K]$ and we define $\gamma^\star = \min\{\gamma_i\}, \forall i \in [K]$ where γ_i is the shadow value defined in Definition 1.

For numerical evaluations, random PSD matrices $\{\mathbf{A}_i\}$ and $\{\mathbf{B}_i\}$ are generated using the formula, unless otherwise stated,

$$\mathbf{A}_i = \mathbf{X}_i \mathbf{X}_i^H, \quad \mathbf{B}_i = \mathbf{Y}_i \mathbf{Y}_i^H, \quad \forall i \in K, \tag{7.47}$$

where $\mathbf{X}_i$ and $\mathbf{Y}_i$ are random matrices in $\mathbb{C}^{N \times N}$ whose elements are i.i.d. circularly symmetric zero-mean complex Gaussian random variables with variance $\sigma^2 = 1$.

7.5.1 Impact of Penalty Coefficient (η)

In section 7.3.2, impact of η on the performance of the optimization algorithm was discussed. Here, we provide an example to illustrate its impact clearly. We consider a scenario where $K = 5$, $N = 5$ and $\|\mathbf{w}\|_2^2 = 1$. A random realization of $\mathbf{A}_i$ and $\mathbf{B}_i$, $\forall i \in [K]$, are generated according to (7.47) and optimization problem $\mathcal{P}_3$ and $\mathcal{P}_4$ are solved for different η. Transition of parameters $\{\gamma_i\}$ and $\{\lambda_i\}$ are shown in Fig. 7.4 for $\eta = 1$ and $\eta = 10$.

Note that while the shadow values $\{\gamma_i\}$ represent the value of the fractional quadratic terms in the original objective $\mathcal{P}_1$, the auxiliary variables $\{\lambda_i\}$ tend to be *as close as possible* to $\{\gamma_i\}$ depending on the weight (η) of the penalty-terms in $\mathcal{P}_3$ and $\mathcal{P}_4$. In Fig. 7.4, we present the transition of variables $\{\gamma_i\}$ and $\{\lambda_i\}$ vs. the

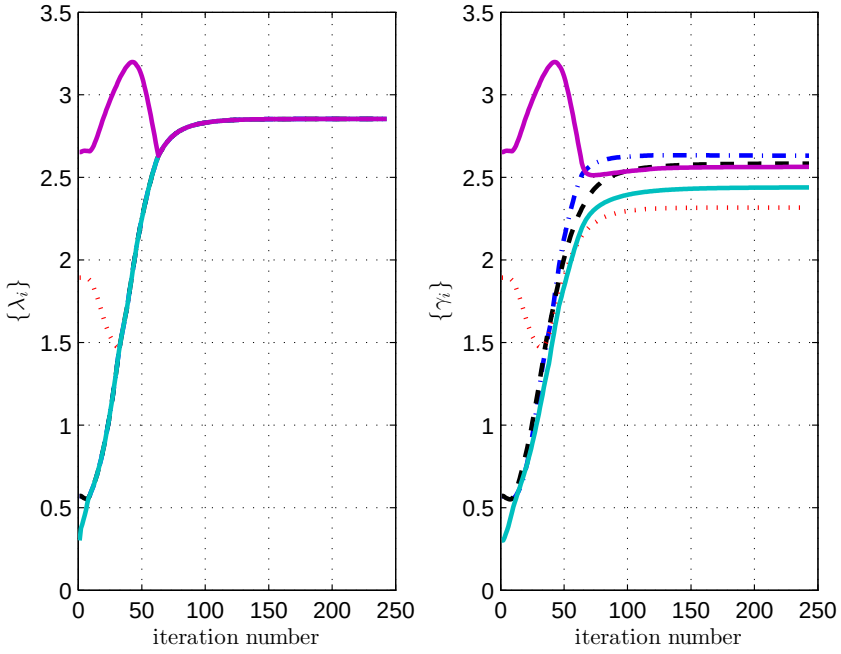

Figure 7.3. Transition of the optimization parameters (distinguished by colors and line-styles) vs. the iteration number for different weights (η) of the penalty-term in $\mathcal{P}_3$ and $\mathcal{P}_4$: (a) $\eta = 1$, and (b) $\eta = 10$.

iteration number for two different settings of η; namely $\eta = 1$ and $\eta = 10$. Although with a larger η one may expect a lower value of the penalty functions in $\mathcal{P}_3$ and $\mathcal{P}_4$, a lower η can play a useful role in speeding up the algorithm. Specifically, one can easily see that if η is large, the value $\lambda^\star$ in (7.30) will be slightly greater than the weighted average of $\{\gamma_k\}_{k\in\Upsilon}$, whereas for smaller values of η, the bounces from the weighted average are much larger—and the convergence can occur much quicker. This phenomenon can also be observed in Fig. 7.4, noting that the aforementioned values of η are chosen to accentuate the trade-off originated from the selection of η.

7.5.2 Comparison with SDR

In order to examine the performance of the proposed method, we compare it with well known SDR method. Considering the total power constraint on the signal,

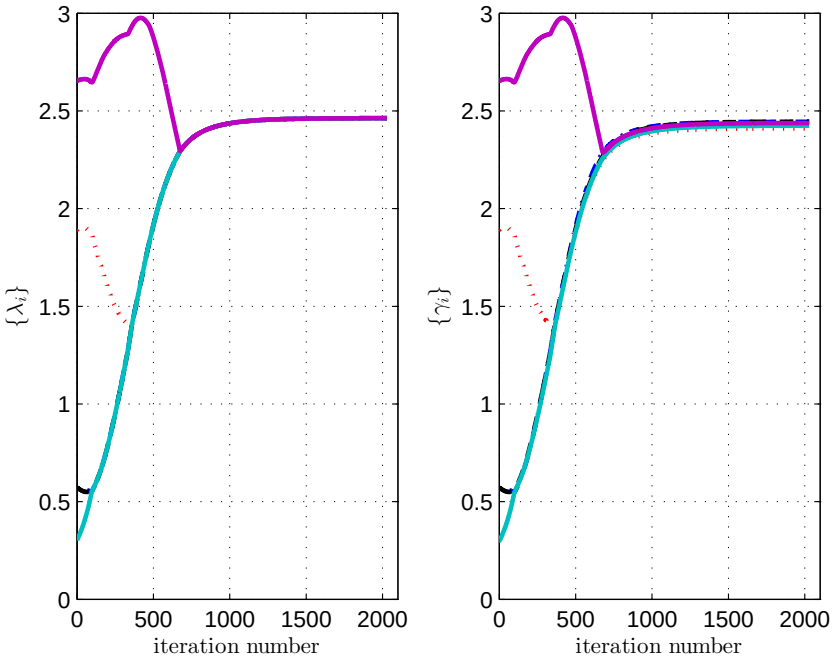

Figure 7.4. Transition of the optimization parameters (distinguished by colors and line-styles) vs. the iteration number for different weights (η) of the penalty-term in $\mathcal{P}_3$ and $\mathcal{P}_4$: (a) $\eta = 1$, and (b) $\eta = 10$.

$\|\mathbf{w}\|_2^2 = 1$, $\mathcal{P}_1$ can be equivalently reformulated as,

$$\begin{aligned} \mathcal{R}_1 : \max_{\mathbf{W}} . \quad & \min_{i\in[K]} \left\{ \frac{\mathrm{Tr}\left(\mathbf{A}_i\mathbf{W}\right)}{\mathrm{Tr}\left(\mathbf{B}_i\mathbf{W}\right)} \right\} \\ \text{s. t.} \quad & \mathrm{Tr}\left(\mathbf{W}\right) = 1\,, \mathbf{W} \succeq 0\,, \mathrm{rank}(\mathbf{W}) = 1, \end{aligned} \tag{7.48}$$

where $\mathbf{W} = \mathbf{w}\mathbf{w}^H$. Relaxing the rank-one constraint and noting that objective function is quasi-concave, we can write the corresponding feasibility problem as follows,

$$\begin{aligned} \mathcal{R}_2 : \textit{find} \quad & \mathbf{W} \\ \text{s. t.} \quad & \frac{\mathrm{Tr}\left(\mathbf{A}_i\mathbf{W}\right)}{\mathrm{Tr}\left(\mathbf{B}_i\mathbf{W}\right)} \geq \upsilon\,, \qquad \forall i \in [K], \\ & \mathrm{Tr}\left(\mathbf{W}\right) = 1\,, \mathbf{W} \succeq 0\,. \end{aligned} \tag{7.49}$$

An optimal value of υ can be found using bisection method. We stop the bisection iteration whenever increment in υ become bounded by 10^{-5}. Note that $\mathcal{R}_2$ along

Table 7.2. Comparison of the performance of GnP and SDR for 100 random realization of $\{\mathbf{A}_i\}$ and $\{\mathbf{B}_i\}$ and $N = 5$. Impact of setting different values for η is also reported.

K	η	Average $\gamma^\star$	Average $\gamma^\star/\upsilon_{\text{SDR}}$	Average $\gamma^\star/\upsilon^\star_{\text{SDR}}$	Average GnP CPU time (sec)	Average SDR time / Average GnP time
5	1	1.9469	0.93	0.9151	0.3702	17.5705
	10	2.0919	0.99	0.9817	3.7486	1.8347
	20	2.0938	1.00	0.9832	6.3256	1.0472
	0.5/10/1000	2.0973	1.00	0.9856	1.1956	5.5039
10	1	1.2742	1.06	0.9047	2.1583	3.3803
	10	1.2977	1.08	0.9210	13.839	0.5178
	20	1.3062	1.09	0.9253	24.4918	0.2919
	0.5/10/1000	1.3290	1.10	0.9419	2.2467	3.1937
15	1	1.0373	1.10	0.8688	3.8869	2.0509
	10	1.0371	1.11	0.8688	33.454	0.2415
	20	1.0376	1.10	0.8689	78.287	0.1082
	0.5/10/1000	1.0707	1.13	0.8960	3.6262	2.1774
20	0.3	0.8470	1.09	0.7938	3.1084	2.9602
	1	0.8876	1.13	0.8324	7.2756	1.2156
	10	0.8796	1.14	0.8256	53.444	0.1658
	20	0.8806	1.14	0.8253	79.958	0.1081
	0.5/10/1000	0.8987	1.15	0.8429	5.4814	1.6111

with bisection procedure is equivalent to $\mathcal{R}_1$. For any given υ, $\mathcal{R}_2$ is a convex optimization problem and can be solved using an standard solver such as CVX [73]. Let us denote the solution of $\mathcal{R}_2$ by $\mathbf{W}^\star$. Due to the rank relaxation in $\mathcal{R}_2$, $\mathbf{W}^\star$ will not, in general, be rank-one. In this case, the Gaussian randomization method [54, 74–76] is used to generate L candidates for optimal solution $\mathbf{w}^\star$. Let us write the eigen-decomposition of $\mathbf{W}^\star$ as $\mathbf{W}^\star = \mathbf{V}\mathbf{\Sigma}\mathbf{V}^H$. Then, the l^{th}, $l \in [L]$, candidate can be generated as $\mathbf{w}_l = \mathbf{V}\mathbf{\Sigma}^{1/2}\mathbf{v}_l$, where $\mathbf{v}_l \in \mathbb{C}^N \sim \mathcal{CN}(\mathbf{0}, \mathbf{I})$ [48]. Note that each $\mathbf{w}_l$ should be scaled in order to satisfy the constraint $\|\mathbf{w}_l\|_2^2 = 1$. We denote the best

candidate by $\mathbf{w}_l^\star$ and corresponding objective value by,

$$\upsilon_{SDR} = \min_{i\in[K]} \left\{ \frac{\mathbf{w}_l^\star \mathbf{A}_i (\mathbf{w}_l^\star)^H}{\mathbf{w}_l^\star \mathbf{B}_i (\mathbf{w}_l^\star)^H} \right\}. \tag{7.50}$$

In order to have fair comparison between our method and SDR approach, we stop Gaussian randomization process whenever $\upsilon_{SDR} \geq \gamma^\star$. To avoid the infinite number of randomizations, we also limit to $L = 1000$. We denote the upper-bound of the objective function of $\mathcal{R}_1$ by,

$$\upsilon_{SDR}^\star = \min_{i\in[K]} \left\{ \frac{\mathrm{Tr}\left(\mathbf{A}_i \mathbf{W}^\star\right)}{\mathrm{Tr}\left(\mathbf{B}_i \mathbf{W}^\star\right)} \right\}. \tag{7.51}$$

Having the upper-bound $\upsilon_{SDR}^\star$, we can use it to examine the goodness of the solutions of our proposed optimization method. Table 7.2 presents the performance comparison of GnP and SDR for 100 random realization of $\{\mathbf{A}_i\}$ and $\{\mathbf{B}_i\}$ with $N = 5$ and a set of values for K and η. These results are obtained on a standard PC with 4GB memory and 2.80GHz processor. It is interesting to note that in all cases, i.e. for different K, there is an η where GnP algorithm outperform SDR in both run-time and accuracy (average $\gamma^\star/\upsilon_{SDR}$). As discussed earlier, increasing η also increases the run-time of the GnP algorithm as can be seen in columns 6 and 7. However, it can be observed that by increasing η from 0.5 to 1000 in two steps, fourth row for each K, the GnP algorithm outperforms the SDR considerably in terms of run-time. It is worth mentioning that when number of constraints are large, e.g. $K = 20$, even very small $\eta = 0.3$ can result in desirable performance.

To sum up, in general a relatively small η, in this example $\eta \approx 1$, may provide good performance in terms of approximate solutions and the run-time. Nevertheless, by starting with a small η and ending with very large η, one can make sure that the GnP algorithm outperforms the SDR approach.

Table 7.3. Comparison of the performance of GnP and SDR for 300 random realization of multi-group multicasting channel($N = 8$, $K = 12$). Impact of setting different values for η and P are also reported.

K	η	Average $\gamma^\star$	Average $\gamma^\star/\upsilon_{\mathrm{SDR}}$	Average $\gamma^\star/\upsilon_{\mathrm{SDR}}^\star$	Average GnP CPU time (sec)	Average SDR time / Average GnP time
12	**1**	0.3353	1.16	0.7796	1.4034	7.5013
	10	0.3859	1.25	0.8827	8.7017	1.2139
	0.5/10/1000	0.3740	1.21	0.8449	2.8303	3.6625

7.5.3 Application in Multigroup Multicast Precoding

In this part, we will use GnP method to solve the Max-Min fair precoding problem for a Multigroup Multicast scenario. In section 7.4, it was show that how this problem can be formulated in $\mathcal{P}_1$ form. We consider a downlink transmitter with $n_{\text{Tx}} = 4$ antennas, as well as $K = 12$ single-antenna users which are divided into $G = 2$ multicast group of 6 users. The entries of the channel vectors $\mathbf{h}_i$ are drawn from an i.i.d. complex Gaussian distribution with zero-mean and unit-variance. The Gaussian noise components received at each user antenna are assumed to have unit variance, i.e. $\sigma_i^2 = 1$ for all $i \in [K]$. We consider normalized total-power constraint, $P = 1$, and stop the optimization iterations whenever the objective increase becomes bounded by $\epsilon = 10^{-6}$.

Table 7.3 summarizes the results of the Max-Min fair precoding design for 300 random realizations of multi-group multicasting channel. Average performance of the GnP method for different η is compared with SDR method. It can be seen that $\eta = 10$ leads to higher accuracy but increases the run time of the algorithm, while increasing η in a few steps, i.e. $\eta = 0.5/10/1000$, provides a good balance between the accuracy and run time that outperform SDR method in both criteria.

7.6 Summary

An optimization framework for efficient precoding/beamforming in fairness-achieving networks was proposed. Thanks to a quadratic reformulation of the original problem, the proposed method can handle different signal constraints by employing the power method-like iterations. Various aspects of the proposed approach were studied.

Chapter 8

Conclusions and Future Work

8.1 Conclusions

In Chapter 3 and Chapter 4, GW transmit diversity was studied for Q/V band feeder link of the multibeam broadband satellite network. The novel aspects of the proposed scheme are the association of GWs into switching pairs based on ordered SNR. Also, considering a dynamic rain attenuation model, the effect of performing switching based on the predicted rain attenuation values have been studied. Expressions for key performance indicators − average outage probability and switching rate− have been derived analytically providing insights into system sizing especially on the relative effect of the number of idle and active GWs. An interesting result is that larger clusters yield better performance for a given ratio of idle and active GWs. It is further seen that an increase in switching threshold, enhances achieved spectral efficiency, but at the cost of higher switching probability.

In Chapter 5, the impact of the phase uncertainty on the precoding was considered. This uncertainty was result of time-varying phase components and long RTD, and was modelled as a random process. The constraints were imposed on the availability and average SINR of the users to render the precoder robust to phase variations. For each of these QoS requirements, probabilistic and expectation based approaches to the design of the precoder were pursued leading to 4 different precoder designs. The choice of different QoS requirements and different approaches provide flexibility to the system designer. The resulting optimization problems were formulated and solved using convex optimization techniques. Numerical evaluations illustrated the detrimental effect of phase uncertainty and vindicate the need for robust designs by showing that the pursued designs achieve the required QoS requirements.

Optimization techniques are vital tool for tackling many signal processing problems including precoder design problem. Chapter 6 and Chapter 7 introduced techniques in order to tackle two NP-hard optimization problems: nonconvex QCQP and Max-Min fractional quadratic programming. These optimization problems have

many applications in signal processing domain including precoder design. The main idea behind the proposed techniques was to transform the constrained problems to unconstrained problems using specialized penalty method. The approximate solutions to the equivalent unconstrained problems then were found by iteratively solving the corresponding subproblems. Comparison with the widely used SDR techniques verified the goodness of the proposed techniques.

8.2 Future Work

Several interesting topics have been identified for future extension of the research activities resulted in this thesis which include,

- **Optical feeder link**: Optical feeder links are an attractive and revolutionary alternative to the RF feeder links in SatCom for capacity expansion. This solution has the following potential advantages with respect to RF links: (a) Optical band has 100 to 1000 times more spectral bandwidth than all of RF bands, (b) Optical bands have no frequency regulation constraints due to the highly directive antennas, (c) With the feeder link moved to the optical band, the spectrum released from the RF feeder link can be allocated to the user links, which will be kept in the RF band and require relatively lower data rates and low cost user terminals. However, there are also some key challenges associated to the use of optical feeder links: (a) The main propagation impairment in optical frequency band is the cloud coverage, which further motivates the investigation of optical ground station (OGS) diversity techniques; (b) Currently, there is no technology mature enough for down-converting the optical signal to RF signal transparently, which further imposes stringent requirements on the payload type (transparent vs. regenerative). These challenges motivate a new research activity in optical feeder link design including new channel model, OGS multiplexing and diversity schemes. It is worth mentioning that SnT is participating in ONSET project (Optical Feeder Links Study for Satellite Networks) and some of ideas developed in this thesis will be considered for switching strategy.

- **Phase uncertainty modeling and robust precoding design**: In Chapter 5, the phase uncertainty was modeled as a Gaussian random variable. It will be very interesting to validate this assumption by using real channel measurements. Another direction could be investigating other approaches for robust precoding design, such as approximating variable y_i using Taylor series expansion. Moreover, it is possible to solve some of the resulted optimization problems by using new techniques proposed in Chapters 6 and Chapter 7.

- **Improving optimization techniques:** In Chapters 6 and Chapter 7, new optimization techniques were introduced to tackle NP-hard problems. Although they have quality performance compared to SDR technique, there is

still room for improvements. Analysis of the approximation accuracy could further shed light on goodness of the proposed methods.

Appendix A

Proof of the Eq. (4.9)

Proof. Since $A_1(n-1)$ and $A_2(n-1)$ are independent, the expression of interest reduces to

$$P_n = \frac{1}{4}\,\mathbf{E}\left\{P\{A_1(n) > \alpha_{\text{th}} | A_1(n-1)\}\right\}\mathbf{E}\left\{P\{A_2(n) > \alpha_{\text{th}} | A_2(n-1)\}\right\}. \quad \text{(A.1)}$$

We now evaluate $\mathbf{E}\left\{P\{A_1(n) > \alpha_{\text{th}} | A_1(n-1)\}\right\}$ and the result in (4.5) follows due to the spatial i. i. d nature of rain attenuation. For simplicity, we rewrite the expression under evaluation as,

$$\begin{aligned}
&\mathbf{E}_y\left\{\Pr\{x > \alpha_{\text{th}} | y\}\right\} = \mathbf{E}_y\left\{\int_{\alpha_{\text{th}}}^{\infty} f(x|y)dx\right\} \\
&= \int_0^{\infty}\int_{\alpha_{\text{th}}}^{\infty} \underbrace{f(x|y)f(y)}_{f(x,y)}\, dx\, dy = \int_{\alpha_{\text{th}}}^{\infty}\int_0^{\infty} f(x,y)\, dy\, dx \\
&= \int_{\alpha_{\text{th}}}^{\infty} f(x)dx = \Pr\{A_1(n) > \alpha_{\text{th}}\} \\
&= 0.5\,\text{erfc}\left(\frac{\ln \alpha_{\text{th}} - m_L}{\sqrt{2}\sigma_L}\right).
\end{aligned}$$

□

Appendix B

Calculation of $\{\mathbf{G}'_i\}$ in (5.20)

The matrix $\mathbf{G}'_i$ can be rewritten as $\mathbf{G}'_i = \mathbf{E}\{\mathbf{q}_i\mathbf{q}_i^\dagger \otimes \mathbf{q}_i\mathbf{q}_i^\dagger\}$. After some calculation, the entry of $\mathbf{G}'_i$ in the rth row and the cth column can be found as,

$$[\mathbf{G}'_i]_{rc} = \mathbf{E}\{e^{\mathbf{j}\mathbf{e}_{i,r_1}} e^{-\mathbf{j}\mathbf{e}_{i,c_1}} e^{\mathbf{j}\mathbf{e}_{i,r_2}} e^{-\mathbf{j}\mathbf{e}_{i,c_2}}\}, \tag{B.1}$$

where,

$$r = (r_1 - 1)K + r_2,\ 1 \le r_1, r_2 \le K, \tag{B.2}$$

$$c = (c_1 - 1)K + c_2,\ 1 \le c_1, c_2 \le K. \tag{B.3}$$

For simplicity, let $\mathbf{G}'_i$ be partitioned as,

$$\mathbf{G}'_i = \begin{bmatrix} \mathbf{G}'_{i,11} & \mathbf{G}'_{i,12} & \cdots & \mathbf{G}'_{i,1K} \\ \mathbf{G}'_{i,21} & \mathbf{G}'_{i,22} & \cdots & \mathbf{G}'_{i,2K} \\ \vdots & \vdots & \ddots & \vdots \\ \mathbf{G}'_{i,K1} & \mathbf{G}'_{i,K2} & \cdots & \mathbf{G}'_{i,KK} \end{bmatrix}, \tag{B.4}$$

where $\{\mathbf{G}'_{i,r_1c_1}\}$ are $K \times K$ matrices. Considering the model used in (5.1) for $\{\mathbf{e}_i\}$ and after some calculation, the submatrices $\mathbf{G}'_{i,r_1c_1}$ can be found as follow,

$$\mathbf{G}'_{i,r_1c_1} = \mathbf{C}_i \quad \text{if} \quad r_1 = c_1, \tag{B.5}$$

where $\mathbf{C}_i$ is defined in (5.6). However, if $r_1 \neq c_1$, the entries of $\mathbf{G}'_{r_1c_1}$ can be obtained as,

$$[\mathbf{G}'_{i,r_1c_1}]_{r_2c_2} = \begin{cases} \rho_i, & \text{if} \quad r_2 = c_2 \\ 1, & \text{if} \quad r_2 = r_1 \quad \text{and} \quad c_2 = c_1 \\ \rho_i^4, & \text{if} \quad r_2 = c_1 \quad \text{and} \quad c_2 = r_1 \end{cases} \tag{B.6}$$

and the rest of the entries (if not defined by (B.6)) are given by

$$[\mathbf{G}'_{i,r_1c_1}]_{r_2c_2} = \begin{cases} \rho_i, & \text{if} \quad r_2 = r_1 \quad \text{or} \quad c_2 = c_1 \\ \rho_i^3, & \text{if} \quad r_2 = c_1 \quad \text{or} \quad c_2 = r_1 \\ \rho_i^2, & \text{otherwise} \end{cases} \tag{B.7}$$

Bibliography

[1] Dantel J Bem, Tadeusz W Wieckowski, and Ryszard J Zielinski. Broadband satellite systems. *IEEE Communications Surveys & Tutorials*, 3(1):2–15, 2000.

[2] Barry G Evans, Paul T Thompson, Giovanni E Corazza, Alessandro Vanelli-Coralli, and Enzo Alberto Candreva. 1945–2010: 65 years of satellite history from early visions to latest missions. *Proceedings of the IEEE*, 99(11):1840–1857, 2011.

[3] Gérard Maral and Michel Bousquet. *Satellite communications systems: systems, techniques and technology.* John Wiley & Sons, 2011.

[4] EN ETSI. Digital video broadcasting (dvb); second generation framing structure, channel coding and modulation systems for broadcasting, interactive services, news gathering and other broadband satellite applications. Technical report, Tech. rep., ETSI, 2005.

[5] EN ETSI. 301 790. *Digital video broadcasting (DVB)*, 499, 2000.

[6] Nicolas Jeannin, Laurent Castanet, Joss Radzik, Michel Bousquet, Barry Evans, and Paul Thompson. Smart gateways for terabit/s satellite. *International Journal of Satellite Communications and Networking*, 32(2):93–106, 2014.

[7] A. Kyrgiazos, B. Evans, P. Thompson, and N. Jeannin. Gateway diversity scheme for a future broadband satellite system. In *Advanced Satellite Multimedia Systems Conference (ASMS) and 12th Signal Processing for Space Communications Workshop (SPSC), 2012 6th*, pages 363–370, 2012.

[8] Helmut Wolf, Markus Schneider, Simon Stirland, and Didier Scouarnec. Satellite multibeam antennas at airbus defence and space: State of the art and trends. In *Antennas and Propagation (EuCAP), 2014 8th European Conference on*, pages 182–185. IEEE, 2014.

[9] Pantelis-Daniel Arapoglou, Bhavani Shankar, Athanasios Panagopoulos, and Björn Ottersten. Gateway diversity strategies in Q/V band feeder links. In *17th Ka and Broadband Communications Conference*, pages 1384–1387, 2013.

[10] O. Vidal, G. Verelst, J. Lacan, E. Alberty, J. Radzik, and M. Bousquet. Next generation high throughput satellite system. In *IEEE First AESS European Conference on Satellite Telecommunications (ESTEL*, pages 1–7, 2012.

[11] M. Marcus and B. Pattan. Millimeter wave propagation; spectrum management implications. *IEEE Microwave Magazine*, 6(2):54–62, 2005.

[12] A.D. Panagopoulos, P.-D.M. Arapoglou, and P.G. Cottis. Satellite communications at KU, KA, and v bands: Propagation impairments and mitigation techniques. *IEEE Communications Surveys Tutorials*, 6(3):2–14, 2004.

[13] ITU-R Recommendation P.676-10. *Attenuation by atmospheric gases*, 2013.

[14] ITU-R Recommendation P.840-6. *Attenuation due to clouds and fog*, 2013.

[15] ITU-R Recommendation P.618-11. *Propagation data and prediction method required for the design of the Earth-space telecommunication systems*, 2013.

[16] S. H. Lin. Statistical behavior of rain attenuation. *Bell System Technical Journal*, 52(4):557–581, 1973.

[17] Joël Lemorton, Laurent Castanet, Frederic Lacoste, Carlo Riva, Emilio Matricciani, Uwe-Carsten Fiebig, Max Van de Kamp, and Antonio Martellucci. Development and validation of time-series synthesizers of rain attenuation for ka-band and Q/V-band satellite communication systems. *International Journal of Satellite Communications and Networking*, 25(6):575–601, 2007.

[18] T. Maseng and P. Bakken. A stochastic dynamic model of rain attenuation. *IEEE Transactions on Communications*, 29(5):660–669, 1981.

[19] ITU-R Recommendation P.1853-1. *Tropospheric attenuation time series synthesis*, 2012.

[20] Pantelis-Daniel Arapoglou, Konstantinos P. Liolis, and Athanasios D. Panagopoulos. Railway satellite channel at ku band and above: Composite dynamic modeling for the design of fade mitigation techniques. *International Journal of Satellite Communications and Networking*, 30(1):1–17, 2012.

[21] Georgios A. Karagiannis, Athanasios D. Panagopoulos, and John D. Kanellopoulos. Multidimensional rain attenuation stochastic dynamic modeling: Application to Earth-Space diversity systems. *Antennas and Propagation, IEEE Transactions on*, 60(11):5400–5411, 2012.

[22] ITU-R Recommendation P.1815-1. *Differential rain attenuation*, 2009.

[23] Gan Zheng, Symeon Chatzinotas, and Björn Ottersten. Generic optimization of linear precoding in multibeam satellite systems. *IEEE Transactions on Wireless Communications*, 11(6):2308–2320, 2012.

[24] Dimitrios Christopoulos, Symeon Chatzinotas, Gan Zheng, Joël Grotz, and Björn Ottersten. Linear and nonlinear techniques for multibeam joint processing in satellite communications. *EURASIP journal on wireless communications and networking*, 2012(1):1–13, 2012.

[25] M.A Diaz, N. Courville, C. Mosquera, Gianluigi Liva, and G.E. Corazza. Non-linear interference mitigation for broadband multimedia satellite systems. In *International Workshop on Satellite and Space Communications, 2007. IWSSC '07*, pages 61–65.

[26] Russell Ju Fu Fang. Spatial diversity satellite communications system with error control, July 4 1978. US Patent 4,099,121.

[27] D. Mignolo, E. Re, A. Ginesi, A. B. Alamanac, P. Angeletti, and M. Harverson. Approaching terabit/s satellite: a system analysis. In *17th Ka and Broadband Communications Conference*, Palermo, Italy, 2011.

[28] P. Angeletti, R. De Gaudenzi, and E. Re. Smart gateway diversity. *Patent Description, European Space Agency*, 2012.

[29] Muhammad Muhammad, Giovanni Giambene, Tomaso de Cola, Matteo Berioli, and Nader Alagha. Network-coding-based gateway handover scheme for terabit satellite networks. In *31st AIAA International Communications Satellite Systems Conference*, 2013.

[30] H. Skinnemoen. Gateway diversity in ka-band systems. In *4th Ka-band Utilization Conference*, Venice, Italy, 1998.

[31] Chaiman Lim, Taesang Yoo, B. Clerckx, Byungju Lee, and Byonghyo Shim. Recent trend of multiuser MIMO in LTE-advanced. *IEEE Communications Magazine*, 51(3):127–135, 2013.

[32] Emil Björnson and Eduard Jorswieck. Optimal resource allocation in coordinated multi-cell systems. *Foundations and TrendsÂ® in Communications and Information Theory*, 9(2), 2013.

[33] ViaSat, Inc. Exede high speed satellite internet services. http://www.exede.com/what-is-exede.

[34] ESA 6B.023. Precoding demonstrator for broadband system forward links. *ARTES 5.1 Statement of Work*, 2014.

[35] ETSI EN 302307-2. *Digital Video Broadcasting (DVB), Second generation framing structure, channel coding and modulation systems for Broadcasting, Interactive Services, News Gathering and other broadband satellite applications; Part II: S2-Extensions (S2-X)*, 2014.

[36] Nihar Jindal. MIMO broadcast channels with finite-rate feedback. *IEEE Transactions on Information Theory*, 52(11):5045–5060, 2006.

[37] Ahmad Gharanjik, Bhavani Shankar Mysore Rama Rao, Pantelis-Daniel. Arapoglou, and Björn Ottersten. Gateway switching in Q/V band satellite feeder links. *IEEE Communications Letters*, 17(7):1384–1387, 2013.

[38] Ahmad Gharanjik, Bhavani Shankar Mysore Rama Rao, Pantelis-Daniel Arapoglou, and Björn. Ottersten. Multiple gateway transmit diversity in Q/V band feeder links. *IEEE Transactions on Communications*, 63(3):916–926, March 2015.

[39] Teresa M. Braun. *Satellite Communications Payload and System, Chapter 7.* John Wiley & Sons, 2012.

[40] A Pascual-Iserte, D.P. Palomar, AI Perez-Neira, and M.-A Lagunas. A robust maximin approach for MIMO communications with imperfect channel state information based on convex optimization. *IEEE Transactions on Signal Processing*, 54(1):346–360, 2006.

[41] B.K. Chalise, S. Shahbazpanahi, A. Czylwik, and A.B. Gershman. Robust downlink beamforming based on outage probability specifications. *IEEE Transactions on Wireless Communications*, 6(10):3498–3503, 2007.

[42] Kun-Yu Wang, Tsung-Hui Chang, Wing-Kin Ma, AM.-C. So, and Chong-Yung Chi. Probabilistic SINR constrained robust transmit beamforming: A bernstein-type inequality based conservative approach. In *IEEE International Conference on Acoustics, Speech and Signal Processing, ICASSP*, pages 3080–3083, 2011.

[43] Kun-Yu Wang, A.M.-C. So, Tsung-Hui Chang, Wing-Kin Ma, and Chong-Yung Chi. Outage constrained robust transmit optimization for multiuser MISO downlinks: Tractable approximations by conic optimization. *IEEE Transactions on Signal Processing*, 62(21):5690–5705, November 2014.

[44] M.B. Shenouda and T.N. Davidson. Outage-based designs for multi-user transceivers. In *IEEE International Conference on Acoustics, Speech and Signal Processing, ICASSP*, pages 2389–2392, 2009.

[45] AB. Gershman, N.D. Sidiropoulos, S. Shahbazpanahi, M. Bengtsson, and B. Ottersten. Convex optimization-based beamforming. *IEEE Signal Processing Magazine*, 27(3):62–75, 2010.

[46] Panos M Pardalos and Stephen A Vavasis. Quadratic programming with one negative eigenvalue is NP-hard. *Journal of Global Optimization*, 1(1):15–22, 1991.

[47] Mats Bengtsson and Björn Ottersten. *Optimal and Suboptimal Transmit Beamforming*. Electrical Engineering & Applied Signal Processing Series. CRC Press, 2001.

[48] Eleftherios Karipidis, Nicholas D Sidiropoulos, and Zhi-Quan Luo. Quality of service and max-min fair transmit beamforming to multiple cochannel multicast groups. *IEEE Transactions on Signal Processing*, 56(3):1268–1279, 2008.

[49] Nicholas D Sidiropoulos, Timothy N Davidson, and Zhi-Quan Tom Luo. Transmit beamforming for physical-layer multicasting. *IEEE Transactions on Signal Processing*, 54(6):2239–2251, 2006.

[50] Yongwei Huang and Daniel P Palomar. Randomized algorithms for optimal solutions of double-sided qcqp with applications in signal processing. *IEEE Transactions on Signal Processing*, 62(5):1093–1108, 2014.

[51] Antonio De Maio, Yongwei Huang, Marco Piezzo, Shuzhong Zhang, and Alfonso Farina. Design of optimized radar codes with a peak to average power ratio constraint. *IEEE Transactions on Signal Processing*, 59(6):2683–2697, 2011.

[52] Augusto Aubry, Antonio De Maio, Marco Piezzo, Mohammad Mahdi Naghsh, Mojtaba Soltanalian, and Petre Stoica. Cognitive radar waveform design for spectral coexistence in signal-dependent interference. In *IEEE Radar Conference*, pages 0474–0478, 2014.

[53] Petre Stoica, Jian Li, and Yao Xie. On probing signal design for MIMO radar. *IEEE Transactions on Signal Processing*, 55(8):4151–4161, 2007.

[54] Zhi-Quan Luo, Wing-Kin Ma, AM.-C. So, Yinyu Ye, and Shuzhong Zhang. Semidefinite relaxation of quadratic optimization problems. *IEEE Signal Processing Magazine*, 27(3):20–34, 2010.

[55] Emmanuel J Candes, Thomas Strohmer, and Vladislav Voroninski. Phaselift: Exact and stable signal recovery from magnitude measurements via convex programming. *Communications on Pure and Applied Mathematics*, 66(8):1241–1274, 2013.

[56] Irène Waldspurger, Alexandre d'Aspremont, and Stéphane Mallat. Phase recovery, maxcut and complex semidefinite programming. *Mathematical Programming*, 149(1-2):47–81, 2015.

[57] Mustafa U Torun, Ali N Akansu, and Marco Avellaneda. Portfolio risk in multiple frequencies. *IEEE Signal Processing Magazine*, 28(5):61–71, 2011.

[58] Alexandre dAspremont and Stephen Boyd. Relaxations and randomized methods for nonconvex QCQPs. *EE392o Class Notes, Stanford University*.

[59] Stephen Boyd and Lieven Vandenberghe. *Convex optimization*. Cambridge university press, 2009.

[60] Kurt M Anstreicher. On convex relaxations for quadratically constrained quadratic programming. *Mathematical programming*, 136(2):233–251, 2012.

[61] Hanif D Sherali and Warren P Adams. *A reformulation-linearization technique for solving discrete and continuous nonconvex problems*, volume 31. Springer Science & Business Media, 2013.

[62] Amir Beck, Aharon Ben-Tal, and Luba Tetruashvili. A sequential parametric convex approximation method with applications to nonconvex truss topology design problems. *Journal of Global Optimization*, 47(1):29–51, 2010.

[63] Barry R Marks and Gordon P Wright. Technical note-a general inner approximation algorithm for nonconvex mathematical programs. *Operations Research*, 26(4):681–683, 1978.

[64] Le-Nam Tran, Muhammad Fainan Hanif, and Markku Juntti. A conic quadratic programming approach to physical layer multicasting for large-scale antenna arrays. *IEEE Signal Processing Letters*, 21(1):114–117, 2014.

[65] Omar Mehanna, Kejun Huang, Balasubramanian Gopalakrishnan, Amit Konar, and Nicholas Sidiropoulos. Feasible point pursuit and successive approximation of nonconvex QCQPs. *Signal Processing Letters, IEEE*, 22(7):804–808, 2015.

[66] M. Schubert and H. Boche. Solution of the multiuser downlink beamforming problem with individual SINR constraints. *IEEE Transactions on Vehicular Technology*, 53(1):18–28, January 2004.

[67] D.W.H. Cai, T.Q.S. Quek, and Chee Wei Tan. A Unified Analysis of Max-Min Weighted SINR for MIMO Downlink System. *IEEE Transactions on Signal Processing*, 59(8):3850–3862, August 2011.

[68] A. Wiesel, Y.C. Eldar, and S. Shamai. Linear precoding via conic optimization for fixed MIMO receivers. *IEEE Transactions on Signal Processing*, 54(1):161–176, January 2006.

[69] Ya-Feng Liu, Yu-Hong Dai, and Zhi-Quan Luo. Max-min fairness linear transceiver design for a multi-user MIMO interference channel. *IEEE Transactions on Signal Processing*, 61(9):2413–2423, May 2013.

[70] Chee Wei Tan, Mung Chiang, and R Srikant. Maximizing sum rate and minimizing MSE on multiuser downlink: Optimality, fast algorithms and equivalence via max-min SINR. *IEEE Transactions on Signal Processing*, 59(12):6127–6143, 2011.

[71] Desmond WH Cai, Tony QS Quek, Chee Wei Tan, and Steven H Low. Max-min SINR coordinated multipoint downlink transmission—duality and algorithms. *IEEE Transactions on Signal Processing*, 60(10):5384–5395, 2012.

[72] G. Dartmann, Xitao Gong, W. Afzal, and G. Ascheid. On the Duality of the Max-Min Beamforming Problem With Per-Antenna and Per-Antenna-Array Power Constraints. *IEEE Transactions on Vehicular Technology*, 62(2):606–619, February 2013.

[73] CVX Research Inc. CVX: Matlab software for disciplined convex programming, version 2.0. http://cvxr.com/cvx, August 2012.

[74] Shuzhong Zhang and Yongwei Huang. Complex quadratic optimization and semidefinite programming. *SIAM Journal on Optimization*, 16(3):871–890, 2006.

[75] Eric Feron. Nonconvex quadratic programming, semidefinite relaxations and randomization algorithms in information and decision systems. In *System Theory*, pages 255–274. Springer, 2000.

[76] Zhi-Quan Luo, Nicholas D Sidiropoulos, Paul Tseng, and Shuzhong Zhang. Approximation bounds for quadratic optimization with homogeneous quadratic constraints. *SIAM Journal on optimization*, 18(1):1–28, 2007.

[77] Ahmad Gharanjik, Bhavani Shankar Mysore Rama Rao, Pantelis-Daniel Arapoglou, Mats Bengtsson, and Björn Ottersten. Phase uncertainty in multibeam satellite channels: Modeling and robust precoding design. *to be submitted to IEEE Transactions on Wireless Communications*, 2016.

[78] Ahmad Gharanjik, Bhavani Shankar Mysore Rama Rao, Pantelis-Daniel Arapoglou, and Björn Ottersten. Large scale transmit diversity in Q/V band feeder link with multiple gateways. In *2013 IEEE 24th International Symposium on Personal Indoor and Mobile Radio Communications (PIMRC)*, pages 766–770, September 2013.

[79] Ahmad Gharanjik, Bhavani Shankar Mysore Rama Rao, Pantelis-Daniel Arapoglou, Mats Bengtsson, and Björn Ottersten. Robust precoding design for multibeam downlink satellite channel with phase uncertainty. In *IEEE International Conference on Acoustics, Speech and Signal Processing, ICASSP*, pages 3083–3087, April, 2015.

[80] Ahmad Gharanjik, Bhavani Shankar Mysore Rama Rao, Pantelis-Daniel Arapoglou, Mats Bengtsson, and Björn Ottersten. Precoding design and user selection for multibeam satellite channels. In *IEEE International Workshop on Signal Processing Advances in Wireless Communications (SPAWC)*, pages 420–424, June, 2015.

[81] Mojtaba Soltanalian, Ahmad Gharanjik, Bhavani Shankar Mysore Rama Rao, and Björn Ottersten. Grab-n-Pull: An optimization framework for fairness-achieving networks. *accepted to IEEE International Conference on Acoustics, Speech and Signal Processing (ICASSP)*, 2016.

[82] Ahmad Gharanjik, Konstantinos Liolis, Bhavani Shankar, and Björn Ottersten. Spatial multiplexing in optical feeder links for high throughput satellites. In *Signal and Information Processing (GlobalSIP), 2014 IEEE Global Conference on*, pages 1112–1116. IEEE, 2014.

[83] Athanasios D Panagopoulos, Pantelis-Daniel M Arapoglou, John D Kanellopoulos, and Panayotis G Cottis. Long-term rain attenuation probability and site diversity gain prediction formulas. *Antennas and Propagation, IEEE Transactions on*, 53(7):2307–2313, 2005.

[84] Hong-Chuan Yang and Mohamed-Slim Alouini. Markov chains and performance comparison of switched diversity systems. *Communications, IEEE Transactions on*, 52(7):1113–1125, 2004.

[85] Ahmad Gharanjik and Kamal Mohamed-Pour. Switch-and-stay partial relay selection over rayleigh fading channels. *IET communications*, 5(9):1199–1203, 2011.

[86] Diomidis S Michalopoulos and George K Karagiannidis. Two-relay distributed switch and stay combining. *Communications, IEEE Transactions on*, 56(11):1790–1794, 2008.

[87] Adnan Abu-Dayya, Norman C Beaulieu, et al. Analysis of switched diversity systems on generalized-fading channels. *Communications, IEEE Transactions on*, 42(11):2959–2966, 1994.

[88] Marvin K Simon and Mohamed-Slim Alouini. *Digital communication over fading channels*, volume 95. John Wiley & Sons, 2005.

[89] Daniel Zwillinger. *Table of integrals, series, and products*. Elsevier, 2014.

[90] Vasileios K Sakarellos, Dimitrios Skraparlis, Athanasios D Panagopoulos, and John D Kanellopoulos. Outage performance analysis of a dual-hop radio relay system operating at frequencies above 10ghz. *Communications, IEEE Transactions on*, 58(11):3104–3109, 2010.

[91] J. Aitchison and J. A. C. Brown. *The Lognormal Distribution*. Cambridge University Press, 1st edition edition, 1957.

[92] M. Luglio. Fade prediction and control systems. In *, 1995 URSI International Symposium on Signals, Systems, and Electronics, 1995. ISSSE '95, Proceedings*, pages 71–75, 1995.

[93] B. Gremont, M. Filip, Paul Gallois, and S. Bate. Comparative analysis and performance of two predictive fade detection schemes for ka-band fade countermeasures. *IEEE Journal on Selected Areas in Communications*, 17(2):180–192, 1999.

[94] A.P. Chambers and I.E. Otung. Neural network approach to short-term fade prediction on satellite links. *Electronics Letters*, 41(23):1290–1292, November 2005.

[95] Steven M Kay. *Fundamentals of statistical signal processing, Volume 1*. Prentice Hall PTR, Englewood Cliffs (N.J.), 1993. 00065.

[96] Thomas H. Cormen, Charles E. Leiserson, Ronald L. Rivest, and Clifford Stein. *Introduction to Algorithms, 3rd Edition*. The MIT Press, 3rd edition edition, 2009.

[97] Herbert A David and Haikady N Nagaraja. *Order statistics*. Wiley-Interscience, Hoboken, NJ, 2003.

[98] P.-D. Arapoglou, A. Ginesi, S. Cioni, S. Erl, F. Clazzer, S. Andrenacci, and A. Vanelli-Coralli. DVB-S2X enabled precoding for high throughput satellite systems. *accepted in Int. J. Satell. Commun. Syst. Network*, 2015.

[99] K. V Mardia. *Statistics of directional data*. Academic Press, London; New York, 1972.

[100] Roger A. Horn and Charles R. Johnson. *Matrix Analysis*. Cambridge University Press, Cambridge; New York, 2 edition edition, December 2012.

[101] S. Kandukuri and S. Boyd. Optimal power control in interference-limited fading wireless channels with outage-probability specifications. *IEEE Transactions on Wireless Communications*, 1(1):46–55, January 2002.

[102] Mats Bengtsson and Björn Ottersten. Signal waveform estimation from array data in angular spread environment. In *Thirtieth IEEE Asilomar Conference on Signals, Systems and Computers*, volume 1, pages 355–359, 1996.

[103] Yongwei Huang and D.P. Palomar. Rank-Constrained Separable Semidefinite Programming With Applications to Optimal Beamforming. *IEEE Transactions on Signal Processing*, 58(2):664–678, 2010.

[104] ETSI EN 302 307 v.1.1.2. *Digital Video Broadcasting (DVB), Second generation framing structure, channel coding and modulation systems for broadcasting, interactive services, news gathering and other broad-band satellite applications*, 2003.

[105] M. Soltanalian and P. Stoica. Designing unimodular codes via quadratic optimization. *IEEE Transactions on Signal Processing*, 62(5):1221–1234, March 2014.

[106] Gene H Golub and Charles F Van Loan. *Matrix computations*, volume 3. JHU Press, 2012.

[107] Antonio Pascual-Iserte, Daniel Pérez Palomar, Ana Pérez-Neira, Miguel Ángel Lagunas, et al. A robust maximin approach for MIMO communications with imperfect channel state information based on convex optimization. *IEEE Transactions on Signal Processing*, 54(1):346–360, 2006.

[108] Alex B Gershman. *Robustness issues in adaptive beamforming and high-resolution direction finding*. New York: Marcel Dekker, 2003.

[109] Seung-Jean Kim and Stephen Boyd. A minimax theorem with applications to machine learning, signal processing, and finance. *SIAM Journal on Optimization*, 19(3):1344–1367, 2008.

[110] A. De Maio, Yongwei Huang, and M. Piezzo. A Doppler robust max-min approach to radar code design. *IEEE Transactions on Signal Processing*, 58(9):4943–4947, sept. 2010.

[111] Mohammad Mahdi Naghsh, Mojtaba Soltanalian, Petre Stoica, Mahmoud Modarres-Hashemi, Antonio De Maio, and Augusto Aubry. A Doppler robust design of transmit sequence and receive filter in the presence of signal-dependent interference. *IEEE Transactions on Signal Processing*, 62(4):772–785, 2014.

[112] Emil Bjornson, Gan Zheng, Mats Bengtsson, and Björn Ottersten. Robust monotonic optimization framework for multicell MISO systems. *Signal Processing, IEEE Transactions on*, 60(5):2508–2523, 2012.

[113] P-A Absil, Robert Mahony, and Rodolphe Sepulchre. *Optimization Algorithms on Matrix Manifolds*. Princeton University Press, 2009.

[114] Alan Edelman, Tomás A Arias, and Steven T Smith. The geometry of algorithms with orthogonality constraints. *SIAM journal on Matrix Analysis and Applications*, 20(2):303–353, 1998.

[115] Eduard Stiefel. Richtungsfelder und fernparallelismus in n-dimensionalen mannigfaltigkeiten. *Commentarii Mathematici Helvetici*, 8(1):305–353, 1935.

[116] Jaehyun Park and Stephen Boyd. A semidefinite programming method for integer convex quadratic minimization. *submitted to SIAM Journal on Optimization, available arXiv:1504.07672*, 2015.

[117] Kejun Huang and Nicholas D Sidiropoulos. Consensus-ADMM for general quadratically constrained quadratic programming. *arXiv preprint arXiv:1601.02335*, 2016.

[118] Aritra Konar and Nicholas D Sidiropoulos. Hidden convexity in QCQP with Toeplitz-Hermitian quadratics. *IEEE Signal Processing Letters*, 22(10):1623–1627, 2015.

[119] Jaehyun Park and Stephen Boyd. Concave quadratic cuts for mixed-integer quadratic problems. *arXiv preprint arXiv:1510.06421*, 2015.

[120] Mojtaba Soltanalian, Bo Tang, Jian Li, and Peter Stoica. Joint design of the receive filter and transmit sequence for active sensing. *IEEE Signal Processing Letters*, 20(5):423–426, 2013.

[121] Mojtaba Soltanalian, Heng Hu, and Petre Stoica. Single-stage transmit beamforming design for MIMO radar. *Signal Processing*, 102:132–138, 2014.

[122] Wei Yu and Tian Lan. Transmitter optimization for the multi-antenna downlink with per-antenna power constraints. *IEEE Transactions on Signal Processing*, 55(6):2646–2660, 2007.

[123] Hao He, Jian Li, and Petre Stoica. *Waveform Design for Active Sensing Systems: A Computational Approach*. Cambridge University Press, 2012.

[124] N. Levanon and E. Mozeson. *Radar Signals*. Wiley, New York, 2004.